CONDENSATION IN MEMBRANE-BASED ENERGY EXCHANGERS

by

Iman Rahgozar Abadi

B.Sc., Sharif University of Technology, 2019

A THESIS SUBMITTED IN PARTIAL FULFILLMENT OF

THE REQUIREMENTS FOR THE DEGREE OF

MASTER OF APPLIED SCIENCE

in

THE FACULTY OF GRADUATE AND POSTDOCTORAL STUDIES

(Mechanical Engineering)

THE UNIVERSITY OF BRITISH COLUMBIA

(Vancouver)

December 2021

The following individuals certify that they have read, and recommend to the Faculty of Graduate and Postdoctoral Studies for acceptance, a thesis entitled:

Condensation in Membrane-Based Energy Exchangers

submitted by Iman Rahgozar Abadi in partial fulfillment of the requirements for

the degree of MASTER OF APPLIED SCIENCE

in Mechanical Engineering

Examining Committee:

Dr. Steven Rogak, Professor, Department of Mechanical Engineering, UBC
Supervisor

Dr. Sheldon Green, Professor, Department of Mechanical Engineering, UBC
Supervisory Committee Member

Dr. Adam Rysanek, Assistant Professor, Architecture and Landscape Architecture, UBC
Supervisory Committee Member

Abstract

Using energy exchangers in winter conditions, and hot and humid summer conditions can result in condensation. Condensation might affect the performance of the exchanger, facilitate the growth of micro-organisms and be a precursor to frost formation at lower temperatures. As a result, information about the impacts of condensation on the performance of the energy exchanger and the operating conditions that result in condensation is essential for the design of ventilation systems and the selection of the proper exchanger.

In this study, a widely used energy exchanger is experimentally tested under various operating conditions. The presence of condensation is inferred from visual observation, investigation of the sensible and latent effectiveness, and measurements of pressure drop. It is shown that condensation increases the sensible effectiveness of the supply side and decreases the sensible effectiveness of the exhaust side. Additionally, the latent effectiveness of both air streams increases when condensation occurs, although the increase in exhaust side latent effectiveness is more significant. Finally, the accumulation of water in the channels significantly increases the pressure drop in the exhaust side while it does not significantly impact the effectiveness.

Additionally, a heat and mass transfer model is developed to investigate condensation in a wide range of operating conditions. The permeability of the composite membrane of the exchanger used in this study, is measured at various temperature and humidities and the effects of membrane orientation and the phase of water (liquid/vapor) on the permeability of the membrane are investigated. An empirical membrane model is then added to the heat and mass transfer model. The heat and mass transfer model is validated against experiments and is then used to determine the operating conditions resulting in condensation and to investigate the effect of variation in the permeability of the membrane on the occurrence of condensation. It is shown that assuming a constant permeability for the membrane can result in errors of up to 25% in the prediction of the rate of condensation. Furthermore, it is shown that condensation in the energy exchanger will be significant only when the indoor air temperature and humidity are high.

Lay Summary

Membrane-based energy exchangers use the temperature and humidity of the indoor air to precondition the fresh air that goes into the ventilation system; thus, they lower the required energy for ventilation. Energy exchangers are similar to heat exchangers; however, instead of plastic or aluminum plates, they have water vapor permeable membranes that permit the transfer of both heat and water vapor. The energy saving ability of energy exchangers is higher in winter conditions; however, using energy exchangers in such weather conditions can result in condensation which has significant effects on the performance of the exchanger. In this study, condensation in energy exchangers is experimentally investigated and a heat and mass transfer model for prediction of condensation is developed. It is shown that condensation enhances the thermal performance of the exchanger and increases the pressure drop; however, it will be significant only when the indoor air temperature and humidity are high.

Preface

This study is the original work of the author, Iman Rahgozar Abadi. The contents of this thesis have been used in research articles that are either published or are under review by scholarly journals. In any such occasion, permission of the journal was obtained; however, manuscripts have had minor changes to fit the formatting style of a thesis.

A version of Chapter 2 has been submitted for publication. The test setup used for the permeability measurements was initially built by previous students in our research group, Dr. Amin Engarnevis and Alexander Sylvester in Aerosol Lab at UBC; however, the setup was adjusted for this study by the author and a fellow MASc student, Behzad Aminian. All of the tests and the following data analysis were performed by the author under the supervision of Dr. Steven Rogak and Dr. Sheldon Green and with the help of Mr. Behzad Aminian. Dr. Ryan Huizing and Mr. Scott Dormian at CORE Energy Recovery Solutions provided the membrane samples and guided the research with their expertise in the area. The author was responsible for the writing of the manuscript and accommodated the comments of the co-authors.

A version of Chapter 3 has been accepted for publication by the journal of Energy and Buildings (In Press, Journal Pre-proof). **I. Rahgozar Abadi**, B. Aminian, M. Rafati Nasr, R. Huizing, S. Green, S. Rogak, Experimental Investigation of Condensation in Energy Recovery Ventilators, Energy and Buildings, 2021. Condensation tests were conducted by the author at CORE Energy Recovery Solutions with the help of Dr. Mohammad Rafati Nasr under supervision of Dr. Sheldon Green and Dr. Steven Rogak. Dr. Ryan Huizing provided guidance for the test planning and analysis of the results. The author was responsible for the data analysis of the test results; however, Mr. Behzad Aminian provided assistance. The author prepared the manuscript and implemented the comments of the co-authors.

A version of Chapter 4 has been submitted for publication. The author was responsible for the development of the model; however, Dr. Steven Rogak and Dr. Sheldon Green provided supervision and scientific assistance. Dr. Mohammad Rafati Nasr and Dr. Ryan Huizing provided guidance for the validation of the heat and mass transfer model and development of empirical membrane model. The author was responsible for the writing of the manuscript and implementing the co-author's comments; however, Mr. Behzad Aminian provided intellectual assistance in the preparation of the manuscript and explanation of the results.

Chapter 1 and Chapter 7 and all of the other materials in this thesis were written by the author with guidance from Dr. Steven Rogak and Dr. Sheldon Green.

Table of Contents

List of Tables

List of Figures

List of Symbols

Symbols

a	Channel Height (m)
A_c	Cross Sectional Area of Channels (m^2)
A_{eff}	Membrane Effective Area (m^2)
b	Channel Width (m)
C	Sutherland's Constant
C_f	Correction Factor
C_p	Specific Heat (J/kg·K)
d_h	Hydraulic Diameter (m)
D_{Kn}	Knudsen diffusivity (m^2/s)
d_{pore}	Pore diameter (m)
D_{wv}	Diffusivity of Water Vapour in Air (m^2/s)
f	Fanning Friction Factor
h	Convection Heat Transfer Coefficient (W/m^2·K)
J	Water Vapour Flux (kg/m^2.s)
k	Mass Transfer Coefficient (m/s)
L	Length of Channels (m)
Le	Lewis Number
LE	Latent Effectiveness
m	Blending Parameter
M	Molar Mass (kg/mol)
$\dot{m}$	Air Mass Flowrate (kg/s)
N	Number of Pores per Unit Area (1/m)
Nu	Nusselt Number

P	Atmospheric Pressure (pa)
Per	Perimeter of the Channel (m)
p_g	Saturation Pressure of Water Vapour (pa)
Pr	Prandtl Number
p_v	Partial Pressure of Water Vapour (pa)
Q	Air Flowrate (m^3/s)
R	Resistance (s/m)
R_a	Air Specific Gas Constant (J/kg.K)
Re	Reynolds Number
RH	Relative Humidity
R_u	Universal Gas Constant (J/mol.K)
R_v	Water Vapour Specific Gas Constant (J/kg.K)
S	Solubility Coefficient (m^3/m^3.pa)
Sc	Schmidt number
SE	Sensible Effectiveness
Sh	Sherwood Number
t	Thickness (m)
T	Temperature (°C or K)
$T_{c_{air}}$	Critical Temperature of Air (K)
T_{c_v}	Critical Temperature of Water Vapour (K)
v	Velocity of Air (m/s)
$V_{c_{air}}$	Critical Specific Volume of Air (m^3/kg)
V_{c_v}	Critical Specific Volume of Water Vapour (m^3/kg)
x_v	Activity of Water Vapour
Z^*	Dimensionless Length

Greek Letters

δ	Membrane Thickness (m)
ε	Surface Porosity
λ	Membrane Thermal Conductivity (W/m·K)
ϵ	Aspect Ratio
μ	Viscosity ($N.s/m^2$)
ρ	Density (kg/m^3)
τ	Pore Tortuosity
Υ	Shape Factor
φ	Pore size Distribution
Φ	Interaction Parameter
ω	Moisture Ratio (kg/kg)

Superscripts

b	Bulk Flow
f	Feed Side
m	Membrane
s	Sweep Side/Supply Side
*	Property at the Coting and Substrate Interface

Subscripts

a	Air
air	Air
b	Bulk Flow
BL	Boundary Layer
c	Coating Layer

Cond	Condensate
e	Exhaust Side
i	Inlet
in	Inlet
LMD	Logarithmic Mean Difference
m	Membrane
mean	Average Value
mem	Membrane Resistance
mix	Mixture of Air and Water Vapor
o	Outlet
out	Outlet
s	Supply Side
sub	Substrate Layer
total	Total Resistance
v	Vapor
0	Reference Property

List of Abbreviations

AHRI	Air Conditioning, Heating and Refrigeration Institute
ASHRAE	American Society of Heating, Refrigerating, and Air-Conditioning Engineers
CA	Cellulose Acetate
CFD	Computational Fluid Dynamics
ERV	Energy recovery Ventilator
HRV	Heat Recovery Ventilator
HVAC	Heating, Ventilation and Air Conditioning
NSERC	Natural Sciences and Engineering Research Council of Canada
PEO	Poly(ethylene oxide)
PU	Polyurethane
SPEEK	Sulfonated poly(ether ether ketone)

Acknowledgements

I would like to show my gratitude to my supervisor, Dr. Steven Rogak who was always patient, encouraging and motivating. None of this work would have been possible without his guidance. I would also like to express thanks to my co-supervisor Dr. Sheldon Green for his dedication and thoughtful guidance. I was truly honored to work under supervision of such great scientists.

I would like to express my gratitude and thanks to my dear friend and colleague, Behzad Aminian who supported me in all stages of this work and provided lots of valuable intellectual assistance. Many thanks to the R&D team at CORE, especially, Dr. Ryan Huizing and Dr. Mohammad Rafati Nasr for their continuous and valuable support and feedbacks and for letting me use their test facility. I would also like to thank my examining committee member, Dr. Adam Rysanek for his valuable comments and recommendations. Many thanks also to my dear friend, Dr. Hamed Nikookar who always made our lab a fun environment and added positive energy.

Finally, appreciation and gratitude are not enough for the dedication and support of my family, my parents and my dear sister. Your love and support always guided me in the hard times of my life, including this research work.

I would also like to acknowledge that this study was funded by the Natural Sciences and Engineering Research Council of Canada (NSERC) [CRD grant GR 14315] and was supported by CORE Energy Recovery Solutions.

Dedication

To my parents and my sister who have always supported me.

Chapter 1: Introduction

1.1 Background

1.1.1 Basics of Energy Recovery

Residential and commercial buildings are responsible for a significant portion of the total energy consumption in the world. For instance, in United States and Canada, building sector is responsible for 41% and 27% of the total primary energy consumption [2,3]. Recent studies have shown that almost half of the energy consumed in the building sector is used by Heating, Ventilation and Air Conditioning (HVAC) systems [4,5]. In order to provide a safe and comfortable environment for the building occupants, the temperature and humidity of the indoor air must be controlled [6,7]. High temperature and humidity may enhance the growth of bio-organisms such as fungi and mites which endanger the health of the occupants and pose risks to the structural stability of the building [1]. In addition to proper temperature and humidity, replacement of the indoor air with fresh outdoor air is also essential for maintaining the indoor air quality. Replacement of indoor air with fresh air, however, imposes a large load on the ventilation system as the fresh air temperature and humidity need to be adjusted to the proper temperature and humidity. As a result, a large fraction of the energy consumed by the HVAC system is used for conditioning of fresh air. Although many new techniques have been developed for decreasing the cooling and heating load on the ventilation system, such as enhanced building insulation, decreased air leakage and smart demand-controlled ventilation systems, the need for using fresh air still exists [1].

Although the need for the continuous addition of fresh air cannot be completely eliminated, the required energy for conditioning the fresh air can be significantly reduced by using air-to-air recovery exchangers also known as recovery ventilators. Recovery ventilators use the energy of the exhaust indoor air to precondition the incoming fresh air. This means that, the energy that was used to condition the current indoor air will not be wasted by exhausting the air and instead, will be reused to condition the incoming fresh air. Two commonly used types of recovery exchangers are heat recovery exchangers and energy recovery exchangers (also known as heat recovery ventilators (HRVs) and energy recovery ventilator (ERVs), respectively). Heat recovery exchangers precondition the incoming fresh air by allowing the transfer of heat between the indoor and outdoor air which results in heating or cooling the fresh air. Similarly, energy recovery exchangers also permit the transfer of heat between the indoor air and outdoor fresh air; however, in addition to heat, they also permit the transfer of moisture between the flows, as a result, the humidity of the incoming fresh air also changes in the exchanger. Figure 1.1 shows the function of an energy exchanger in summer and winter conditions.

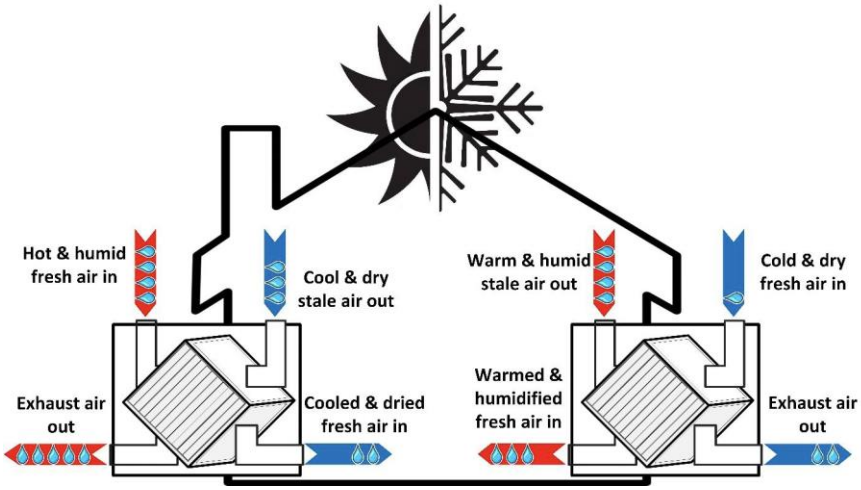

Figure 1.1) Function of an energy exchanger in winter and summer conditions, picture from [1]

As is shown in the figure, in winter, the humidity and temperature of the outgoing indoor air is higher than the incoming fresh air, as a result, in the exchanger, the temperature and moisture transfers from the indoor air to the outdoor air and the temperature and humidity of the incoming fresh air increases. In summer, however, the humidity and temperature of the indoor air is lower than the outdoor air, as a result, the temperature and humidity of the incoming fresh air decreases in the exchanger. Using an efficient energy exchanger can reduce the required energy for conditioning of fresh air by 65% and the total energy consumption of the HVAC system by 20% [8–10].

1.1.2 Flat-Plate Membrane-Based Energy Exchangers

Energy recovery exchangers are classified based on their geometry and flow arrangement. Some of the most common types of energy recovery exchangers are energy wheels, switching chambers, plenum chambers and flat-plate membrane-based energy exchangers [11]. In the recent years, however, flat-plate membrane-based energy exchangers have gained more attention due to their compact structure, low price and high efficiency [10,12,13], Flow arrangement in flat-plate membrane-based energy exchangers can be cross-flow, counter-flow or quasi counter-flow. Due to their manufacturability and simple structure, cross-flow exchangers are the most widely used type. As a result, in this study, flat-plate membrane-based energy exchangers with cross-flow arrangement (hereafter called energy exchangers for simplicity) are studied; however, many of the findings of this study can be generalized to other exchanger types and flow arrangements. The schematic of a typical cross-flow energy exchanger is shown in Figure 1.2.

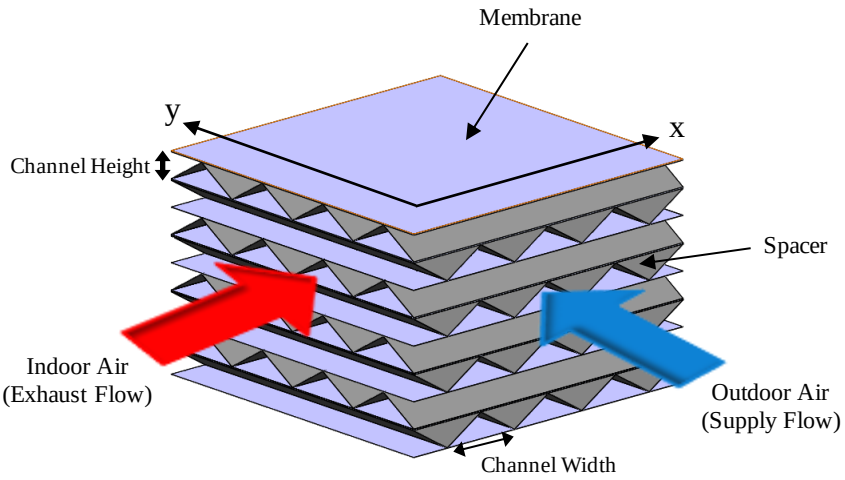

Figure 1.2) Schematic of a typical cross-flow energy exchanger

As is shown in the figure, in the exchanger, indoor air stream (exhaust flow) and outdoor air stream (supply flow) are separated by sheets of water vapor permeable membranes (that allow the transfer of both heat and moisture) and corrugated aluminum sheets are used as spacers between the membrane sheets.

1.2 Motivation

Air-to-air energy exchangers have become a crucial part of the ventilation system of the modern buildings. In the recent decades, many codes, standards, and mandates have been introduced by governments that demand or encourage the use of recovery ventilators in the ventilation system of the residential and commercial buildings [14,15]. This means that energy exchangers are used in various locations all around the world with different weather conditions including hot and humid summer conditions and cold and dry winter conditions.

Although energy exchangers have a higher energy saving potential in extreme weather conditions, these weather conditions might result in condensation and frost formation in the exchanger, and it has been shown that condensation and frost formation could have significant effects on the performance of the exchanger and the ventilation system [16]. Despite the significance of their impacts, however, studies on condensation and frost formation are rare in the literature [16] and virtually all of these studies have investigated condensation that accompanies frosting in sub-zero temperatures and condensation without frosting is neglected. This is surprising considering the fact that, unlike frost formation, condensation can occur in both summer and winter conditions, and it does not require extremely cold weather conditions, as a result, the chances of the occurrence of condensation are higher than frost formation while it could equally affect the performance.

Information about condensation is helpful for both the costumers and manufacturers of energy exchangers. Being able to predict the occurrence of condensation could help the users of energy exchangers to design proper drainage systems to avoid the accumulation of water in the energy recovery unit. Additionally, the manufacturers can implement changes in their exchangers to decrease condensation or propose exchangers that result in the lowest amount of condensation to their customers.

As a result, investigating the effects of condensation on the performance of energy exchangers and developing tools that enable prediction of operating conditions that result in condensation are of crucial importance.

1.3 Research Objectives and Thesis Outline

The main aim of this study is to determine the operating conditions that result in condensation in energy exchangers and to investigate the impacts of condensation on the performance factors of the exchanger such as sensible and latent effectiveness and the pressure drop.

In order to investigate condensation, however, detailed information about the permeation properties of the membrane media is needed, since the heat and mass transfer processes in the exchanger are significantly affected by the membrane properties. As a result, in Chapter 2 of this study the permeation properties of the membrane media used in the energy exchanger studied in this thesis are investigated. Membrane permeability is measured at different temperature and humidities and the effect of membrane orientation (which side of the membrane is in contact with the flows with higher humidity) on the permeability is investigated. The results of this chapter are then used in Chapter 3 and Chapter 4.

In Chapter 3, condensation in a commercially used energy exchanger is experimentally investigated. Visual inspection of the exchanger, investigation of sensible and latent effectiveness and measurement of pressure drop are used for detection of condensation. The operating conditions that result in condensation are determined and short-term and long-term impacts of condensation on effectiveness and pressure drop are determined. The results of the experiments in this chapter are also used in Chapter 4.

As determination of condensation in a wide range of operating conditions with experimental tests is not practically possible, in Chapter 4, a heat and mass transfer model is developed to predict condensation in a wide range of operating conditions. The results of the permeability measurements in Chapter 2 are used to develop an empirical membrane model which is added to the heat and mass transfer model to account for variations in the permeability of the membrane.

The developed model is then used to investigate the occurrence of condensation in energy exchangers in a wide range of operating conditions. Furthermore, the effect of variations in the permeability of the membrane due to temperature, humidity and phase of water (liquid/vapor) are investigated.

In Chapter 5, a summary of the conclusions of this study are presented, limitations of this study are explained, and recommendations are made for future works and extension of thes research.

Chapter 2: Orientation Dependent Permeability in Asymmetric Composite Membranes

2.1 Introduction

Membranes with high water vapor permeability and selectivity have a wide range of applications, such as dehumidification of air, flue and natural gas [17–19], and in packaging materials [20] and wearable fabrics [21]. In the past decade, water vapor permeable membranes have become ubiquitous in membrane-based energy exchangers [22]. Hydrophilic dense polymers are among the best options for energy exchangers due to their high selectivity and permeability for water vapor [1]. In order to achieve mechanical stability, dense polymer membranes must be made with a high thickness; however, increasing the thickness significantly decreases the permeability [23]. Additionally, dense polymers are prone to swelling when used in highly humid environments [23]. As a result, dense polymer membranes used in membrane-based energy exchangers are mostly used as a selective layer on top of a microporous substrate with high structural stability forming a composite asymmetric structure [24].

The latent effectiveness of an energy exchanger, which quantifies its ability to transfer moisture between the flows, is directly related to the permeability of the membrane. Membrane permeability, however, often varies with temperature and humidity, complicating the prediction of energy exchanger effectiveness. Many of the studies that have modelled heat and mass transfer in energy exchangers have assumed a constant permeability for the membrane [22,25–31]; however, Engarnevis et al. [32] showed that this assumption can result in deviations in effectiveness of up to 15%. As a result, measurement of permeability at different temperatures and water vapor activities is salient. Permeability measurements of membranes are mainly done by varying the feed flow humidity while keeping the sweep flow dry [33–36], although a few studies that have considered the effect of sweep flow humidity have observed significant effects [1,37–40] . For instance, Prabhakar et el. [38] developed a model to explain the temperature and concentration dependent behavior of permeability of rubbery polymers. Additionally, they experimentally measured the permeability of propane in PDMS to validate the results of their model. The results of both their model and their experiments showed that the vapor pressure of propane in the sweep flow can significantly affect the permeability. They explained that changing the concentration of both feed and sweep flows changes the concentration of the penetrant in the membrane and if the membrane permeability is concentration dependent, this changes the permeability of the membrane.

Composite membranes are made up of layers with completely different permeation properties, so water vapor concentration is likely to have a different impact on each layer. This means that, it is possible to test a membrane at similar operating conditions with different orientations (i.e., varying the layer of the membrane in contact with the feed flow) and get different values for permeability. Although membranes used in energy exchangers are fixed (i.e., their orientation does not change), the humidity of the indoor and outdoor air streams might differ depending on the season. In summer, the outdoor air humidity is usually higher than indoor air humidity while in winter the indoor air humidity is higher. This means that in different seasons the layer of the composite membrane which is contact with the humid flow changes. Change in the orientation of the membrane is likely to influence the permeability of the membrane, although, it is mostly neglected in permeability measurements of composite membranes and the membrane is only tested maintaining the same layer in contact with the feed flow throughout all experiments [41–43]. A few studies, however, have investigated the impact of membrane orientation.

Koester et al. [37] investigated the effect of sweep side humidity and membrane orientation on water vapor permeability of single-layer and composite membranes. They revealed that for membranes with a concentration dependent permeability, membrane orientation can significantly affect the permeability. In contrast, for membranes with concentration independent permeability, the orientation of the membrane does not change the permeability. They speculated that the possible cause for the concentration dependent behavior of permeability might be the pressure loss in the substrate layer; however, they did not perform extra experiments to prove this supposition. Additionally, their results showed that the permeability of single-layer and composite membranes can be significantly affected by the humidity of the sweep flow. They showed that the permeability can increase, decrease, or be unaffected by changes in the sweep flow humidity. In a more recent study, Engarnevis et al. [32] developed a model that predicts the permeability of composite membranes at different temperature and water vapor activities. They used solution-diffusion model for the mass transfer in the dense coating layer and the dusty gas model for the flux in the substrate layer. The results of their model showed that permeability of the composite membrane was a function of the water vapor activity at both sides of the membrane, which results in different permeabilities even at different locations in a single energy exchanger. Additionally, they revealed that the orientation of the composite membranes with concentration dependent coating layer can significantly change the permeability of the membrane, and this can increase or decrease the latent effectiveness of the energy exchanger depending on the operating conditions. They speculated that this orientation dependence of permeability is due to the existence of a substrate layer; however, they did not verify this idea.

Other studies have investigated the effects of substrate layer on the permeability of composite membrane, including the effect of pore size, porosity and roughness of the support layer on the permeation properties of the composite membrane [44,45], the effect of support layer on

concentration inhomogeneities in the dense coating layer [46] and the effect of substrate mass transfer resistance on the permeation properties of the composite membrane [41], but a study of the role of substrate layer in the orientation dependence of the permeability of composite membranes has not been conducted previously.

In this study, the permeability of two asymmetric composite membranes is measured at various combinations of feed and sweep activities and at different temperatures. Additionally, the effect of membrane orientation on the permeability of the composite membranes is investigated by repeating the tests for membranes with both substrate-on-feed and substrate-on-sweep orientations. A new method for presentation of permeability at different operating conditions is proposed and is compared with the conventional method for presentation of permeability. Finally, using the proposed method, the orientation dependence of the permeability of composite membranes and the effect of sweep flow activity are explained.

2.2 Background

2.2.1 Mass Flux Through the Membrane

Considering the asymmetric nature of the composite membranes investigated in this study, there are two possible configurations for the membrane when it is placed between the two flows, feed stream which is the flow with higher water vapor concentration flowing on the coating side of the membrane (Coating-on-Feed) or sweep stream which is the dry flow or the flow with lower water vapor concentration flowing on the coating side of the membrane (Coating-on-Sweep). The two possible configurations are shown in Figure 2.1. In the figure, subscripts b, in and out refer to bulk, inlet and outlet flows, superscripts f and s refer to feed and sweep sides and ω denotes the humidity ratio.

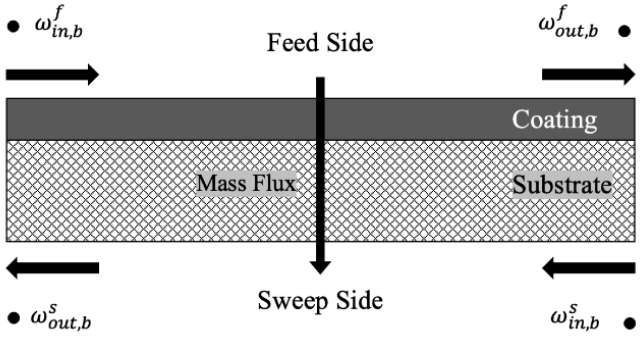

a)

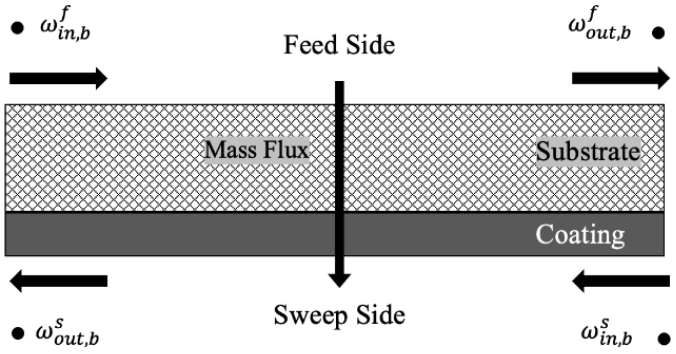

b)

Figure 2.1) Membrane configuration: a) Coating-on-Feed, b) Coating-on-Sweep

In both orientations of the membrane, the water vapor flux through the membrane is from the feed side to the sweep side.

2.2.2 Resistance in Series Model

The water vapor permeation from the feed flow to the sweep flow through the membrane occurs in following steps:

- Diffusion of water vapor in the feed flow to the surface of the membrane.
- Permeation of water vapor into the surface of the substrate or coating layer (depending on the orientation of the membrane).
- Transportation of water vapor through the coating or substrate layer to the intersection between the two layers.
- Permeation of water vapor through the next layer (coating or substrate depending on the orientation of the membrane).
- Permeation of water vapor from the membrane surface to the air.
- Diffusion of water vapor in the sweep bulk flow.

The mathematical investigation of the above process can be done using the diffusivity and permeability of the water vapor in air streams and the membrane, but the so-called resistance-in-series model has been shown to make the mass flux calculations much easier [32,47].

The resistance-in-series model states that, the resistance of different media (coating layer, substrate layer, air streams) to the transport of the water vapor can be added to each other and the mass transfer in the system can be calculated using the concentration of the water vapor at the feed and sweep bulk flows and total resistance between the two sides. Using this model, the humidity distribution for both membrane orientations can be presented as shown in Figure 2.2.

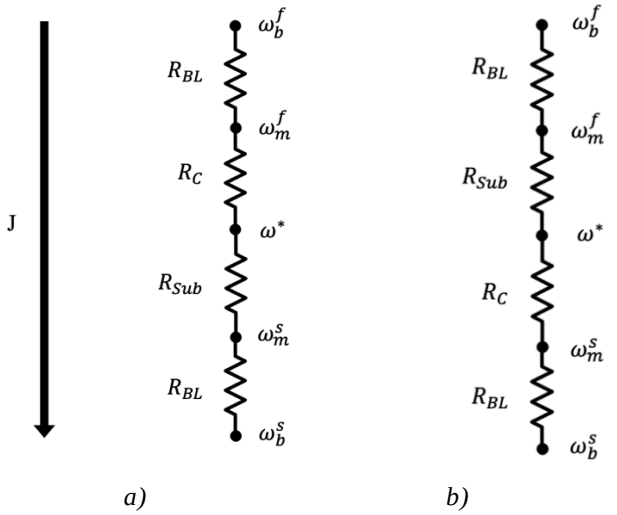

Figure 2.2) The presentation of the humidity distribution using the resistance-in-series model: a) Coating-on-Feed, b) Coating-on-Sweep

In the figure, R_{BL} denotes the boundary layer resistance in the feed and sweep flows (which is the resistance of the bulk flow to the flux of water vapor from the flow to the surface of the membrane), R_C is the coating layer resistance and R_{Sub} is the substrate layer resistance. It is shown in the next section that, the resistance of the boundary layer in the test cell is a function of temperature, flowrate, size of the channels and the properties of the fluid. Since this study the structure of the channels of the feed and sweep sides are the same, the same fluid is used in both sides, the flowrate of the feed and sweep streams are equal and tests are done in isothermal chambers, the boundary layer resistance to the water vapor flux is the same for both feed and sweep flows.

In terms of the resistance-in-series model, the main purpose of the moisture permeation measurements is finding the resistance of the asymmetric composite membranes ($R_{mem} = R_C + R_{Sub}$). The resistance of the substrate layers of the membranes used in this study do not significantly change with the water vapor concentration and temperature. Additionally, the boundary layer resistance is mainly a function of the structure of the channels and temperature and can be measured separately. This makes the resistance of the coating layer the only unknown resistance in the series of resistances.

2.2.3 Boundary Layer Resistance

Different methods have been used to measure the boundary layer resistance in studies using a moisture transfer test cells similar to the test cell used in this study [22,47–50]. The method used in this study was introduced by Metz et al. [49] and has been used frequently in other studies in recent years [32,47]. In this method, single-layer membranes with various thicknesses are tested in the test module under the same operating conditions and the total resistance of the test cell to the water vapor transport is measured. The total resistance is then plotted vs the thickness of the membrane and a linear curve is fitted to the results, the intercept of which then gives an estimate of the total boundary layer resistances in the test cell (feed side+ sweep side). To measure the boundary layer resistance of the moisture transfer test cell in this study, layers of Celgard® 2500 monolayer membrane are stacked together to create membranes with a thickness of 25 µm, 50 µm, 75 µm and 100 µm. Each membrane is tested at 30 °C and 50 °C with a feed inlet relative humidity of 50% and a dry sweep with flowrates ranging from 5 to 8 SLPM. The boundary layer resistance of the test cell at different temperatures and flowrates is then calculated by plotting the total resistance against the membrane thickness for each case. In order to be able to calculate the boundary layer resistance at various temperatures and flowrates, a model is also developed using the results of the experiments. Sherwood correlations that follow the following form can be used to estimate the mass transfer resistance in channels and ducts [48,51].

$$Sh = aRe^{b}Sc^{c}\left(\frac{d_h}{L}\right)^{d} \quad (1)$$

In the above equation, Sh, Re, Sc, d_h and L denote Sherwood number, Reynolds number, Schmidt number, hydraulic diameter and channel length, respectively. Also, a, b, c and d are coefficients specific to the test cell and can be determined experimentally.

Sherwood number is defined by the following equation, where k is the mass transfer coefficient, d_h is the hydraulic diameter of the channel and D_{wv} is the diffusivity of water vapor in the air.

$$Sh = \frac{kd_h}{D_{wv}} \quad (2)$$

The Reynolds number is given by equation (3), where ρ is the density of the humid air, μ is the viscosity of the humid air and v and d_h denote the velocity of the air in the channel and hydraulic diameter of the channel, respectively.

$$Re = \frac{\rho v d_h}{\mu} \quad (3)$$

The velocity and hydraulic diameter are calculated using equations (4) and (5):

$$v = \frac{Q}{A_c} \tag{4}$$

$$d_h = \frac{4A_c}{Per} \tag{5}$$

In the above equations, A_c denotes the cross-sectional area of the channels, Per is the perimeter of the channels and Q is the volumetric flow.

Schmidt number can also be calculated using the following equation:

$$Sc = \frac{\rho\mu}{D_{wv}} \tag{6}$$

Schmidt number is a characteristic of the flow and hardly changes in the range of temperatures and water vapor concentrations of the tests done in this study. Furthermore, the $\left(\frac{d_h}{L}\right)$ value is constant for all the tests as the structure of the test cell does not change. As a result, equation (1) can be reduced to:

$$Sh = a\ Re^b \tag{7}$$

Where, $a = a\mathrm{Sc}^{\mathrm{c}} \left(\frac{d_h}{L}\right)^d$ in equation (1).

By fitting equation (7) to the measured boundary layer resistances, the values of a and b are found to be 0.07636 and 0.604, respectively. Details of the boundary layer resistance measurement and modelling are explained in Appendix A.

2.2.4 Resistance of the Substrate Layer

In microporous membranes, the so-called Pore-Flow mechanism is the main mechanism responsible for the transport of the water vapor between the two sides of the membrane [52,53]. In the Pore-Flow model, the properties of the pores of the membrane such as porosity and pore diameter have a more significant effect on the mass transfer resistance of the membrane than the properties of the material itself [53,54]. As a result, it can be assumed that the effect of the temperature and humidity on the transport properties of the microporous substrate layers used in this study are less significant compared to the permeability variations of the dense coating layers in which the solution-diffusion mechanism is responsible for the transport of water vapor. In order to further investigate changes in the permeability of the substrate layer with water vapor

concentration and temperature, the so-called dusty gas model is also used to calculate the permeability. The details of the model are explained in Appendix B.

Using the permeability of the substrate and the ideal gas law, it is possible to calculate the resistance of the substrate layer:

$$R_{sub} = \frac{t_{sub}}{Permeability_{sub} R_u T} \quad (8)$$

In the above equation, R_{sub} is the substrate water vapor resistance, R_u is the universal gas constant and $Permeability_{sub}$ is the permeability of the substrate layer.

2.2.5 Flux Calculations

The average water vapor flux through the membrane can be calculated from the humidity ratios of the inlets and outlets of the feed and sweep sides. Using the feed side humidity ratios:

$$J = \frac{\dot{m}_{dry\,air} \left(\omega^f_{in,b} - \omega^f_{out,b}\right)}{A_{eff}} \quad (9)$$

Where, J is the water vapor flux through the membrane, $\omega^f_{in,b}$ and $\omega^f_{out,b}$ are the humidity ratios of the bulk flow at the feed inlet and outlet measured by S1 and S2, respectively, and A_{eff} is the effective membrane area.

Using the sweep side humidity measurements:

$$J = \frac{\dot{m}_{dry\,air} \left(\omega^s_{out,b} - \omega^s_{in,b}\right)}{A_{eff}} \quad (10)$$

In the above equation, $\omega^s_{out,b}$ denotes the humidity ratio at the sweep outlet measured by the hygrometer or S4, and $\omega^s_{in,b}$ is the humidity ratio measured by S3.

If the sweep flow is dry, equation (10) becomes:

$$J = \frac{\dot{m}_{dry\,air}\, \omega^s_{out,b}}{A_{eff}} \quad (11)$$

2.2.6 Membrane and Coating Resistance and Permeability

Now that the average water vapor flux through the membrane and the resistances of the boundary layers and substrate layer are calculated, it is possible to calculate the average permeability and water vapor resistance of the composite membrane and the coating layer.

The total resistance of the test cell to the water vapor flux can be defined as:

$$R_{total} = \frac{\Delta\omega_{LMD}\ \rho_{air}}{J} \tag{12}$$

Here, $\Delta\omega_{LMD}$ is the logarithmic mean humidity ratio given as

$$\Delta\omega_{LMD} = \frac{\left(\omega^{f}_{in,b} - \omega^{s}_{out,b}\right) - \left(\omega^{f}_{out,b} - \omega^{s}_{in,b}\right)}{ln\left(\frac{\left(\omega^{f}_{in,b} - \omega^{s}_{out,b}\right)}{\left(\omega^{f}_{out,b} - \omega^{s}_{in,b}\right)}\right)} \tag{13}$$

Now, based on the resistance-in-series model:

$$R_{mem} = R_{total} - 2R_{BL} \tag{14}$$

$$R_c = R_{mem} - R_{sub} \tag{15}$$

Where, R_{BL} is the boundary layer resistance of the feed or sweep side, R_{mem} is the resistance of the membrane and R_c is the resistance of the coating layer.

Finally, the permeability and permeance of the membrane and coating layer can be calculated from the following equations:

$$Permeability_c = \frac{t_c}{R_c R_u T} \tag{16}$$

$$Permeability_{mem} = \frac{t_{mem}}{R_{mem} R_u T} \tag{17}$$

$$Permeance_c = \frac{Permeability_c}{t_c} \tag{18}$$

$$Permeance_{mem} = \frac{Permeability_{mem}}{t_{mem}} \quad (19)$$

Where, the subscripts c and m refer to the coating and membrane, respectively.

2.2.7 Mean RH of the Coating Layer

As the mass flux between the feed and sweep sides is not high compared to the amount of the water vapor in the flows, the humidity ratio of the flow does not significantly change after passing over the membrane. Considering this low difference between the humidity ratio at the inlet and outlet of each flow, the following equations can be used for estimating the average humidity ratio of the feed and sweep bulk flows:

$$\omega^{f}_{mean,b} = \frac{\omega^{f}_{in,b} + \omega^{f}_{out,b}}{2} \quad (20)$$

$$\omega^{s}_{mean,b} = \frac{\omega^{s}_{in,b} + \omega^{s}_{out,b}}{2} \quad (21)$$

Using the calculated water vapor flux through the membrane and the resistance of the bulk flow (boundary layer) for water vapor at the feed and sweep sides it is possible to estimate the average humidity ratio on the surface of the membrane at the feed and sweep sides, $\omega^{f}_{mean,m}$ and $\omega^{s}_{mean,m}$, respectively.

$$\omega^{f}_{mean,m} = \omega^{f}_{mean,b} - \frac{R_{BL} \cdot J}{\rho_{air}} \quad (22)$$

$$\omega^{s}_{mean,m} = \omega^{s}_{mean,b} + \frac{R_{BL} \cdot J}{\rho_{air}} \quad (23)$$

Having the moisture ratio on the surface of the membrane and the resistance of the substrate layer, it is also possible to calculate the average moisture ratio at the intersection of the coating and

substrate layer (ω^*_{mean}). The location of the abovementioned values for the coating-on-feed scenario are shown in Figure 2.3.

For coating-on-feed scenario:

$$\omega^*_{mean} = \omega^s_{mean,m} + \frac{R_{sub} \cdot J}{\rho_{air}} \quad (24)$$

And for coating-on-sweep scenario:

$$\omega^*_{mean} = \omega^f_{mean,m} - \frac{R_{sub} \cdot J}{\rho_{air}} \quad (25)$$

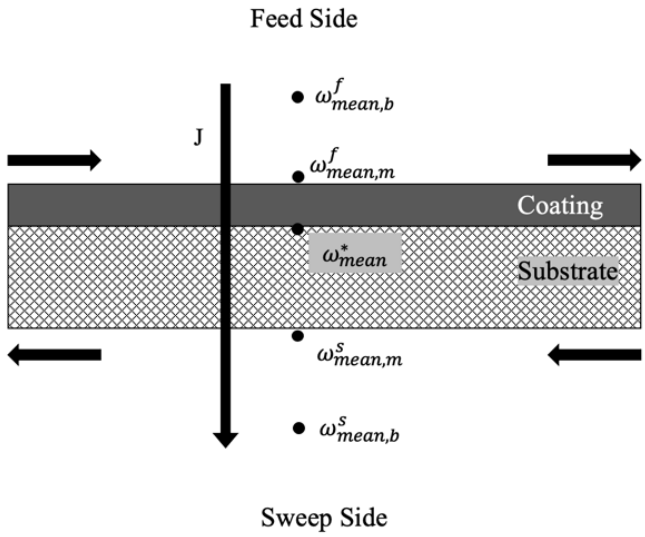

Figure 2.3) Humidity distribution in the test cell

The average humidity ratio at the two sides of the coating can then be calculated using the following equations:

For coating-on-feed:

$$\omega_{mean,c} = \frac{\omega^f_{mean,m} + \omega^*_{mean}}{2} \quad (26)$$

For coating-on-sweep:

$$\omega_{mean,c} = \frac{\omega^{s}_{mean,m} + \omega^{*}_{mean}}{2} \quad (27)$$

Using the test temperature, the average humidity ratio can be converted to activity:

$$activity_{mean,c} = \frac{\omega_{mean,c} P}{(0.622 + \omega_{mean,c}) p_g} \quad (28)$$

Where P is the atmospheric pressure, and p_g is the saturation vapor pressure at the test temperature.

Finally, it should be noted that the calculated water vapor concentration on the surface of the membrane are in the air and not in the membrane. In order to calculate the water vapor concentration in the membrane at the contact surface of the membrane and the air the solubility of the membrane is required.

$$Concentration = S \times p_v \quad (29)$$

Where S is the solubility of the membrane for water vapor and p_v is the partial pressure of the water vapor in the air adjacent to the membrane surface. In this study, the average activity and humidity ratio of the coating is calculated using the humidity values in the air for simplicity.

2.3 Materials

Two widely used asymmetric composite membranes with high water vapor permeability known with commercial names of "T4 (also known as MX4)" and "HP2", purchased from CORE energy recovery solutions, are investigated in this study [24,55]. Table 1 provides a summary of the materials used in the membranes provided by the supplier. Both membranes are made up of a thin coating layer with high permeability and selectivity for water vapor and a microporous substrate layer which provides mechanical stability to the thin coating layer.

Table 2.1) Properties of the T4 and HP2 composite membranes

Membrane	Coating Material	Substrate Material	Thickness (μm)
T4 (MX4)	Polyethylene Oxide-Polyurethane (PEO-PU)	Silica-Polyethylene	100-110
HP2	Blend of SPEEK and CA	Polypropylene	20-30

In order to calculate the variable permeability of the coating layer for each membrane the permeability of the substrate layer is required. Table 2 summarizes the permeability of the substrate layers of the T4 and HP2 membranes reported by the supplier.

Table 2.2) The water vapor permeability of the T4 and HP2 substrates

Substrate Material	Permeability (Barrer)
Silica-Polyethylene	2053590
Polypropylene	776583

2.4 Experimental Setup

Various methods for permeability measurements of membranes can be found in the literature [49,56–58] . In this study, a moisture permeation test apparatus is used to measure the permeability of the composite membranes under different operating conditions. This apparatus is proposed in ASTM F2298 [59] and has been used in several other studies in the literature [32,47,60]. The water vapor transport rate (WVTR) testing method is then used to measure the permeability of the membrane samples [1,47]. In this method, two air streams with different water vapor concentrations flow over the membrane. Due to the water vapor gradient across the membrane, water vapor permeates through the membrane from the high concentration side (feed) to the low concentration side (sweep). Finally, using the water vapor concentrations at the inlets and outlets of the test cell, it is possible to calculate the permeability of the membrane.

As mentioned earlier, unlike most of the studies in the literature that have used dry air as the sweep flow, in this study, the concentration of the water vapor in the sweep flow is changed similar to the feed flow to enable measuring the permeability at different combinations of the feed and sweep water vapor concentrations.

2.4.1 Test Apparatus

The schematic of the test apparatus is shown in Figure 2.4. Room air is pumped into the system using a compressor and is filtered using a HEPA capsule filter #1602051 before entering the system. The main air stream is split into two branches; one stream enters the first moisture exchanger and the other one passes through a polycarbonate DRIERITE dehumidifier. In order to lower the risk of the presence of the water droplets in the air stream, a two-step humidification process is used to control the humidity of the air stream in the feed and sweep sides. dPoint Px1-32 humidifiers are used as the moisture exchangers (EXG 1&2). The first branch of the main air stream with a flow rate of 30 LPM and hot water with a flowrate of 3.2 LPM enter the first exchanger (EXG1). The temperature of the water is controlled using a StableTemp model WB10 water bath and a RIDGID model AC11301 submersible pump circulates the water in the exchanger. Air entering EXG1 becomes humid and leaves the exchanger at a saturated state. This saturated air is then used to humidify the feed and sweep air streams. The second branch of the main air stream (dry air) is divided into two separate streams to be used as the feed and sweep flows and mass flow controllers MFC1 and MFC2 (Alicat Scientific MCS) control the flowrate of the feed and sweep air streams, respectively. Due to the size of the test cell and to decrease the uncertainty of the final measured permeability, a flowrate of 6 SLPM is chosen for the feed and sweep sides. After the mass flow controllers (for both feed and sweep sides), air stream is split into two branches; one air stream passes through EXG2 (EXG3 for the sweep side) in which it becomes humid, and the other stream remains dry. These two air streams are then mixed to produce the air stream with the desired humidity. The humidity of the final flow is manually controlled by changing the ratio of the humid and dry flows via gate valves. The humidity and temperature of the feed and sweep inlets and outlets are dynamically measured using 4 TE HTM2500LF polymer RH and temperature sensors (S1-S4). In order to increase the accuracy of the measurements, a dew-point hygrometer (EdgeTech DewMaster S2SCPT) also measures the humidity and temperature of the sweep outlet. This hygrometer is also used to calibrate the polymeric humidity sensors. The calibration process and the uncertainty of the sensors are further discussed in Appendix C. In order to eliminate the effect of temperature difference between the flows and to control the temperature of the tests, the exchangers, RH sensors, hygrometer and the moisture transfer test module are placed in a temperature-controlled chamber (MT Model OF-22GW for 35°C and 50°C tests and ESPEC BTZ-133 for 5°C tests).

Overall, the design of the moisture permeation test apparatus enables creating feed and sweep flows with an activity of 0-0.95 in the temperature range of 5-70 °C.

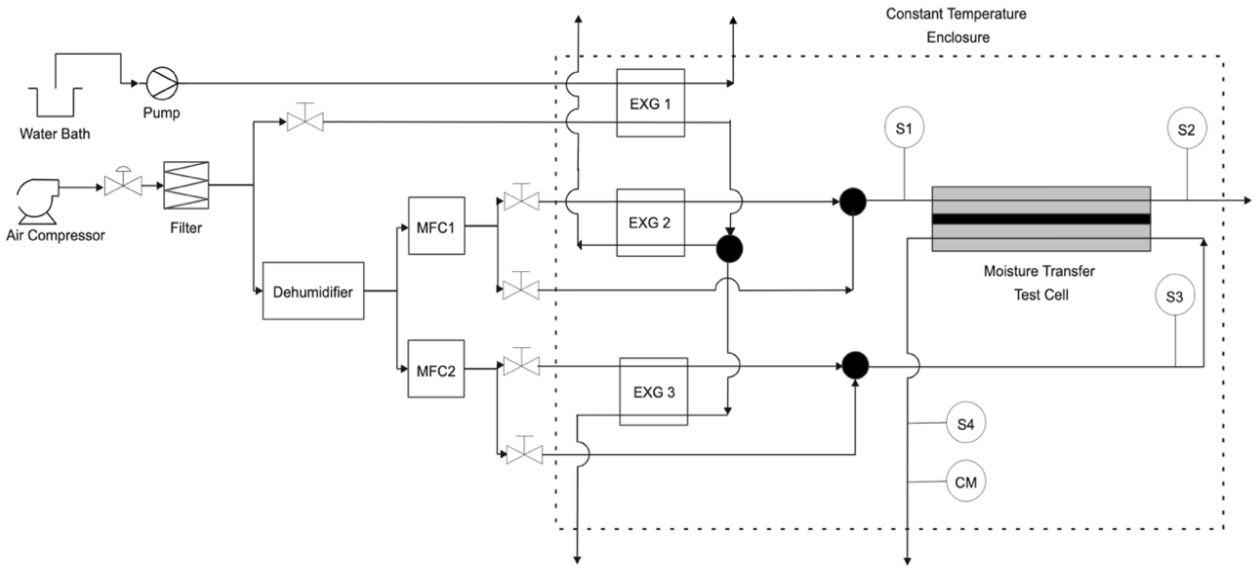

Figure 2.4) Schematic of the test apparatus

2.4.2 Moisture Transfer Test Cell

The moisture transfer test cell used in this study is similar to the test cell used in [47,61]. The schematic of the test cell is shown in Figure 2.5. Flow tubes are connected to the test cell through 4 push-to-connect elbow connectors in a counter flow arrangement. On each side of the test cell, air flows through seven channels with a depth of 1.5mm, width of 3mm and length of 17cm. Rectangular membrane samples (18 cm $\times$ 5 cm) are placed between the two pieces of the test cell and the module is sealed by applying pressure to both sides. The effective membrane area that participates in the moisture transfer process is 45.6 cm^2 [47].

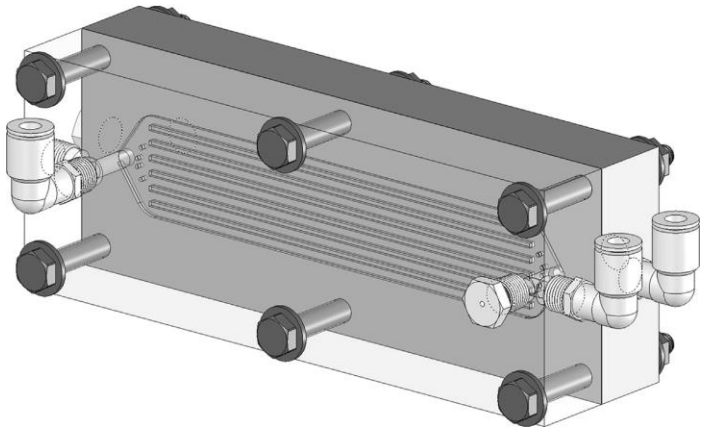

Figure 2.5) Moisture transfer test cell [47,61]

2.5 Results and Discussion

2.5.1 The Effect of RH and Temperature

Permeability is typically presented as a function of the water vapor activity of the feed flow [38]. Following this convention, the permeability of the T4 and HP2 membranes with a coating-on-feed orientation is shown in Figure 2.6. The measurements are performed at 3 different temperatures of 5°C, 35 °C and 50 °C with a dry sweep and feed inlet activities ranging from 0.20 to 0.95. Each measurement was repeated at least 3 times and a repeatability error of less than 5% is measured for the permeability values. Error bars are the standard deviations of the measured permeability values.

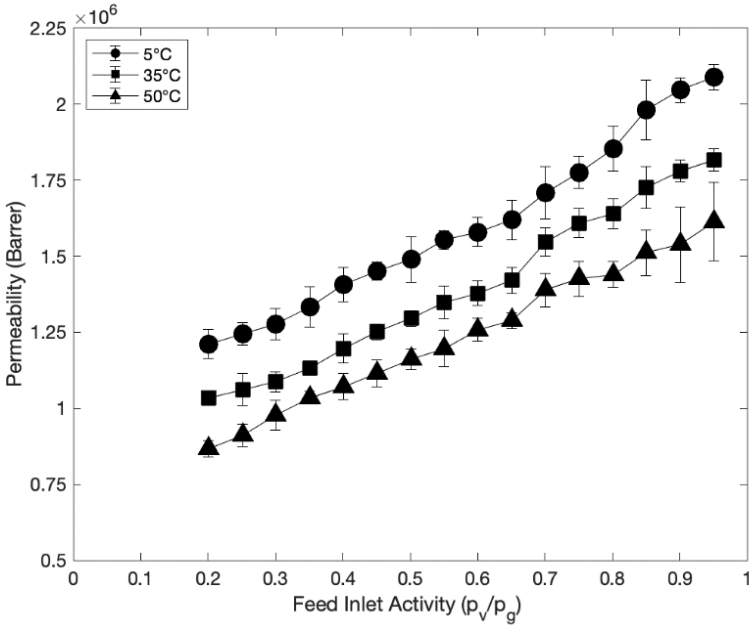

a) T4

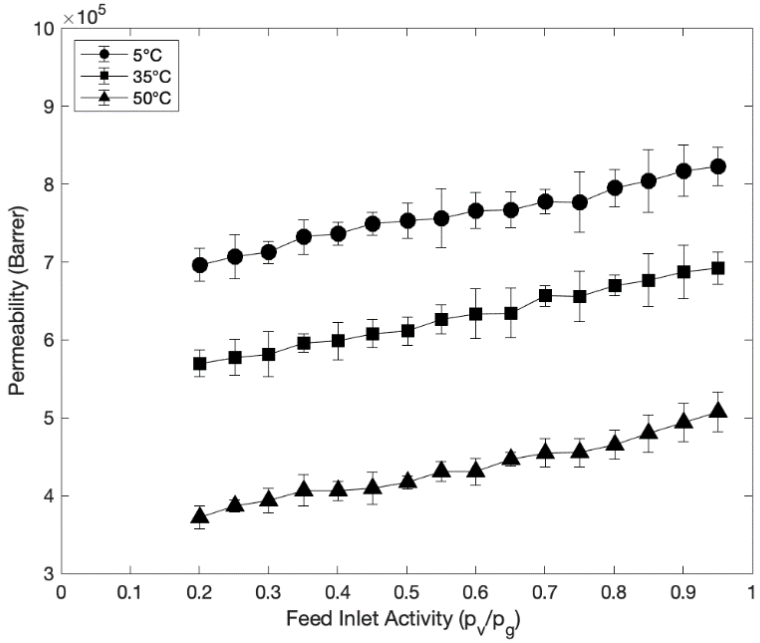

b) HP2

Figure 2.6) The effect of temperature and humidity on permeability

For both T4 and HP2 membranes, permeability increases with increasing feed flow water vapor activity. Increasing temperature decreases the permeability significantly for HP2 but only slightly for T4. Furthermore, the permeability of the T4 membrane changes more notably with humidity compared to HP2 membrane. This humidity dependent behavior has been observed in another study investigating a membrane similar to the T4 membrane [37] However, no studies reporting on the humidity or temperature dependence of the HP2 membrane are available in the open literature. Although the same composite membranes are not extensively studied in the literature, the observed behavior is in agreement with the results of studies that have investigated membranes made up of similar dense coating polymers. The observed behavior for the T4 membrane is compatible with the results of studies investigating membranes made up of PU-PEO polymers [1,23] or other PEO based polymers [62]. Studies investigating membranes with blends of SPEEK and CA are rare in the literature; however, similar dependence of permeability on activity and temperature has been observed in studies that have investigated SPEEK and CA alone or mixed with other polymers [18,63–65].

2.5.2 The Effect of Orientation

In order to investigate the effect of membrane orientation on the permeability, membranes are tested with a coating-on-sweep orientation with feed flow activities ranging from 0.20 to 0.95 and a dry sweep. Each measurement is repeated 3 times and a repeatability error of less than 5% is

calculated for the measured permeability values. The permeability of the membranes for both coating-on-feed and coating-on-sweep orientations at 5°C, 35°C and 50°C is shown in Figure 2.7.

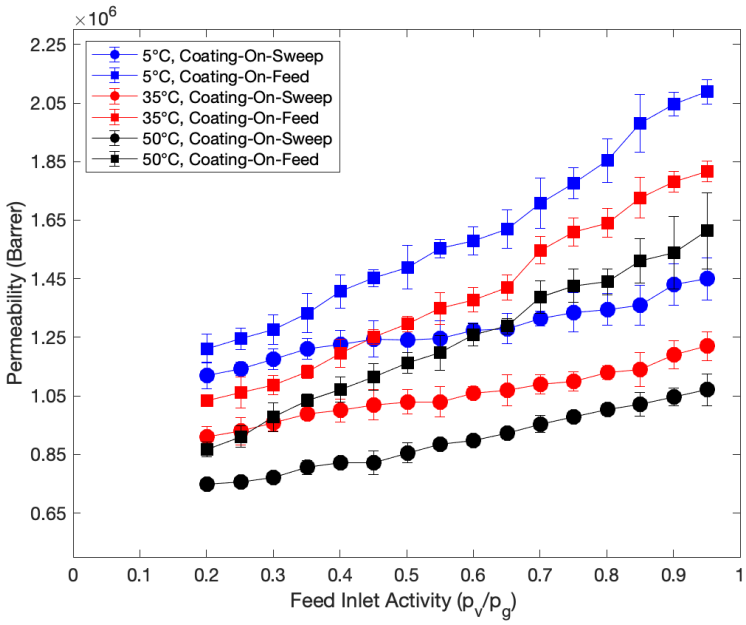

a) T4

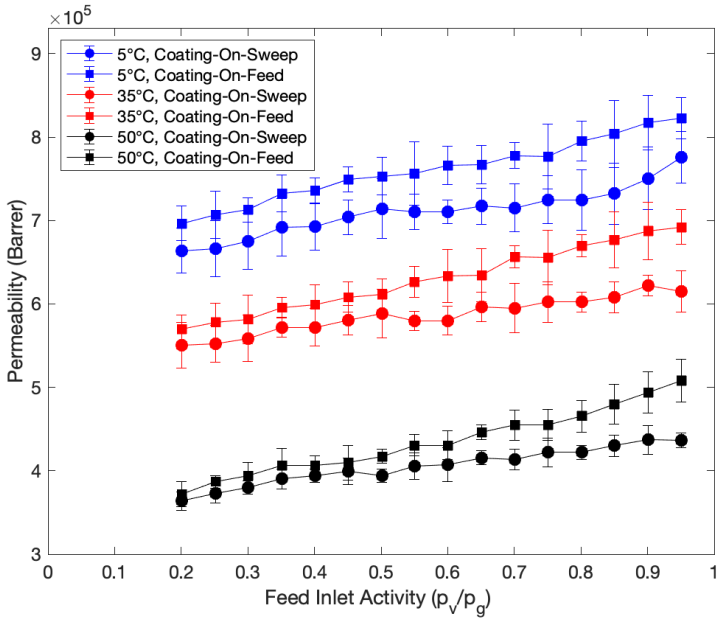

b) HP2

Figure 2.7) The effect of membrane orientation on the permeability of membranes

As is shown in Figure 2.7a, changing the orientation of the T4 membrane from coating-on-feed to coating-on-sweep decreases the permeability of the membrane, at all temperatures studied. This

behavior is similar to the behavior observed in [37] for a membrane similar to the T4 membrane used in this study. The decrease in permeability is larger at higher activities.

The HP2 membrane behaves in a qualitatively similar manor to the T4 membrane (Figure 2.7b): the permeability likewise decreases as the membrane orientation is switched from coating-on-feed to coating-on-sweep. As for the T4 membrane, the change in permeability increases with increasing activity.

In order to explain this orientation-dependent behavior of the membranes, it is essential to investigate the behavior of the dense polymer coating layer and the microporous substrate layer comprising them.

The permeation properties of many types of polymers, including the dense polymers of the membranes studied in this paper, have been shown to be significantly affected by the water vapor concentration of the polymer adjacent flows [18,51,62,66]. This stems from the fact that the sorption of the polymers can be directly affected by the humidity of the flow at the surface of the membrane and the concentration of water vapor in the polymer can influence the diffusivity.

Additionally, as explained earlier, it is reasonable to assume the permeability of the microporous substrate layers of the T4 and HP2 membranes to be independent of the operating conditions. Figure 2.8 shows the effect of temperature and activity on the permeability of the substrate layers computed using the method explained in Appendix B beside the measured membrane permeability. As is indicated in the figure, the effect of temperature and humidity on the permeability of the substrate layer is negligible compared to the effect on the membrane permeability. As a result, the variations in the permeability of the membranes are mainly due to the permeability variations of the dense coating layer.

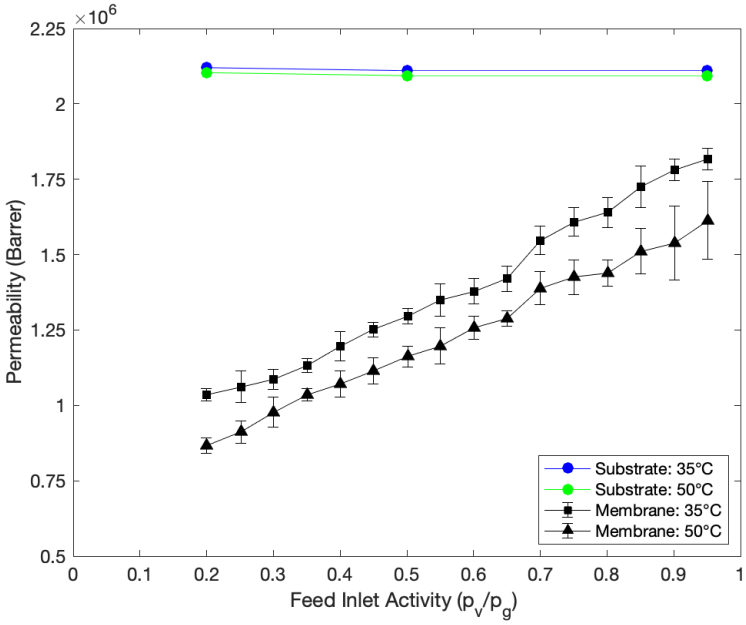

a) T4

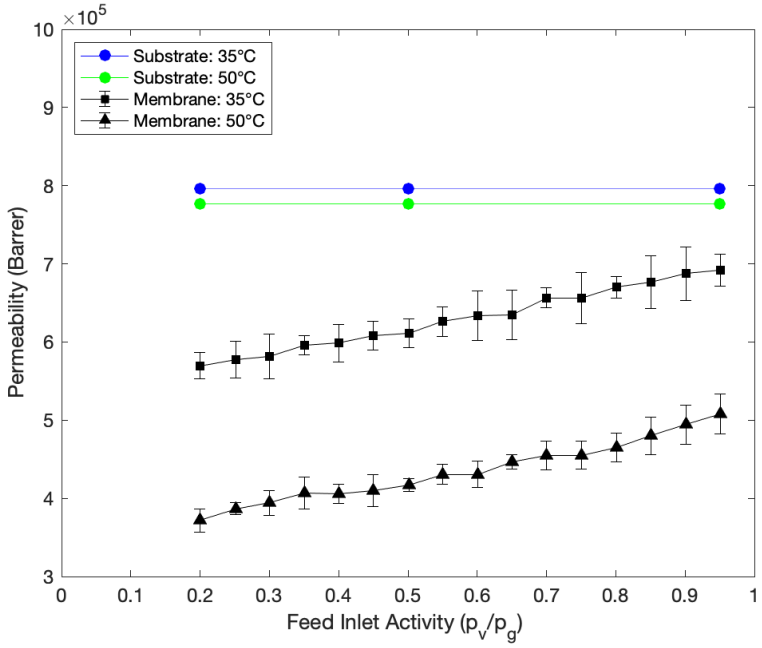

b) HP2

Figure 2.8. The effect of temperature and humidity on the substrate permeability

Subtracting the mass transfer resistance of the substrate layer from the resistance of the membrane, it is possible to calculate the permeability of the dense coating layer. Figure 2.9 indicates the calculated permeability of the dense coating layers of HP2 and T4 membranes at different feed inlet activities. Each measurement is repeated at least 3 times and a repeatability error of less than

10% is observed for the coating permeability values. Error bars are the standard deviations of the coating permeability values.

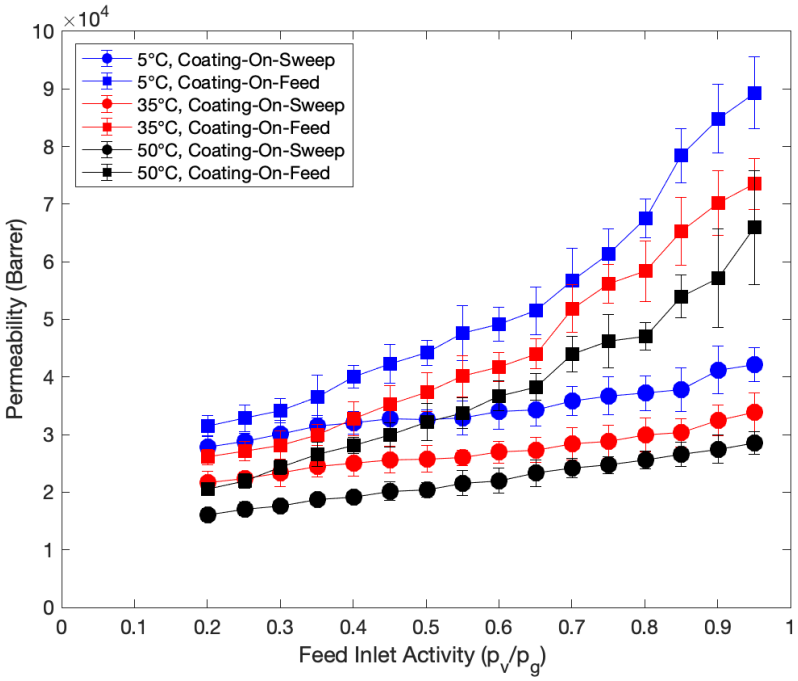

a) T4 Coating

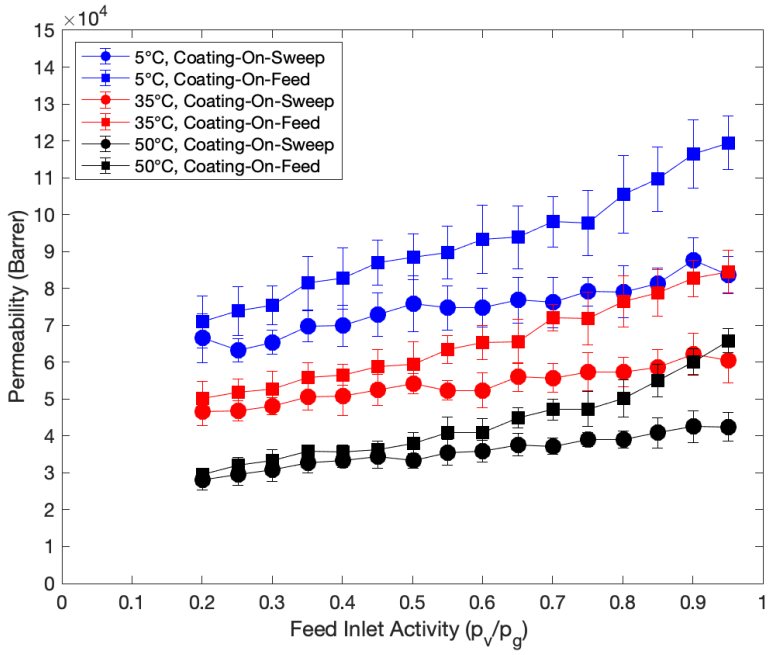

b) HP2 Coating

Figure 2.9. Permeability of the dense coating layer of T4 and HP2 membranes

Compared to the composite membranes, it can be observed that the dependence of the permeability on the activity of the flow is more significant for the dense coating layers. This is reasonable considering the fact that in the composite membrane, the impact of the permeability variation of the coating layer is diminished due to the existence of a substrate layer with relatively constant permeability. Finally, as expected, the permeability of the coating layer decreases when the orientation of the membrane changes from coating-on-feed to coating-on-sweep. This effect is caused by the lower humidity experienced by the coating layer when the coating layer is exposed to the sweep flow (the sweep is dry). Similar to the composite membrane, the permeability of the coating layer of T4 considerably increases with activity while the effect of temperature is less significant, especially at lower activities. The permeability variations of the HP2 coating layer is similar to the composite membrane as well, the effect of temperature is more significant compared to the T4 coating but the effect of activity is less significant. It should be noted that although the effect of activity on permeability is not as significant as T4, it is still considerable.

Although the presentation of permeability values in Figure 2.9 reveals this dependence of permeability on the activity of the flow, it cannot fully explain the main source of this phenomenon. The permeability of the dense coating layer is affected by the activity of the flow at both sides of the membrane; however, the presentation method used in Figure 2.9 relates the permeability to the feed inlet activity while the feed side flow is not directly in contact with the coating layer in the coating-on-sweep orientation. As a result, in order to better visualize the changes in the permeability of the membranes, the average activity of the flow at the two sides of the dense polymer layer is calculated and it is our hypothesis that this average activity is the main variable responsible for the permeability variations in the dense coating layer. Figure 2.10 shows the coating permeability as a function of the mean coating activity. As shown in the figure, the measured permeability becomes independent of the membrane orientation when the results are presented against the mean activity of the flow at the two sides of the coating. This collapse of the data supports our hypothesis that the mean activity is the relevant variable (with the temperature) determining the permeability of the coating.

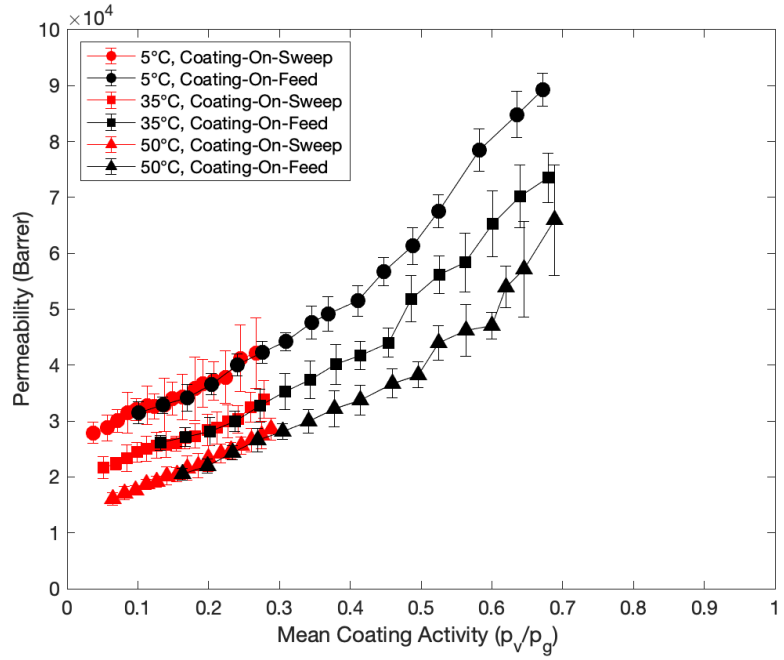

a) T4 Coating

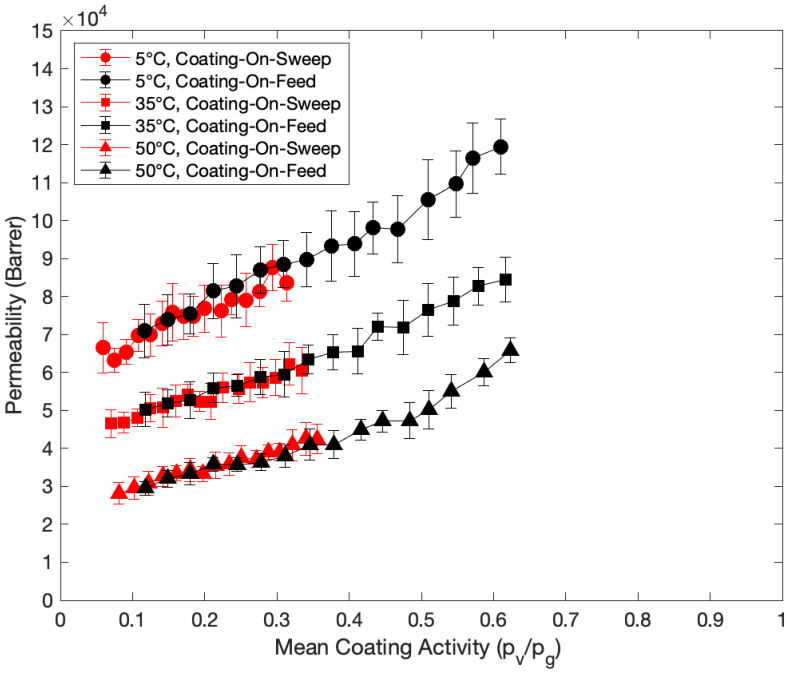

b) HP2 Coating

Figure 2.10. Permeability of the T4 and HP2 coatings as a function of the mean activity of the flow at the two sides of the coating

Following the same pattern, Figure 2.11 shows the membrane permeability of the T4 and HP2 membranes against the mean activity of the flow at the two sides of the coating layer. Similar to the coating layers, the permeability of the membranes at the coating-on-feed and coating-on-sweep orientations are equal at equal mean coating activities which makes the permeability independent of the membrane orientation.

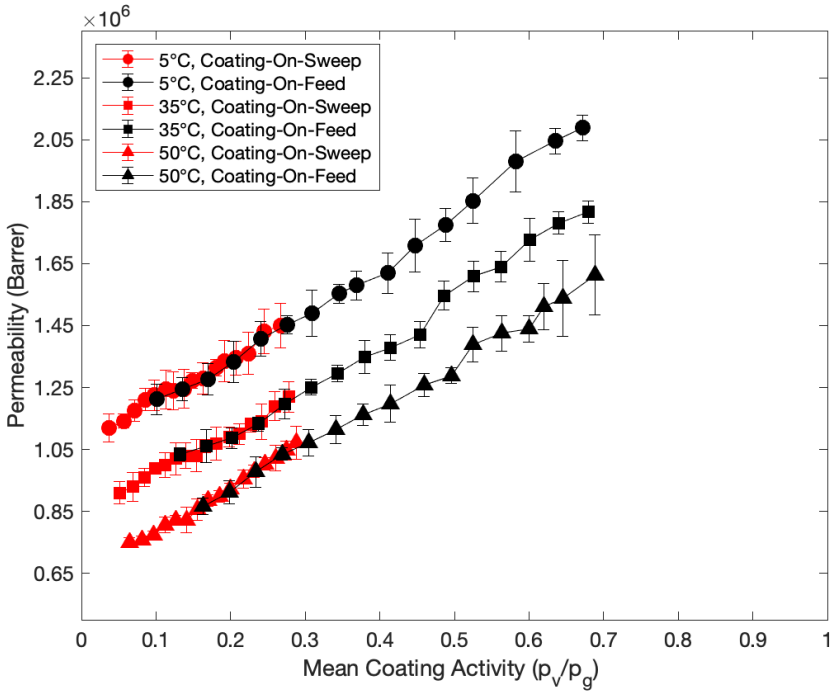

a) T4

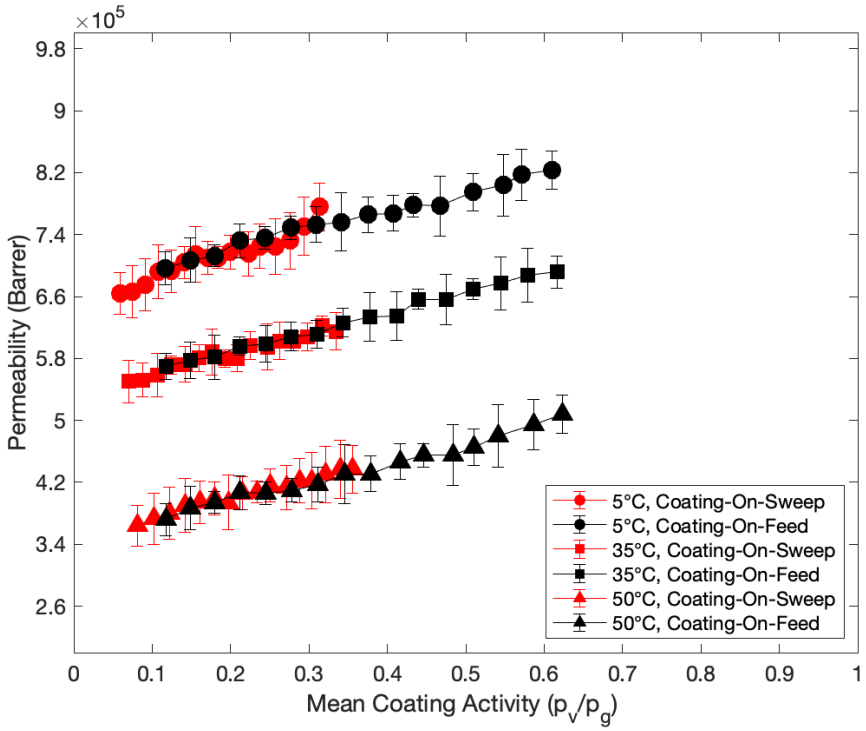

b) HP2

Figure 2.11. Permeability of the T4 and HP2 membranes as a function of the average activity of the flow at the two sides of the coating

2.5.3 The Effect of Sweep Side Humidity

One of the parameters that is often ignored in measuring and reporting the permeability of composite membranes is the effect of sweep flow humidity. Most studies that have used moisture permeation techniques to measure the permeability of composite membranes have kept the sweep flow dry, with only the humidity of the feed flow varied. However, the humidity of the sweep flow can also influence the permeability of the membrane.

In the previous section we showed that the permeability of the coating layer of a composite membrane is a direct function of the average activity of the flow at the two sides of the coating. Changing the activity of the sweep flow changes the mean activity of the flow at the coating layer in both coating-on-feed and coating-on-sweep orientations, and as a result, it can be expected that changing the sweep side humidity would affect the permeability of the composite membrane.

To test this idea, membranes are tested with a humid sweep flow. The feed inlet activity is changed from 0.60 to 0.95 while a 0.15 activity difference is maintained between the feed and sweep inlets ($0.45 < Activity^{s}_{in,b} < 0.80$). Each measurement is repeated at least 3 times and repeatability errors of less than 5% and 10% are observed for the membrane and coating permeabilities,

respectively. The permeability of the coating and the composite membranes is shown in Figure 2.12, error bars represent the standard deviation of different measurements.

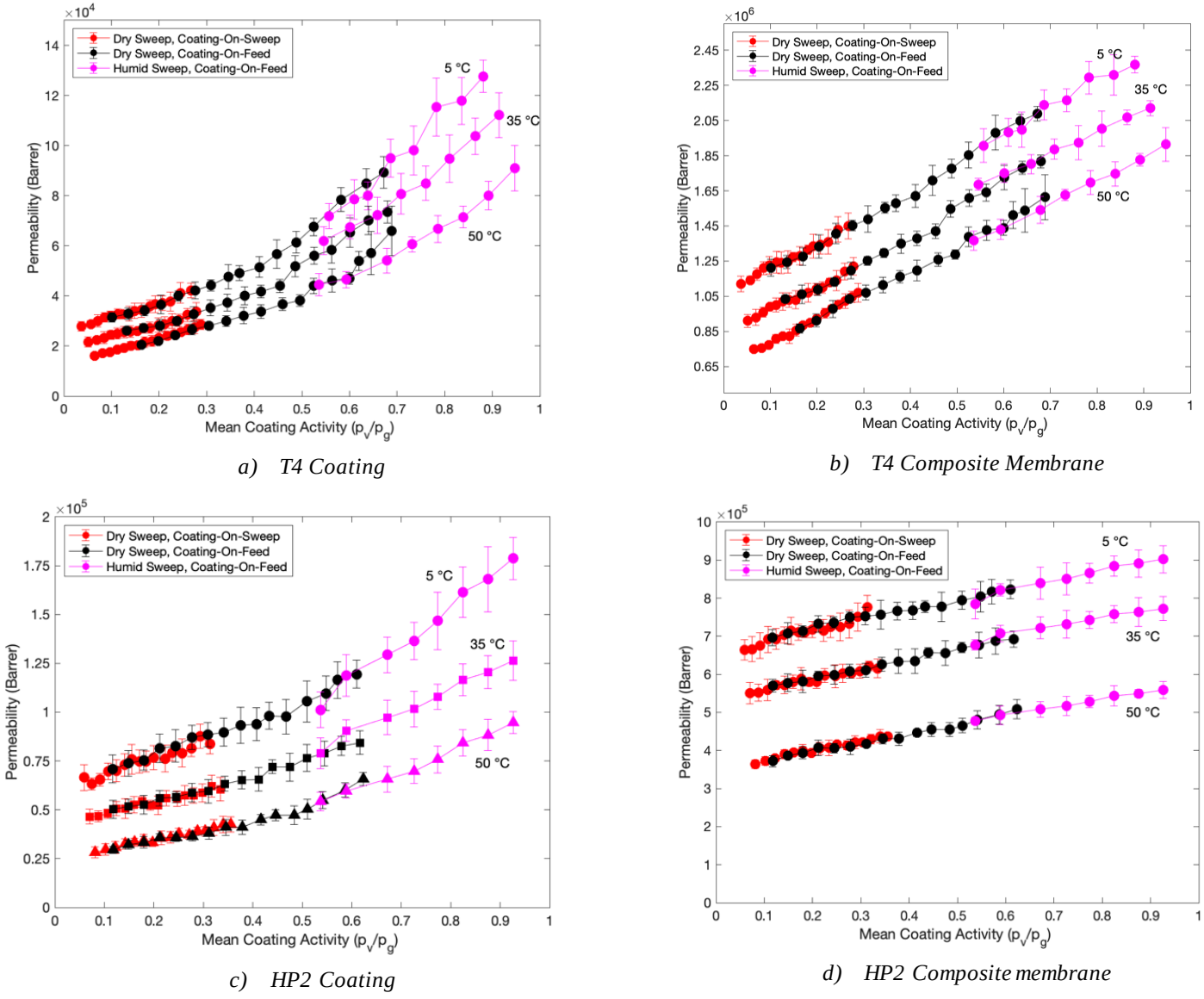

a) T4 Coating

b) T4 Composite Membrane

c) HP2 Coating

d) HP2 Composite membrane

Figure 2.12) Effect of sweep side humidity on the permeability of the coating and composite membranes

As expected, having a humid sweep flow increases the permeability of the coating and membrane for both T4 and HP2 membranes. Additionally, the overlap between the "Humid Sweep" and "Dry Sweep" graphs is evidence that the permeability of the membrane is independent of the feed flow or sweep flow activities provided that the mean activity at the coating layer is constant. However, it can be seen that the measured permeability for the T4 coating at dry sweep condition at 50°C is not completely compatible with the measured coating permeability at humid sweep. This can be

attributed to the fact that the accuracy of the measurement equipment is lower at very high temperatures and water vapor concentrations which results in a lower accuracy in measured permeability value. Finally, use of variable sweep flow humidity permits the measurement of permeability over a much wider range of activity than can be achieved with the conventional approach of maintaining a dry sweep.

2.6 Conclusion

In this study, the impact of membrane orientation and sweep flow water vapor concentration on the permeability of two commercially used asymmetric membranes ("T4 (MX4)" and "HP2") were studied through moisture permeation tests. Membranes with coating-on-feed and coating-on-sweep orientations were tested at 3 different temperatures of 5°C, 35°C and 50°C for various feed and sweep water vapor concentration combinations. It was shown that the permeability of the composite membranes and their coating layers is a function of membrane orientation when the permeability is presented as a function of feed flow inlet activity. However, plotting permeability against the mean activity at the coating layer eliminates the orientation dependence of permeability. This finding means that the concentration dependence of the permeability of the composite membranes and their coating layers is due to the variations in the mean activity of the flow at the coating layer. Furthermore, it was revealed that the humidity of the sweep flow can significantly affect the permeability of membranes. However, as was also the case with membrane orientation effects, if the permeability is plotted against the mean activity of the coating, the permeability dependence on sweep flow humidity is eliminated. Additionally, increasing mean coating activity increases the permeability of both T4 and HP2 membranes, though the impact on T4 is more significant. Increasing the membrane temperature decreases the permeability of both membranes, though the impact on HP2 is more significant. Finally, the new proposed method for presentation of permeability values showed that testing membranes with a coating-on-sweep orientation results in lower water vapor concentrations at the coating layer, as a result, it enables permeability measurements at lower water vapor concentrations. In the same manner, using humid sweep flow increases the mean water vapor concentration at the coating, so it can be used to measure the permeability at higher humidity. This is especially helpful when the results of the permeability measurements from the moisture permeation test methods are used to validate measurements from other methods. However, it should be noted that the proposed method in this study is only useful in the presentation of the data when the permeability of one or several layers of a composite membrane are concentration dependent. In the case of membranes with concentration independent layers, using the mean activity of one of the layers will not be as helpful.

Chapter 3: Experimental Investigation of Condensation in Energy Exchangers

3.1 Introduction

Although energy exchangers are useful in all weather conditions, they are more effective in extreme hot or cold climates. Using energy exchangers in cold weather conditions, however, can result in condensation and frost formation in the exchanger [67]. Frost formation in energy exchangers can decrease the sensible and latent effectiveness. Frost can also increase the pressure drop in the exchanger by partially or completely blocking the channels. This increase in pressure drop increases the fan power required to maintain the needed flowrate [16]. In a similar way, condensation can also affect the effectiveness and pressure drop in heat exchangers and decrease their energy saving capacity [68]. Additionally, condensation can accelerate the growth of fungi and other bio-organisms in the exchanger or even other equipment in the ventilation system if water is carried away by the flow [1]. This poses health risks to the occupants and could compromise the structural integrity of the building [69]. Moreover, the presence of water in the energy exchanger and the ventilation system also hastens frost formation if the temperature decreases to sub-zero temperatures. Several methods are proposed in the literature for protection against condensation and frost formation in recovery exchangers [70–75]; however, most of these methods require extra equipment and constant monitoring [76].

Although frost formation can only occur in sub-zero temperatures, condensation can occur in even mild winter conditions. Many studies have investigated the performance of air-to-air exchangers including energy exchangers, heat recovery exchangers and energy wheels in dry conditions [26,27,77–83], but studies on condensation and frost formation in such exchangers are very limited, mainly due to the required testing equipment and the long duration of the tests [16]. The structure of heat recovery exchangers is similar to energy exchangers. In energy exchangers supply and exhaust flows are separated using water vapor permeable membranes that allow the transfer of both heat and moisture between the two flows. In heat recovery exchangers, in contrast, the supply and exhaust flows are separated with plate fins made up of impermeable materials such as plastic and aluminum. As a result, in heat exchangers the supply and exhaust flows can only transfer heat and there is no moisture transfer between the two flows. Energy wheels have a completely different structure compared to heat and energy exchangers as the heat transfer media rotates between the two flows.

Han et al. [84] and Nam et al. [85] experimentally investigated the effect of condensation on the effectiveness of an heat exchanger and developed a CFD model to predict the effectiveness of the exchanger when condensation happens. Both their experiments and model showed that

condensation increases the sensible effectiveness of the supply side. Furthermore, they showed that increasing the exhaust inlet relative humidity and supply inlet temperature magnifies the changes in sensible effectiveness. Gendebien et al. [68] developed a semi-empirical model for condensation in heat exchangers and validated their model with experimental results. Their experiments showed that condensation increases the pressure drop in the exhaust side of the exchanger although as time passes the rate of increase in condensation diminishes and the heat exchanger reaches a steady state. Using their model, they also performed a parametric analysis to find the effects of operating conditions on condensation and frost formation. Their results revealed that condensation could increase the total heat transfer rate in the exchanger by 8.3% and that the share of the latent heat transfer could become even larger than sensible heat transfer at very high indoor air relative humidity. In a more recent study, Anisimov et al. [86], developed a numerical model to predict the location of condensation and frost formation in an heat exchanger and calculate the heat exchanger performance with and without condensation and frost formation. They showed that, at low exhaust inlet relative humidity, the exchanger is divided into only dry and frost regions and increasing humidity increases the ratio of the frost and dry regions. However, at higher exhaust inlet relative humidity, not all of the condensed water freezes, and the exchanger is divided into dry, condensation and frost regions. Increasing the humidity while holding other variables constant increases the area of the condensation while decreasing the dry and frost regions. Furthermore, similar to other studies, their model predicted that the sensible effectiveness of the exchanger increases with humidity. Other studies have also investigated the effects of condensation and frosting on effectiveness, frost deposition pattern and the limits of frosting in heat exchangers [71,87–91]. Although different aspects of condensation and frost formation in heat exchangers have been investigated in the literature, many of the conclusions and behaviors cannot necessarily be generalized to energy exchangers owing to the transfer of water vapor through the energy exchanger membrane.

Research on condensation and frost formation in energy exchangers is rare [16], and most of this has investigated different methods of detection of frost, limits of frosting and condensation and their effect on effectiveness and pressure drop [67,70,76,92]. Fisk et al. [70] compared frosting limits in heat exchangers and energy exchangers. They used visual observation and pressure drop measurements to reveal the occurrence of frosting in heat and energy exchangers. They noted that visual observation was faster than the pressure measurements in identifying the onset of frosting in both heat and energy exchangers. They also found that the frosting limit for the energy exchanger was lower than an equivalent heat exchanger because the transport of water vapor between the flows in an energy exchanger decreases the humidity in the exhaust air flow. In a recent study, Rafati et al. [93] investigated the methods of detection of frost formation in energy exchangers. They used 4 different methods to detect frost formation in the exchanger: visual inspection of the exchanger for frost, measurement of pressure drop over the exchanger, investigation of effectiveness of the supply and exhaust sides and the temperature distribution at

the outlet of the exchanger. Their results showed that temperature and pressure measurements are the fastest and clearest methods of detecting frosting. In their experiments, pressure drop in an exchanger with frost formation continuously increased over time. Additionally, sensible and latent effectiveness both decreased as the frost grew in the exchanger. Deshko et al. [67] developed a heat and mass transfer model that predicts the location of condensation and frost formation in energy exchangers and calculates the sensible and latent effectiveness but only validated their results with an heat exchanger; the energy exchangers model was not directly validated. Similar to the work of Anisimov et al. [86], they divide the exchanger into dry, condensation and frost formation regions and used different heat and mass transfer equations for each region. The results of their model showed that increasing the permeability of the membrane significantly decreased the condensation zone in the exchanger while the frost zone slightly increased at first but then decreased at higher permeabilities. Furthermore, their model predicted that increasing room air relative humidity increases the frost and condensation zones. Decreasing outdoor air temperature, however, slightly decreased the condensation zone portion while it significantly increased the frost zone portion. In a more recent study, Shen et al [94] investigated the occurrence of condensation in energy exchangers in summer conditions. Using their previously developed model for the dry conditions they calculated the maximum relative humidity of air at the surface of the membrane and marked the operating conditions that resulted in a surface relative humidity of 100% as the condensation limit. However, they did not validate the predictions of their model with experimental measurements. They also investigated the effect of properties of the membrane on the operating conditions that result in condensation and concluded that membranes with higher permeability decrease the chances of occurrence of condensation. Moreover, they did not investigate the effects of condensation in the exchanger on the effectiveness or the pressure drop.

Overall, the authors have not been able to find any studies on the investigation of condensation without frost formation in the energy exchangers. Many of the previous studies have studied frosting or ice formation in energy exchangers. Frosting/icing is associated with completely different physics than condensation as condensed water can permeate through the membrane or be moved by the flowing air while ice cannot be moved out of the exchanger or permeate through the membrane. Other studies have investigated condensation in heat exchangers, but heat exchangers do not have water vapor permeable membranes in their structure and thus have a completely different heat and mass transfer process. Thus, the goal of the present research is, for the first time, to investigate condensation without ice formation in energy exchangers and determine its limits, performance impacts, and phenomenology. As a result, a membrane-based energy exchanger is tested under various operating conditions and short-time and long-time effects of condensation are investigated using visual observation and effectiveness and pressure drop methods. The effects of indoor air relative humidity, temperature, and flowrate on the limits of condensation and performance of the exchanger with condensation are investigated. Finally, the results of this study

are compared with the results of other studies on condensation and frost formation in energy exchangers and heat exchangers.

3.2 Background

In an air-to-air flat plate energy exchanger, due to the temperature and moisture gradient between the flows, heat and water vapor transfer through the flat sheet membrane [32]. In winter, the temperature and moisture content of the outdoor air (hereafter called supply air) are both lower than the indoor air (hereafter called exhaust air), and as a result both heat and mass fluxes are from the exhaust air to the supply air. It should be noted that the relative humidity of the supply air might be high in winter conditions and even exceed the relative humidity of the exhaust air but because of the lower temperature, the moisture content of the supply air remains lower than the exhaust air. Figure 3.1 shows the heat and mass transfer between the flows in an energy exchanger in winter conditions. In the figure, subscripts *s* and *e* denote supply and exhaust and superscripts *b* and *m* refer to the bulk flow and surface of the membrane. The intensity of the color of each point represents the level of temperature and humidity. As is indicated in the figure, it can be assumed that the process of heat and mass transfer takes place in 3 steps: from the exhaust bulk flow to the surface of the membrane then thorough the membrane and finally from the surface of the membrane at the supply side to the supply bulk flow. The heat and mass transfer through the membrane can be assumed to be only in the vertical direction through the thickness of the membrane and the heat and mass fluxes in the direction of the width or depth of the membrane are negligible [32]. Convective flows in the passages dominate heat and mass transfer in the plane of the membranes.

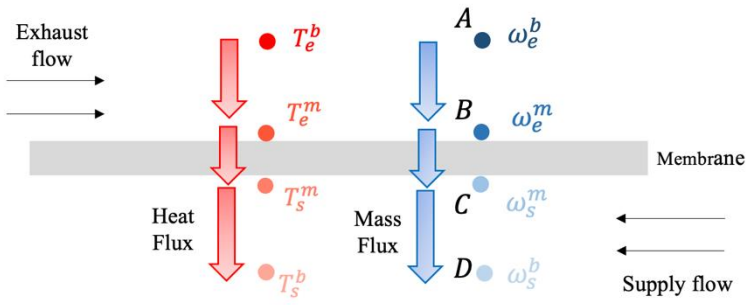

Figure 3.1) Heat and mass transfer in the energy exchanger

At the exhaust side, both temperature and moisture content at the surface of the membrane are lower compared to the bulk flow. Decreasing the temperature increases the relative humidity while decreasing the moisture content lowers the relative humidity. If the temperature at the surface of

the membrane at the exhaust side becomes equal or less than the dew point temperature of the air at the surface (i.e., relative humidity reaches 100%), water condenses on the membrane.

3.3 Methodology

3.3.1 Experimental Setup

The schematic of the experimental setup is shown in Figure 3.2. Supply and exhaust flows with desired conditions are created in two separate loops, with a fraction of the flow created in each loop passed through the exchanger to perform the tests. As shown in the figure, a fan is used in each main loop to control the flowrate (Fan 1 in the exhaust loop and Fan 2 in the supply loop). The cooling coils of an air-cooled chiller dehumidify the air and lower its temperature. Then, if necessary, the temperature of each flow is increased by means of separate heaters and the humidity of the flow is adjusted using two humidifiers. To extract the required flow from the main loops and to adjust the pressure at the inlets of the test cell, two smaller fans are used (Fans 3&6 for the exhaust flow and Fans 4&5 for the supply flow). The flowrates at the main loops are inferred from the measured dynamic and static pressure of the air. The dynamic pressure of the air is measured via a pitot-static tube connected with MKS 226A pressure transducers. The static pressure is measured via Omega PX653 pressure transducers. To measure flowrate at the inlets and outlets of the test cell, an orifice plate is used in each duct. The pressure difference between the two sides of the orifice is measured via VALIDYNE P305D pressure transducers. The pressure drop across each side of the exchanger is measured using Dwyer 616KD-A-03-V pressure transmitters.

Figure 3.3 shows the location of the temperature and humidity measurement sensors. Measurements at the supply and exhaust inlets are done using 6 type T thermocouples spread at the surface of the exchanger. Since the outlet temperature varies between different channels of the exchanger, flow mixers are used at the outlet of the test cell to create a more uniform temperature field in the duct. After the mixers, 12 type T thermocouples spread inside the duct are used to measure the temperature. At each outlet and inlet, two ROTRONIC HygroClip 2 RH sensors are used for humidity measurements. Like temperature, humidity also varies between different channels at the outlet of the exchanger. As a result, to have a more uniform humidity distribution in the duct at the location of humidity measurement, sensors are placed after the mixers and further downstream. LabVIEW 2018 is used to control different equipment and set the required operating conditions.

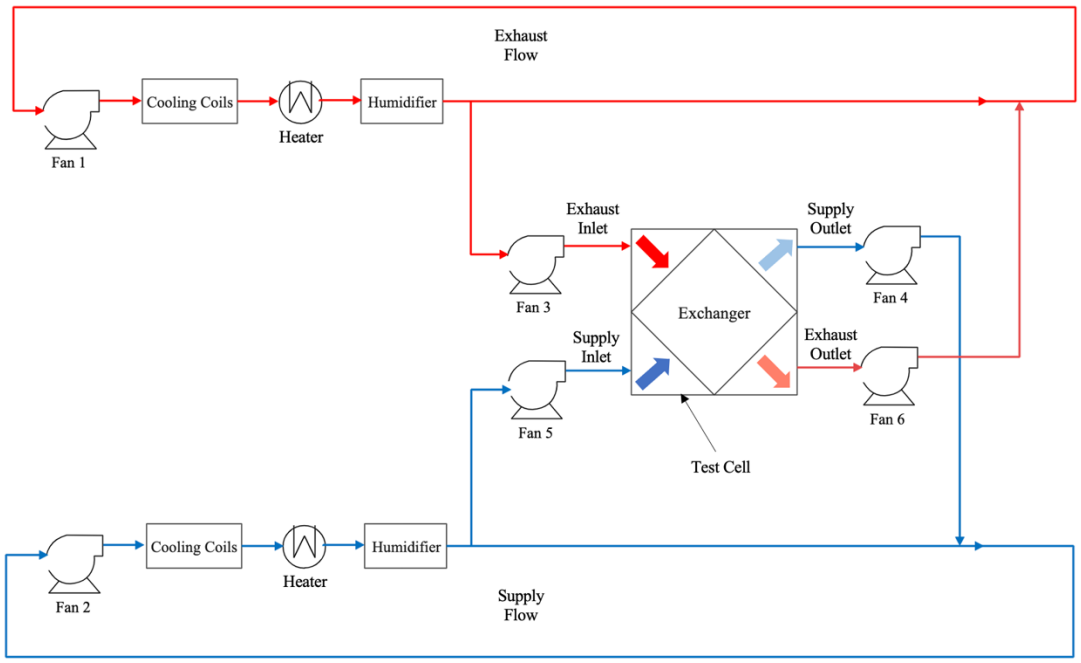

Figure 3.2) Schematic of the test setup

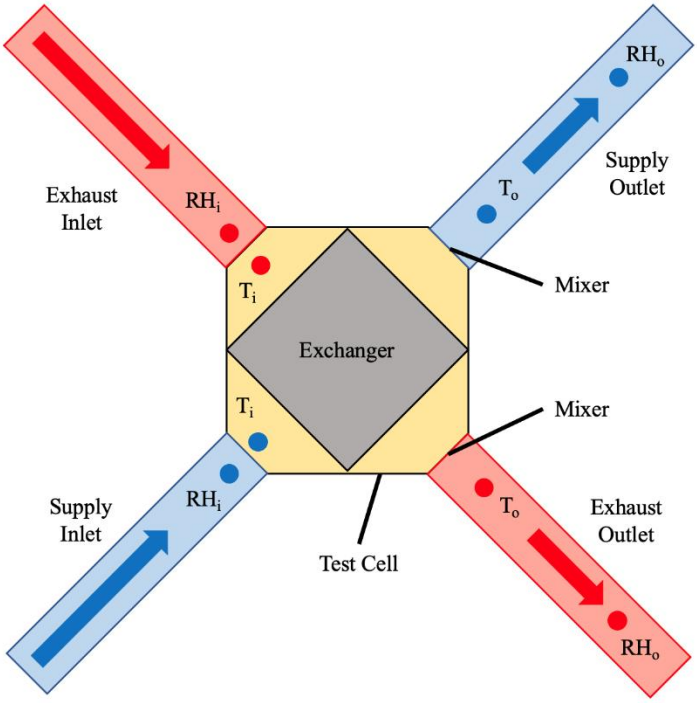

Figure 3.3) Location of the temperature and humidity sensors

3.3.2 Uncertainty Analysis

The flowrate in the main loops is calculated by measuring the dynamic and static pressure of the air with an uncertainty of ±30 Pa and ±2.5 Pa, respectively. This results in errors of up to ±30 CFM in the typical flowrates at the main loops (500 CFM). The flowrates of the supply and exhaust flows entering and leaving the exchanger are calculated by measuring the pressure drop across the orifice plates at the inlet and outlets with an accuracy of ±10 Pa. The manufacturer reports expected errors of up to 1 CFM in the measured flowrate of the exchanger. The thermocouples used for measurement of temperature at the inlets and outlets of the exchanger have an uncertainty of ± 0.1°C. The uncertainty in the sensible effectiveness is calculated by error propagation in equations (30) and (31) and using the uncertainty of the thermocouples, which results in expected absolute errors of 1-2% in sensible effectiveness. The RH sensors used for measurement of humidity are calibrated with a dew-point hygrometer to have an uncertainty of ±0.06 gr/kg. Similar to sensible effectiveness, the uncertainty in the latent effectiveness is calculated by error propagation in equations (32) and (33). Absolute errors of 1-5% are expected in the calculated latent effectiveness. Finally, the pressure drop across the exchanger is measured with an accuracy of ±10 Pa. All the tests in this study are repeated at least 3 times and a repeatability error of less than 5% was observed.

3.3.3 Exchanger Specifications

The energy exchanger studied (Figure 1.2 and Figure 3.4) has a cross flow configuration; supply and exhaust channels are separated by sheets of water vapor permeable polymer membranes and aluminum corrugated fins are used as spacers between the membrane sheets.

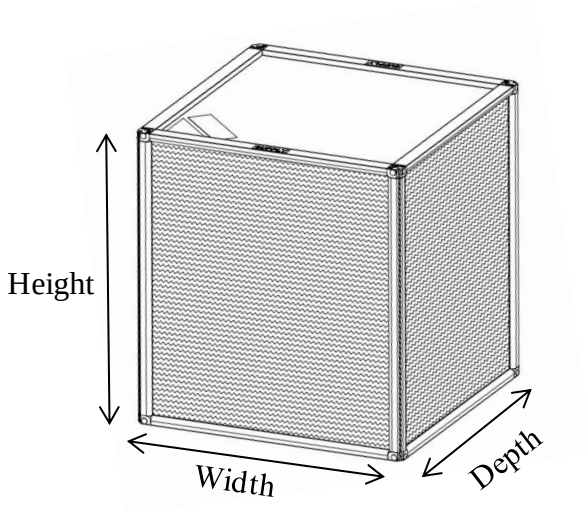

Figure 3.4) Schematic of the exchanger

The exchanger was a model X-ERV provided by CORE Energy Recovery Solutions with specifications listed in Table 1.

Table 3.1) Specifications of the exchanger

Height (mm)	Width (mm)	Depth (mm)	Channel Height (mm)	Channel Width (mm)	Membrane
250	213	213	2	6.5	T4 (MX4)

The membrane (trade names MX4, T4) used in the exchanger is a composite consisting of a thin (1-2 μm) coating of Polyethylene Oxide-Polyurethane (PEO-PU) on a substrate of silica polyethylene. The composite is 100-110 microns thick and has a permeability of 1.1×10^6 Barrer at 50 °C and 50% RH (as explained in Chapter 2). In the studied exchanger, the coating layer of the membrane is faced towards the exhaust side, where condensation occurs. The contact angle of the coating material is approximately 48° as reported by the manufacturer (CORE Energy Recovery Solutions). The substrate and aluminum fins are believed to be more hydrophobic, with contact angles of 120^0 [23] and 81^0 as reported by the manufacturer (CORE Energy Recovery Solutions), respectively. We suspect that these surface properties have only a small influence on the problem because in the real world, surface contamination will generally make the surface more hydrophilic. Furthermore, models developed for this problem in Chapter 4 show good agreement with the experiments when it is assumed that condensation occurs without any supersaturation.

3.3.4 Experiment Procedure

The exchanger is placed in the test cell horizontally (flow passages are parallel with the ground) and is sealed prior to the start of the test. In order to make sure that the exchanger is completely dry at the start of testing, the condensed water inside the exchanger is drained and the exchanger is continuously exposed to dry air at 35 °C and the pressure drops at the supply and exhaust sides are measured as a function of time. When the pressure drops equal the values measured with dry air conditions, there should be no remaining macroscopic water particles in the exchanger. However, as a precaution, the drying process continues for another 45 minutes after the time when the pressure drop measurements would suggest that the energy exchanger is dry.

In order to minimize the effect of transient temperature and humidity, after drying the exchanger, the temperature of the supply and exhaust inlets are set to the test temperatures while the flows are kept dry. After the test temperatures are met, the humidifiers are turned on to increase the humidity of the flows. The humidity of the flows reaches the test level after at most 5 minutes. The recording starts when all test operating conditions at inlet are met and are at steady state. If the tests are aimed to investigate the effect of condensation on the effectiveness, testing only continues for 20 minutes. The short time for testing is enough to analyze the effect of condensation on effectiveness because both sensible and latent effectiveness are very sensitive to the condensation, and they change almost immediately when condensation occurs. Investigation of the effect of condensation on pressure drop requires testing for longer times, and as a result, these tests are only performed under

3 different operating conditions. The details of each test operating conditions are explained later. Finally, tests with various operating conditions are repeated at least twice and a repeatability error of less than 5% is observed.

Temperature and humidity of the outdoor and indoor air (i.e., temperature and humidity at the supply and exhaust inlets), flowrate and the specifications of the exchanger are the salient factors in the performance of the energy exchangers [32]. As a result, the operating conditions resulting in condensation in the exchanger can be assumed to be affected by these factors as well. However, experimental investigation of all factors would be extremely time-consuming; only a representative selection of these factors is investigated in this study.

The main factor investigated is the relative humidity of the exhaust inlet, and all short tests are performed for a wide range of exhaust inlet relative humidity. Under each fixed operating condition, the relative humidity of the exhaust inlet is changed to detect any changes in the sensible and latent effectiveness. Due to the equipment limitations, temperature and humidity of the supply inlet is kept constant, although the effects of exhaust inlet temperature and flowrate are investigated.

3.3.5 Methods of Detection of Condensation

In studies investigating condensation and frost formation in heat exchangers and energy exchangers various approaches are used for detection of condensation and frost formation [16]. In this study, condensation is detected via investigation of the effectiveness of supply and exhaust sides, changes in pressure drop in the exchanger, and visual inspection of the exchanger. These methods are explained below.

3.3.5.1 Effectiveness

In the ideal situation without condensation, energy and mass do not accumulate in the exchanger and the effectiveness (latent and sensible) is the same whether measured using the exhaust flow or the supply flow. Condensation is an exothermic process that results in the release of heat in the energy exchanger at the location of condensation. Depending on where the generated heat is absorbed, it can change the temperature of the air at the exhaust and supply sides which results in a different sensible effectiveness for the two flows. Condensation also affects the latent effectiveness. Condensation in the exhaust flow results in accumulation of liquid water on the membrane. This will then transfer through the membrane to the supply side, although the rate of condensation is not necessarily equal to the rate of transfer of liquid water through the membrane. Consequently, the amount of extracted water vapor from the exhaust side is not precisely equal to the amount of water vapor received by the supply side. As a result, the occurrence of condensation can cause the latent effectiveness to differ between the supply and exhaust sides.

Usually, sensible effectiveness is calculated using the average change in the temperature of both flows; however, in this study, to be able to compare the temperature change of the supply and exhaust flows in the exchanger, sensible effectiveness is calculated separately for the supply and exhaust sides. Sensible effectiveness of the exhaust side is calculated using the following equation assuming equal flowrate for both sides [27,32]:

$$SE_e = \frac{T_{e,i} - T_{e,o}}{T_{e,i} - T_{s,i}} \quad (30)$$

In the above equation, SE_e denotes the sensible effectiveness of the exhaust side, T is the temperature and subscripts e, s, i and o refer to exhaust side, supply side, inlet, and outlet. In the same way, the sensible effectiveness of the supply side is calculated using the following equation:

$$SE_s = \frac{T_{s,o} - T_{s,i}}{T_{e,i} - T_{s,i}} \quad (31)$$

Similarly, latent effectiveness of the supply and exhaust sides are calculated using the following equations, assuming equal flowrate for both flows [27,32]:

$$LE_e = \frac{\omega_{e,i} - \omega_{e,o}}{\omega_{e,i} - \omega_{s,i}} \quad (32)$$

$$LE_s = \frac{\omega_{s,o} - \omega_{s,i}}{\omega_{e,i} - \omega_{s,i}} \quad (33)$$

In the above equations, LE is the latent effectiveness and ω is the moisture content of the flow.

3.3.5.2 Pressure Drop

As mentioned in the previous section, all of the condensed water will not necessarily permeate through the membrane, and as a result the condensed water can accumulate in the channels and block them. This blockage of the channels can then result in an increase in pressure drop in the exchanger. However, changes in pressure drop are expected to happen only at the exhaust side, where condensation is expected to occur. In this study the pressure drops at both supply and exhaust sides are measured and are compared to the case without condensation. Although measuring pressure drop can be used as a method for detecting condensation, it should be noted that pressure drop is not as sensitive to condensation as sensible and latent effectiveness; to detect condensation via pressure drop requires that tests be conducted for longer periods of time.

3.3.5.3 Visual Inspection

Visual inspection of the channel outlets is a reliable but qualitative method to detect condensation after long tests; this method is only used as a confirmation that condensation has occurred.

3.4 Results and Discussion

3.4.1 Onset of Condensation

Condensation should affect the sensible and latent effectiveness of the supply and exhaust sides. The effects of condensation on the sensible and latent effectiveness should be measurable almost immediately after the condensation operating conditions are met. In this section we discuss only tests carried out for a short duration, during which the physical blockage of channels by condensation is negligible. For such short duration tests the effectiveness is not affected by the channel blockage and changes in the flow distribution in the exchanger. The effects of channel blockage on effectiveness are discussed in section 3.4.3.

3.4.1.1 Effect of Exhaust Inlet Relative Humidity

Figure 3.5 shows the sensible and latent effectiveness of the supply and exhaust sides against exhaust inlet relative humidity. The supply inlet temperature and relative humidity are kept at 4°C and 78% respectively, the exhaust inlet temperature is 25°C and both flows have a flowrate of 90 CFM. Error bars show the uncertainty in the measured sensible or latent effectiveness calculated based on the accuracy of the measurement equipment.

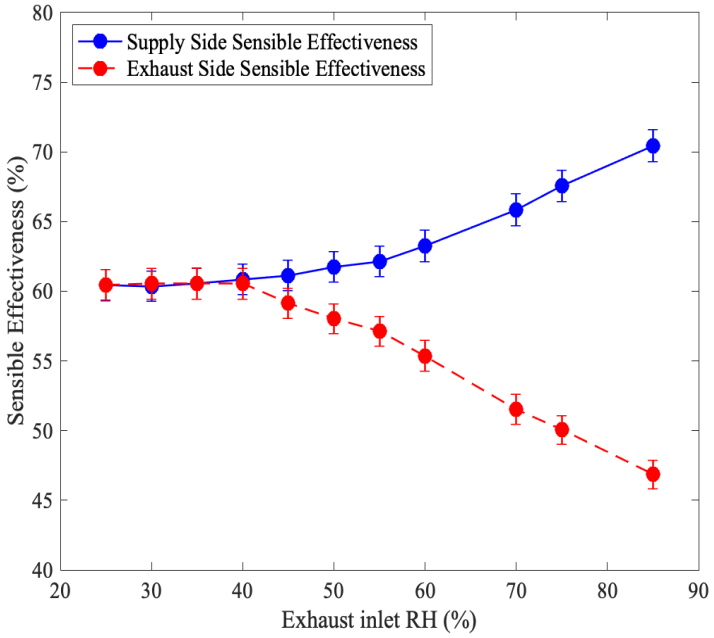

a) Sensible Effectiveness

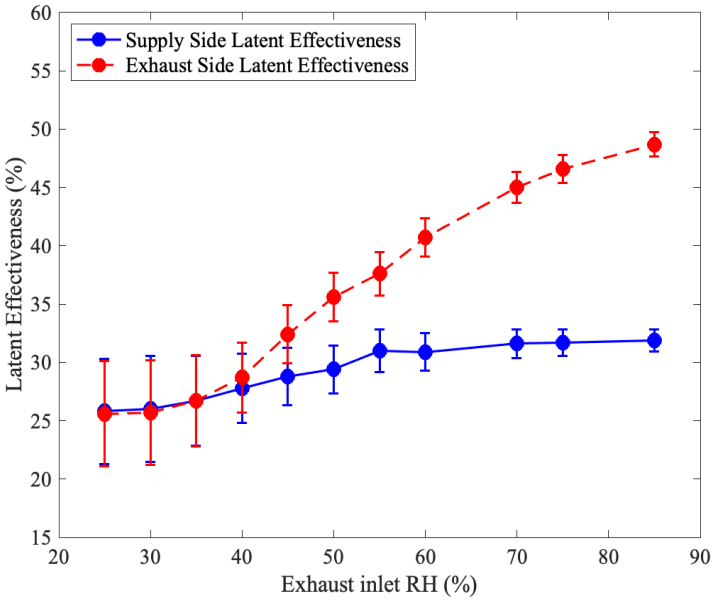

b) Latent Effectiveness

Figure 3.5) The effect of exhaust inlet relative humidity on the occurrence of condensation, supply inlet temperature = 4 ℃, supply inlet relative humidity = 78%, exhaust inlet temperature = 25 ℃, flowrate = 90 CFM.

At low exhaust inlet relative humidity, the sensible effectiveness of the supply and exhaust sides are equal, but they gradually diverge as the humidity increases. The point at which the sensible

effectiveness of the two sides starts to diverge marks the onset of condensation. Condensation is an exothermic process that releases heat in the exchanger. The generated heat eventually increases the temperature of both supply and exhaust flows. This means that, compared to the case without condensation, the outlet temperature of both supply and exhaust sides are higher when condensation happens. Using equations (30) and (31), it is clear that increasing the outlet temperature of the supply side increases the supply side sensible effectiveness while increasing the outlet temperature of the exhaust side decreases its sensible effectiveness.

The effect of condensation on the latent effectiveness is more complicated. Similar to the sensible effectiveness, at low relative humidity the latent effectiveness of the supply and exhaust sides are equal, and they diverge when the relative humidity increases. The point at which the latent effectiveness of the two sides starts to diverge can be assumed to be the start point of condensation; however, as the uncertainty in the measured latent effectiveness value is comparatively high, sensible effectiveness is a more reliable measure of the onset of condensation. Unlike sensible effectiveness, the latent effectiveness of both supply and exhaust sides increases with relative humidity but the increase in the exhaust side latent effectiveness is much more significant.
Increasing the exhaust inlet relative humidity results in an overall higher relative humidity experienced by the membrane. The permeability of the polymer membrane used in the exchanger was shown to be concentration dependent and increase with increasing humidity in Chapter 2, and since the latent effectiveness of an energy exchanger is a function of permeability of the membrane, the overall latent effectiveness of the exchanger increases with humidity. If the temperature at the surface of the membrane at the exhaust side reaches the dew point temperature of the air, the excess water vapor condenses on the surface of the membrane. If condensation occurs in the exchanger at the imaginary location shown in Figure 3.1, the state of the air at the bulk flows and the surfaces of the membrane will be as shown in Figure 3.6. If air could be supersaturated and have a relative humidity of more than 100% without condensing the excess water, the state of the air at the surface of the membrane at the exhaust side could be represented by point B'. However due to the presence of many nucleation sites, the relative humidity of the air cannot exceed 100 % and the excess water condenses on the surface of the membrane. Owing to latent heat effects, condensation of water vapor on the surface of the membrane also increases the temperature of the air at the surface of the membrane.

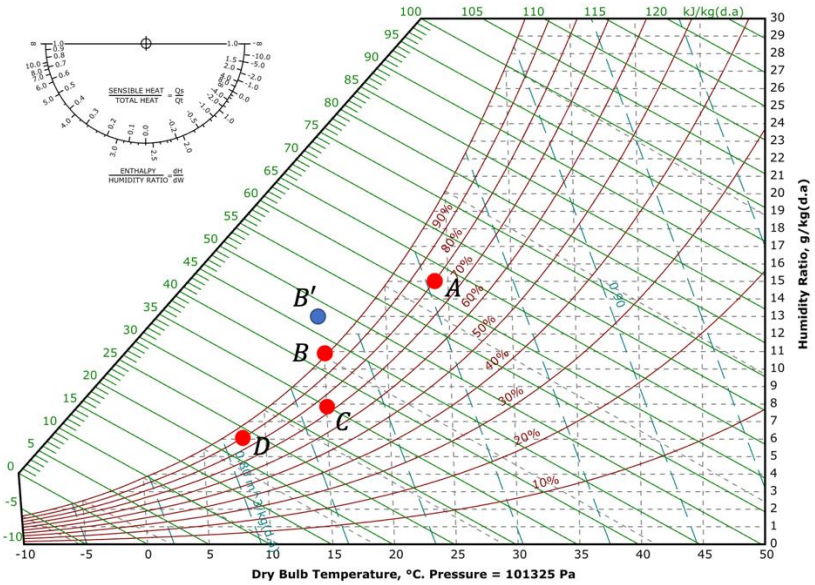

Figure 3.6) State of the air at the imaginary location shown in Figure 3.1 (psychrometric chart extracted from [95])

As is indicated in Figure 3.6, the amount of condensed water is higher than the amount of water vapor that would have permeated through the membrane if condensation hadn't occurred. As a result, the moisture content of the air at the exhaust outlet is lower when condensation occurs, which increases the latent effectiveness (equation (32)). The condensed water on the surface of the membrane then permeates through the membrane to the supply side. If the rate of permeation of the liquid water through the membrane is higher than water vapor without condensation, then the outlet moisture content of the supply side increases, which results in a higher latent effectiveness (equation (33)). Figure 3.6 shows that condensation of water vapor can actually result in a lower moisture content at the surface of the membrane compared to the case if condensation hadn't occurred (compare points B and B′), lowering the flux of water vapor through the membrane. On the other hand, the permeability of the membrane to liquid water is not necessarily equal to that of water vapor and both have been measured. The procedure and equipment used for those measurements are explained in detail in Chapter 2. To measure the permeability of the membrane for water vapor, a feed flow at 50°C and 95% RH and a dry sweep flow are used and by using the moisture content of the flow at the inlets and outlets, the permeability of the membrane is calculated. To measure the permeability for liquid water, the feed flow is replaced with liquid water while using a dry sweep. As explained in [52], the permeation of liquid water at temperature T through the membrane is similar to the permeation of saturated water vapor at temperature T through the membrane, and therefore similar equations are used to calculate the permeability for liquid water.

The permeability of the membrane for water vapor at 50 °C and 95 % RH and liquid water are 1600000 and 5900000 Barrer, respectively. The permeability of the membrane for liquid water is

thus about 3.7 times higher than the permeability of the membrane to water vapor, and as a consequence the flux of water vapor through the membrane is greater at locations where condensation has occurred.

In summary, for the exhaust flow the condensation of the excess water vapor in air and overall increase in the permeability of the membrane at higher relative humidity result in a significant increase in the latent effectiveness. On the other hand, for the supply flow, increasing the exhaust inlet relative humidity and the presence of the liquid water increase the permeability of the membrane, which in turn increases the latent effectiveness. However, in areas with condensation, the moisture content difference at the two sides of the membrane decreases, which results in lower water vapor flux through the membrane and lower latent effectiveness. Based on Figure 3.5b, at lower exhaust inlet relative humidity, the effect of increase in permeability is dominant and the latent effectiveness at the supply side increases, whereas at higher humidity and condensation rate, the aforementioned factors approximately negate each other, resulting in less significant changes in the latent effectiveness.

The effect of exhaust inlet relative humidity on condensation and frost formation in heat exchangers and energy exchangers has also been investigated by others. Nam et al. [85], showed that condensation in heat exchangers increases the sensible effectiveness of the supply side, similar to the behavior shown in Figure 3.5a. They attributed the increase in effectiveness to the heat release of the condensation. Anisimov et al. [86] showed with their model that increasing the relative humidity of the indoor air increases the combined sensible effectiveness of the heat exchanger. Rafati et al. [93] compared the effect of long-time frost formation on the sensible and latent side effectiveness of supply and exhaust sides of an energy exchanger and an heat exchanger. They reported the time-dependent graph of effectiveness for only one operating condition. It can be inferred from their results that, for both energy exchangers and heat exchangers, the sensible effectiveness of the exhaust side was higher than the supply side compared to the beginning of the test prior to frost formation, although the sensible effectiveness at both sides decreased over time. This is in contrast to the findings of this study and other studies for condensation in heat exchangers where the sensible effectiveness of the exhaust side increases with the occurrence of condensation. Rafati et al. attributed the increase in sensible effectiveness to the fact that the roughness of the frost layer enhances the convective mass transfer coefficient of the air in the exhaust side, which in turn increases the sensible effectiveness of the exhaust side. Their results also showed that the latent effectiveness of the exhaust side was higher than the supply side when frost formation occurred, which is consistent with the results of this study.

3.4.1.2 Effect of Exhaust Inlet Temperature

In order to examine the effect of indoor air temperature, the exchanger is tested at two different exhaust inlet temperatures (20°C and 25°C) at various exhaust relative humidities. The supply inlet temperature and relative humidity are kept constant at 4°C and 78%, respectively, and the flowrate is 90 CFM. Figure 3.7 compares the sensible and latent effectiveness of the exchanger against the exhaust inlet relative humidity at exhaust inlet temperatures of 20°C and 25°C. Error bars represent the bounds of error calculated using the accuracy of the measurement equipment.

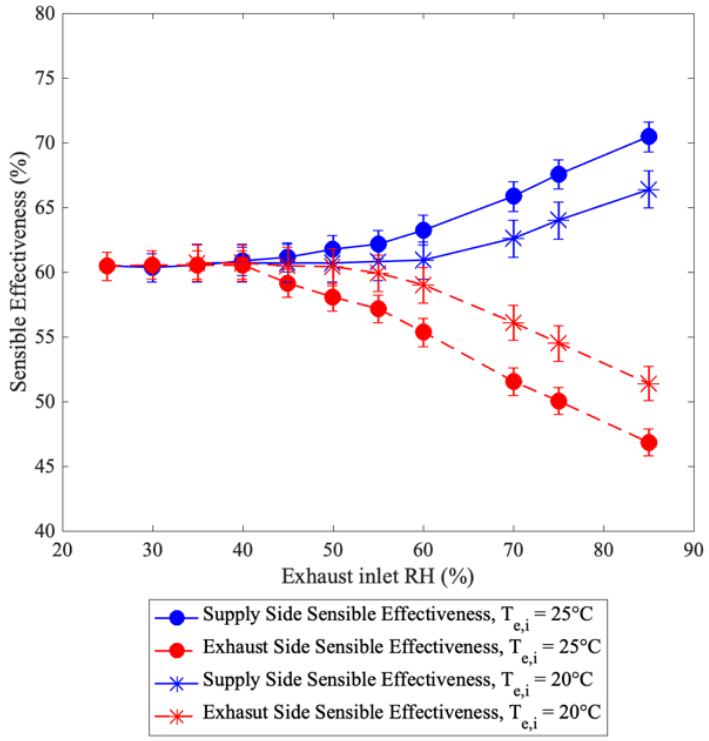

a) Sensible Effectiveness

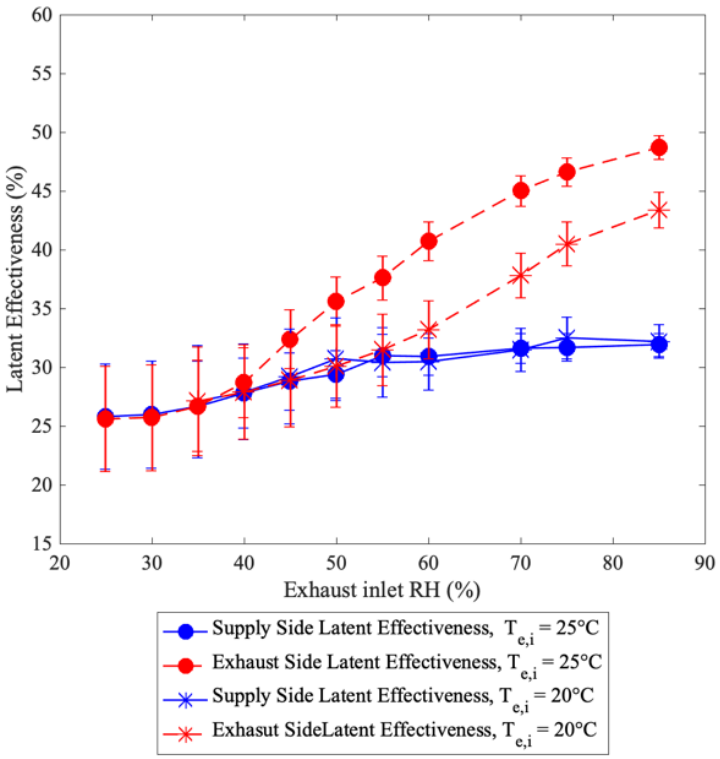

b) Latent Effectiveness

Figure 3.7) Effect of indoor temperature on condensation in the exchanger, $T_{e,i}$ = exhaust inlet temperature, supply inlet temperature = 4 ℃, supply inlet relative humidity = 78%, flowrate = 90 CFM.

Based on the sensible and latent effectiveness graphs, condensation begins at higher exhaust inlet relative humidity when the exhaust inlet temperature is lower. This is due to the fact that, at equal relative humidity, the moisture content in the air is much lower at lower temperatures. As a result, the moisture content of the air reaches the required limit for condensation at higher relative humidity when the temperature is lower. The effect of condensation on both sensible and latent effectiveness is less significant at the lower exhaust inlet temperature. This is due to the fact that, at equal exhaust inlet relative humidity, the rate of condensation is lower at lower temperature, which decreases the significance of the effect of condensation on the effectiveness.

3.4.1.3 Effect of Flowrate

In this section, the exchanger is tested at two different flowrates of 60 CFM and 90 CFM. The supply inlet temperature is kept at 4°C, supply inlet relative humidity is 78% and exhaust inlet temperature is kept constant at 25°C. Figure 3.8 shows the effect of flowrate on sensible and latent effectiveness of the exchanger with and without condensation. Error bars show the uncertainty in

the measured values calculated based on the accuracy of the measurement equipment. Generally, increasing flowrate decreases the sensible and latent effectiveness of the energy exchangers [32]. As indicated in the figure, at low relative humidity without condensation, increasing the flowrate decreases the sensible and latent effectiveness independent of the exhaust inlet relative humidity. Additionally, both the exhaust inlet relative humidity at which the condensation starts to occur and the difference between the sensible and latent effectiveness of the supply and exhaust sides are independent of the flowrate. The results of other studies on condensation in heat exchangers have also shown that increasing the flowrate decreases the effectiveness of the exchanger, although it does not affect the limits of occurrence of condensation [85].

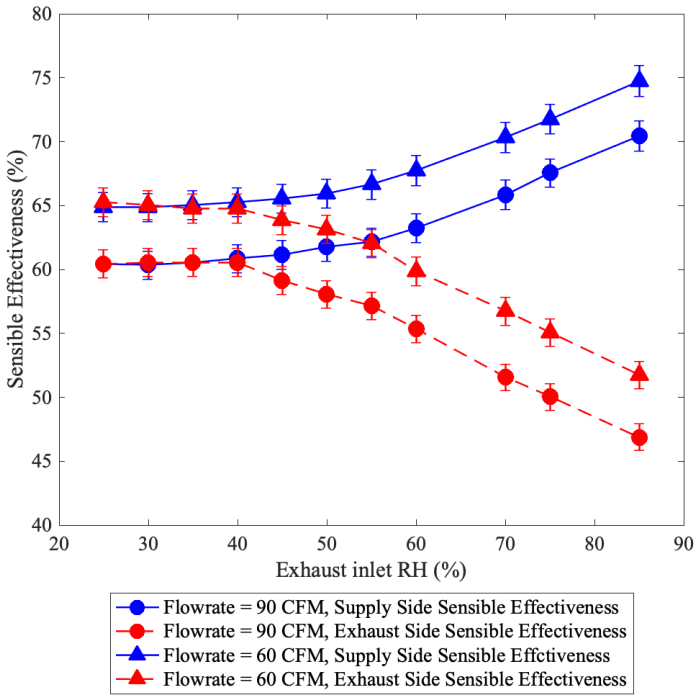

a) Sensible effectiveness

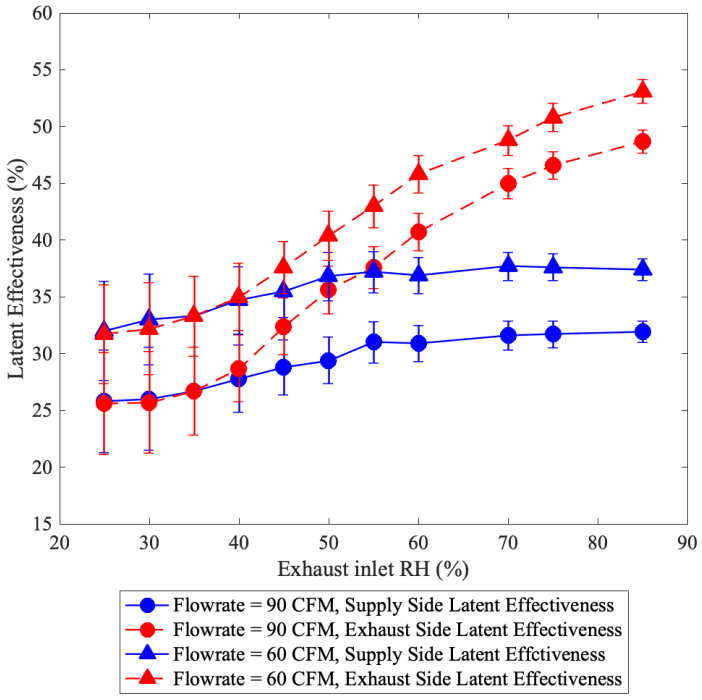

b) Latent effectiveness

Figure 3.8) Effect of flowrate on the occurrence of condensation in the exchanger, supply inlet temperature = 4 ℃, supply inlet relative humidity = 78%, exhaust inlet temperature = 25 ℃.

3.4.1.4 Rate of condensation

Using the moisture content at the supply and exhaust inlets and outlets and the flowrate of air, for equal supply and exhaust mass flow rates, it is possible to calculate the rate of condensation in the exchanger via the following equation.

$$\dot{m}_{cond} = \dot{m}_{air}\left(\omega_{e,in} + \omega_{s,in} - \omega_{e,out} - \omega_{s,out}\right) \qquad (34)$$

In the above equation, $\dot{m}_{cond}$ is the rate of condensation of water, $\dot{m}_{air}$ is the air flowrate, ω is the moisture content and subscripts *e, s, in,* and *out* denote exhaust, supply, inlet and outlet.

Rate of condensation for the tests discussed in sections 3.4.1.2 and 3.4.1.3 and Figures 3.7 and 3.8 are calculated using equation (34). Figure 3.9 shows the effect of exhaust inlet temperature and relative humidity and the air flowrate on the rate of condensation. Error bars are the uncertainty in the condensation rate calculated based on the uncertainty of the measured flowrate and moisture

content values. Consistent with Figures 3.7 and 3.8, increasing the exhaust inlet temperature and flowrate increases the rate of condensation at a constant exhaust inlet relative humidity.

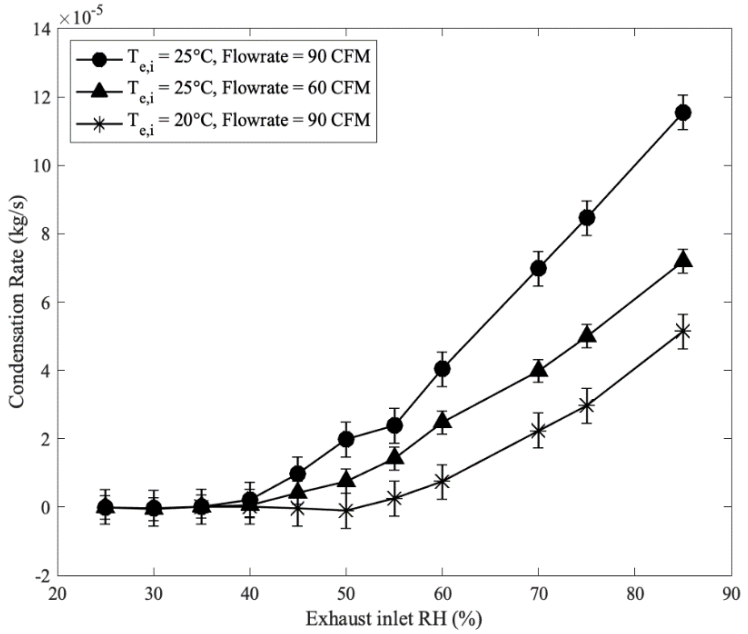

Figure 3.9) Rate of condensation in the exchanger, $T_{e,i}$ = exhaust inlet temperature, supply inlet temperature = 4 ℃, supply inlet relative humidity = 78%.

3.4.2 Transient Development of Condensation

Condensed water on the surface of the membrane can accumulate and partially or completely block the channels of the exchanger. If the channels get blocked by water, the pressure drop over the exchanger increases. To study this phenomenon, the exchanger is tested for more than 2 hours under operating conditions that result in condensation. For these tests operating conditions are chosen to ensure a high rate of condensation. To investigate the effect of exhaust inlet relative humidity and flowrate, the exchanger is tested under 3 different operating conditions. In all tests supply inlet temperature and relative humidity are kept at 4°C and 78% and the exhaust inlet temperature is set to be 25°C.

Figure 3.10 shows the pressure drop at the supply and exhaust sides over time under these different operating conditions. Error bars represent the uncertainty in the measured pressure drop calculated from the accuracy of the measurement equipment. For the operating condition with the highest flowrate and humidity (90 CFM flowrate and 80% exhaust inlet RH), condensation can significantly increase the pressure drop in the exchanger. At the beginning of the test the pressure drop in both sides is equal. However, after a relatively short time, the pressure drop at the exhaust side increases whereas the supply side pressure drop remains constant. The constancy of the

pressure drop in the supply side is consistent with the notion that condensation occurs only in the exhaust side. As the condensed water accumulates in the channels the rate of increase of pressure drop rises and after about 70 minutes there is an inflection point after which the pressure drop asymptotically approaches its steady state value. This steady state pressure drop is 4 times larger than the pressure drop prior to significant condensation. Figure 3.11 shows the partial and complete blockage of channels due to condensation. While condensation of water on the surface of the membrane increases the blockage of the channels, which in turn increases the pressure drop, permeation of water through the membrane decreases the amount of accumulated water in the channels. Additionally, when the amount of water in the channels is sufficiently large, the flow of air can push the water out of the exchanger. This axial displacement of water can be observed as liquid water present at the exhaust outlet of the energy exchanger. The authors believe that during the first 100 minutes of testing the rate of condensation is higher than the rate of permeation of water through the membrane and the flow of water out of the exchanger, but thereafter the effects become balanced, and the condensation reaches a steady state.

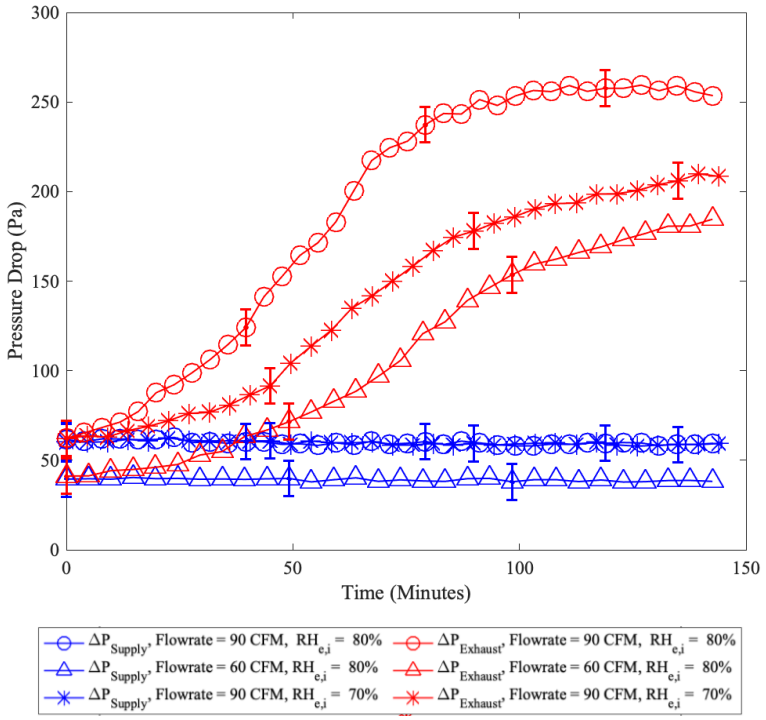

Figure 3.10) Effect of flowrate and exhaust inlet relative humidity on pressure drop, $RH_{e,i}$ = exhaust inlet relative humidity, supply inlet temperature = 4 ℃, supply inlet relative = 78%, exhaust inlet temperature = 25 ℃

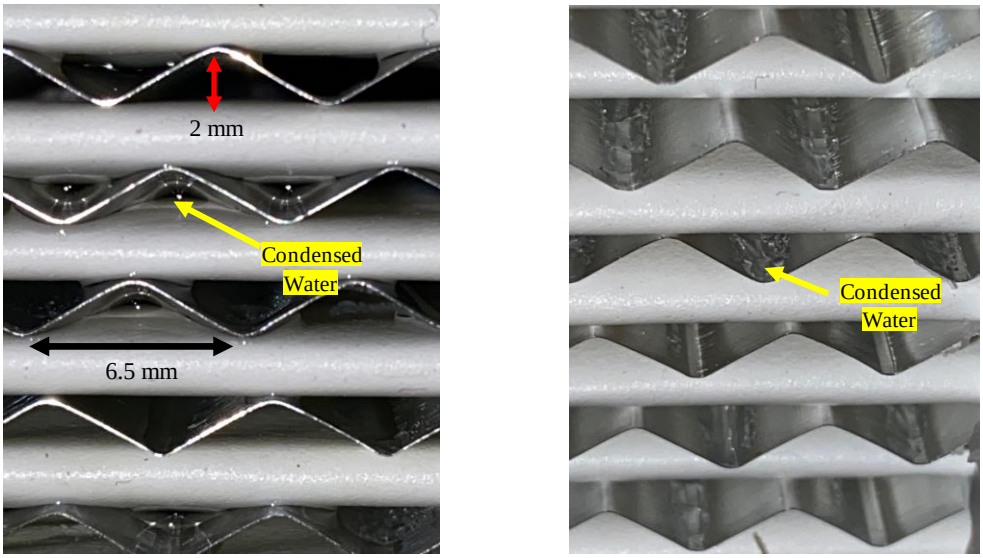

Figure 3.11) The complete (left) and partial (right) blockage of channels due to condensation

As one might speculate, decreasing the exhaust inlet relative humidity decreases the rate of increase in pressure drop, resulting in a longer time to achieve steady state. The steady state pressure is also lower for the lower exhaust inlet relative humidity but the effect of condensation on pressure drop is still significant. The changes in pressure drop can be explained by the fact that at lower exhaust inlet relative humidity, condensation occurs at a smaller area in the exchanger, so the rate of condensation and the amount of condensed water is lower. As a result, it takes more time for the level of condensed water to reach the level required to make the outflow of water from the exchanger match the rate of increase in channel blockage. So, when the pressure drop reaches steady state, the channels are less blocked, and this results in lower pressure drop. The exhaust inlet relative humidity, however, does not affect the pressure drop at the supply side. Figure 3.12 shows the relative growth of the condensation region due to the increase in exhaust inlet RH.

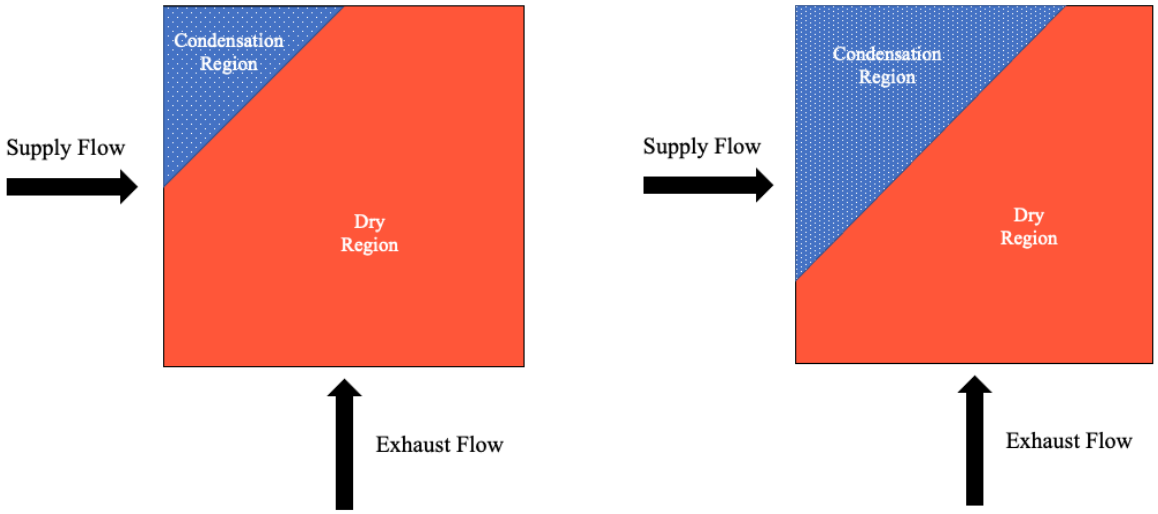

a) Exhaust inlet RH 70%

b) Exhaust inlet RH 80%

Figure 3.12) Growth of condensation region due to the increase in exhaust inlet RH

Decreasing flowrate decreases the pressure drop in an exchanger and as a result the pressure drops with condensation (Figure 3.10) are overall lower for both supply and exhaust sides relative to the high flowrate case. Even at low flowrate, the effect of condensation on pressure drop is significant and the steady state pressure drop is almost 4.5 times higher than pressure drop without condensation. Similar to the case with the lower exhaust inlet relative humidity, the pressure drop reaches the steady state at a longer time (~145 minutes) and the absolute increase in pressure drop due to condensation is lower compared to the case with the higher flowrate. Both of these findings are intuitive given the lower condensation rates and lower pressure drops associated with lower flowrates.

The results of this study can be compared to the results of other studies investigating condensation and frost formation in heat exchangers and energy exchangers. Gendebein et al. [68] and Fernandez et al. [96] investigated the pressure drop in an heat exchanger with condensation. Their experiment also showed that the pressure drop increased with the occurrence of condensation, rising to a steady state value. In contrast with the present study their heat exchangers were placed vertically, and the condensed water was drained continuously from the exchanger by gravity. However, in agreement with the current work, those studies indicate that the drainage of condensed water from the exchanger can be an influential factor in the steady state behavior during long duration tests. Rafati et al. [93] also investigated the effect of frost formation on the pressure drop in heat exchangers and energy exchangers. In contrast to the results of this study, frost formation continuously increased the pressure drop in the exchanger and the rate of increase in pressure drop increased with time. This difference in behavior can be explained by the fact that in frost formation, the

formed ice cannot leave the exchanger and accumulated ice continuously increases the pressure drop, whereas the condensed water can be pushed out of the exchanger by the air movement.

3.4.3 Channel Blockage and Effectiveness

Figure 3.13 shows the effect of channel blockage on sensible and latent effectiveness. Error bars show the uncertainty in the measured sensible or latent effectiveness calculated based on the accuracy of the measurement equipment. Changes in sensible and latent effectiveness due to channel blockage are minor compared to changes in pressure drop.

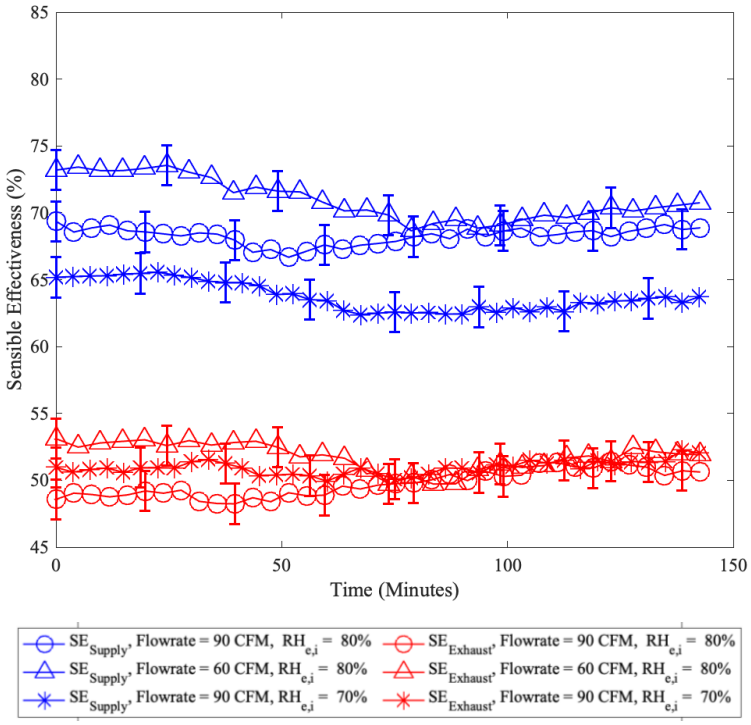

a) Sensible Effectiveness

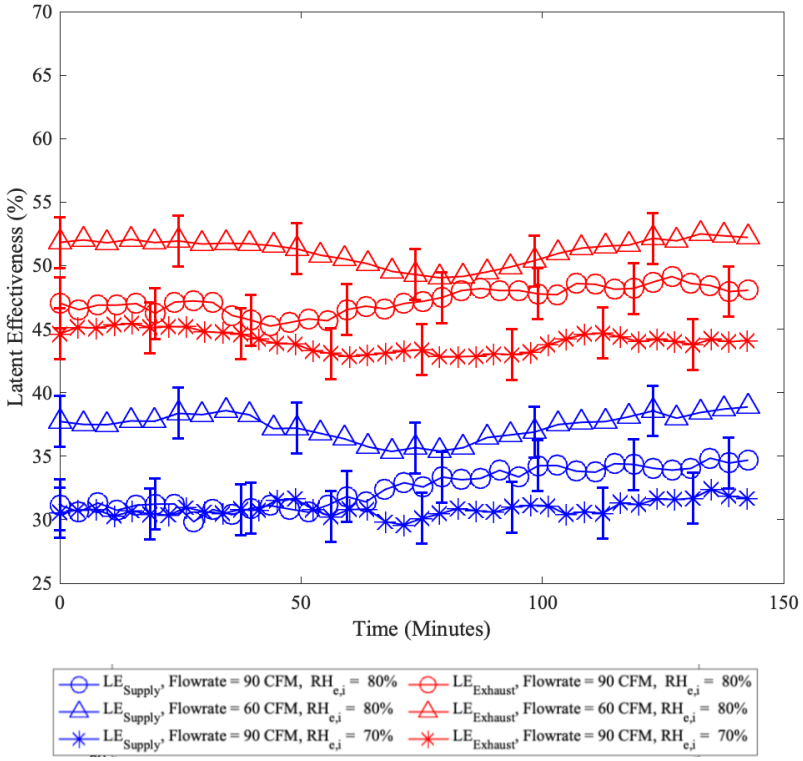

b) Latent Effectiveness

Figure 3.13) Effect of channel blockage on effectiveness, SE = sensible effectiveness, LE = latent effectiveness, supply inlet temperature = 4 ℃, supply inlet RH = 78%, exhaust inlet temperature = 25 ℃. Effectiveness and supply side pressure drop reach steady state in approximately 1 hour. Exhaust side pressure drop, where condensation occurs, nearly reaches steady state in 2 hours.

3.5 Conclusion

The occurrence of condensation in a crossflow, flat plate, membrane-based energy exchanger in winter operating conditions was investigated. It was shown that, compared to the case without condensation, when condensation occurs it increases sensible effectiveness of the supply side while it decreases sensible effectiveness of the exhaust side. Furthermore, the latent effectiveness of both supply and exhaust sides increased when condensation occurred although the rate of increase in the latent effectiveness of the exhaust side was much more significant.

The effect of exhaust inlet relative humidity, exhaust inlet temperature and flowrate on condensation were investigated. Increasing the exhaust inlet relative humidity increased the area at which the relative humidity of the flow at the surface of the membrane could reach 100%, and as a result, the rate of condensation was higher at higher exhaust inlet relative humidity. At lower exhaust inlet temperatures, the exhaust inlet relative humidity over which condensation starts to

occur was higher and the rate of condensation was lower. Changing flowrate did not change the operating conditions at which condensation starts to occur and changes in the sensible and latent effectiveness of the supply and exhaust sides remained independent of the flowrate. Increasing flowrate did, however, increase the rate of condensation.
The effect of condensation and channel blockage on pressure drop and effectiveness was also studied. It was shown that condensation significantly affects the pressure drop at the exhaust side while it does not affect the pressure drop at the supply side. At high exhaust inlet relative humidity, pressure drop started to increase only a few minutes after the start of the test, the increase in pressure drop continued until it reached a plateau. At lower exhaust inlet relative humidity, the time at which the pressure drop reached the steady state was longer and the steady state pressure decreased. Lowering the flowrate also increased the time required to reach steady state and decreased the absolute increase in the pressure drop of the exhaust side, although the effect of condensation on pressure drop remained significant. The effect of channel blockage on effectiveness was not significant.

The results of this study show that condensation can occur in energy exchangers in mild winter conditions and at higher room temperature and humidity. For instance, at outdoor temperature and relative humidity of 4°C and 78%, condensation could occur at room temperature and relative humidity of 25°C and 50-60%. As a result, exchanger selection should be made based on system design and the expected operating window of indoor and outdoor climate conditions to minimize the impacts or occurrence of condensation.

Chapter 4: Modelling Condensation in Energy Exchangers with Variable Permeability Membranes

4.1 Introduction

Membrane energy exchangers, also known as Energy Recovery Ventilators, are frequently used in ventilations systems of modern buildings due to their potential for energy saving [26,78]. Energy exchangers use the outgoing indoor air to precondition the incoming fresh air, which decreases the ventilation system load [97]. Using energy exchangers in cold weather conditions is associated with a risk of condensation and frost formation. Frost formation in the exchanger increases the pressure drop, which increases the required fan power [93,98], and it also negatively affects the thermal performance of the exchanger by decreasing the heat and mass transfer between the flows [70]. Condensation also results in partial or complete blockage of the channels and an increase in pressure drop, it may enhances the growth of bio-organisms that pose health risks to the building residents [99], and may facilitate fouling of the membrane [100]. Condensation is more likely to occur than frost formation as frosting occurs only under extremely cold weather conditions whereas condensation can occur even in mild winter conditions. In view of the high likelihood of occurrence and significant impacts of condensation, developing models that can predict the onset of condensation and the performance of the exchanger under condensation conditions is essential.

Heat and mass transfer models for energy exchangers under dry conditions have been developed using CFD [82,101,102], finite-difference [103,104] and ε-NTU methods [105,106]. In most of these studies the permeability of the membrane is assumed constant. In a recent study, Engarnevis et al. [32] developed a heat and mass transfer model that considered the variations in the membrane permeability due to humidity and temperature. They showed that assuming a constant permeability for the membrane can result in errors of up to 15% in the predicted performance of the exchanger. They also showed that, for an asymmetric composite membrane, the orientation of the membrane (whether the coating layer is at the supply side or the exhaust side) affects the performance. Compared to the heat and mass transfer models for dry conditions, heat and mass transfer models for air-to-air exchangers under condensation and frost formation conditions are rare [16].

Most models for air-to-air exchangers under condensation and frosting conditions are focused on heat recovery exchangers (also known as HRVs), where moisture cannot be transferred from one stream to the other. Anisimov et al. [86] developed a heat and mass transfer model that could predict the location of condensation and frosting in the heat exchanger and its performance. They divided the exchanger to dry, condensation and frosting zones and used different sets of heat and mass transfer equations for each region. They used their model to determine the effect of operating

conditions on the size of different regions in the exchanger. They found that at low indoor relative humidity all of the condensed water in the exchanger freezes and as a result the exchanger is only divided into dry and frosted regions. In contrast, at high indoor relative humidity not all of the condensed water freezes, and the exchanger has dry, condensation, and frost regions. Other studies have also investigated condensation and its effects on heat exchangers using CFD tools [85], Simulink [89,91] and the ε-NTU method [68]. The similarities between energy exchangers and heat exchangers might suggest that heat exchanger models can be used as a baseline for energy exchanger models. However, the permeability of the membrane in an energy exchanger makes the heat and mass transfer more complicated and models developed for heat exchangers cannot be directly used for energy exchangers.

Only a handful of studies have investigated condensation and frosting in energy exchangers. Liu et al. [92] used the ε-NTU method and developed a theoretical model that predicted the operating conditions that result in frosting in energy exchangers and heat exchangers. They determined frosting limits for two geometrically similar heat exchanger and energy exchanger and showed that the frosting limit for the energy exchanger was 5-10°C lower than the heat exchanger. Although their model was validated against experimental results and could successfully predict the occurrence of frosting in the exchanger, it could not predict the location of frost in the exchanger or the performance of the exchanger under frosting. Deshko et al. [67] introduced a heat and mass transfer model for heat exchangers and energy exchangers under condensation and frosting but they only validated their model against experimental measurements on a heat exchanger. Similar to the work of Anisimov et al. [86], they divided the exchanger into dry, condensation and frosting regions. They determined the state of each region by comparing the surface temperature of the membrane and the dew point temperature of the air. They investigated the effects of operating conditions and membrane permeability on the size of each region in the exchanger. They showed that increasing the permeability of the membrane significantly decreases the frost region while it only slightly affects the condensation region. Furthermore, they showed that increasing indoor relative humidity and decreasing outdoor temperature increased the relative size of condensation and frost regions in the exchanger. One limitation of their model is that it neglects the variability of the membrane permeability. Moreover, although their model could be used to study condensation without frosting in the exchanger, they did not use their model for this purpose. In a recent study, Shen et al. [94], used the model developed for dry conditions to predict the occurrence of condensation in summer conditions. They calculated the relative humidity on the surface of the membrane and determined the operating conditions that resulted in a relative humidity of 100% on the surface of the membrane. Using their model, they determined the limits of condensation in summer; however, they did not validate the predictions of their model with experimental measurements. Furthermore, they did not extend their model to investigate the performance of the energy exchanger when condensation occurs.

Overall, the authors were unable to find any model of condensation without frost formation in energy exchangers that considers the variable permeability of the membrane. Furthermore, none of the previous studies has investigated the condensation limits and the performance of the exchanger in a wide range of operating conditions. In the present study, a heat and mass transfer model is developed that considers, for the first time, variations in membrane permeability due to condensation, humidity and temperature and their effects on condensation. The model is used to predict the operating conditions resulting in condensation, location of condensed water in the exchanger and the performance of the exchanger under condensation.

4.2 Model Description

The complete model involves specifying the geometry of the energy exchanger, the heat and mass transfer resistances from one side to the other, an empirical membrane permeability model, and the heat and mass balances for the entire energy exchanger considering that some locations may have condensation occurring while others do not. Only steady-state behavior is modelled, which implies validity only for short durations after condensation starts. The entire set of equations is iterated until the steady balances are achieved.

4.2.1 Energy Exchanger Configuration

The modelled exchanger (Figure 1.2) has a crossflow arrangement in which sheets of membrane are separated using corrugated aluminum spacers that create triangular flow passages on each side. For notational convenience we let the x direction be the flow direction of the indoor air (also referred to as the exhaust air) and the y direction as that of the outdoor air (also referred to as the supply air). Owing to the fact that the exchanger consists of multiple stacked identical channels in the z-direction, only a single layer (one set of indoor air channels and one set of outdoor air channels) is modelled.

Heat and mass transfer between each channel in the supply side and each channel in the exhaust side take place at the overlapping region of the two channels (Figure 4.1). For simplicity, the temperature and moisture are spatially averaged over the indoor and outdoor air channel volumes corresponding with a single overlapping region. Thus, for each overlap region the heat and mass transfer become one-dimensional, normal to the membrane.

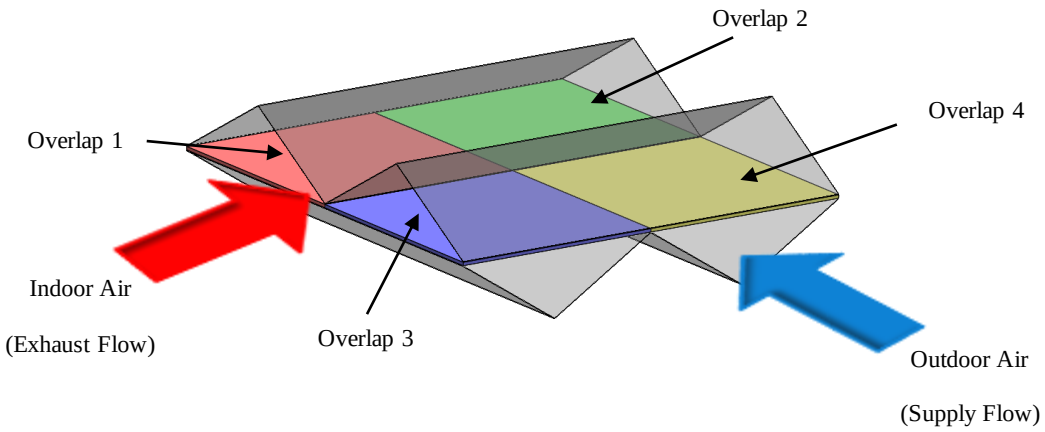

Figure 4.1) Heat and mass transfer areas between the channels

4.2.2 Heat and Mass Transfer Resistances and Balances

Figure 4.2 is a schematic of the supply and exhaust flows at the overlap of the two channels, shown for the case with and without liquid water condensation on the exhaust side. Condensation may also occur in extreme summer conditions at the supply side and is briefly discussed at the end of this paper. Heat transfer between the flows is governed by the convective heat transfer in the exhaust and supply bulk flows and the conduction heat transfer in the membrane. In the case without condensation, mass transfer between the two flows occurs in three steps [23]:

1. Diffusion of water vapor in the exhaust side from the bulk flow to the surface of the membrane.
2. Permeation of water vapor into the membrane from the surface at the exhaust side to the surface at the supply side.
3. Diffusion of water vapor from the surface of the membrane into the supply side bulk flow.

In the case without condensation, the water vapor concentration is always below the saturation value and is computed so that the water vapor flux is the same through bulk flows and the membrane. When there is condensation, however, the mass balance must allow for liquid water accumulation and the heat balance must allow for the heat of condensation; this results in extra unknowns but the condition of saturation at the water surface allows closure.

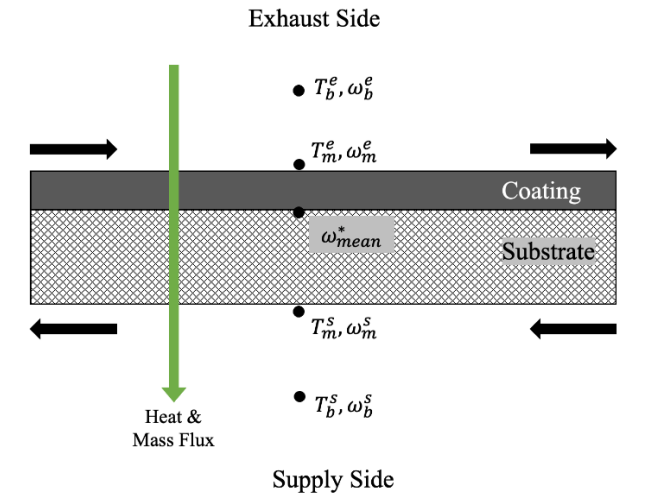

a)

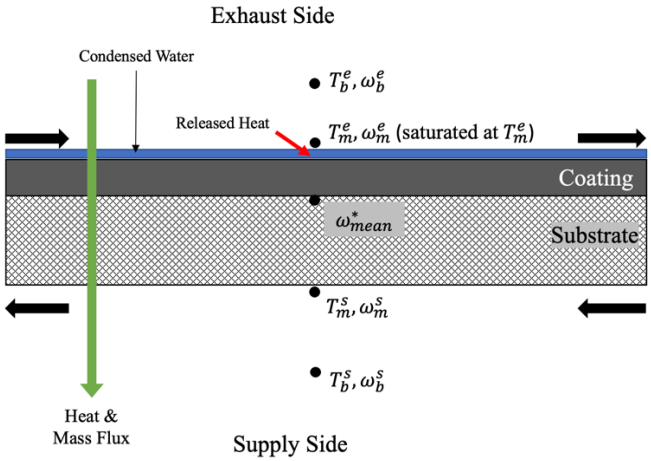

b)

Figure 4.2) Heat and mass flows from exhaust side downward to supply side. a) The case without condensation b) The case with condensation which results in heat release at the liquid water surface.

As in previous models [67,86], the exchanger is divided into dry (without condensation) and wet (with condensation) regions. In order to develop the condensation model, the following assumptions are made [32,67,86]:

- Steady-state heat and mass transfer.

- Diffusion of vapor and heat conduction in the air stream is negligible relative to the heat and mass convection in the bulk flow.
- Membrane is in equilibrium with the adjacent air.
- Heat and mass transfer in the membrane is one-dimensional through the thickness of the membrane as the thickness of the membrane is much lower than its width and length.
- The effect of the thickness of the condensed water on heat resistance and flow distribution is neglected, as we are only modeling conditions up to the onset of condensation.
- The temperature of the condensed water on the membrane is equal to the surface temperature of the membrane.
- Permeation of liquid water and water vapor in the membrane can be calculated with the same equations [52].

The "resistance in series" analogy for heat and mass transfer is used which is appropriate for steady 1-D transport [32]. Figure 4.3 shows the heat and mass transfer resistance of each medium at the overlap of two channels.

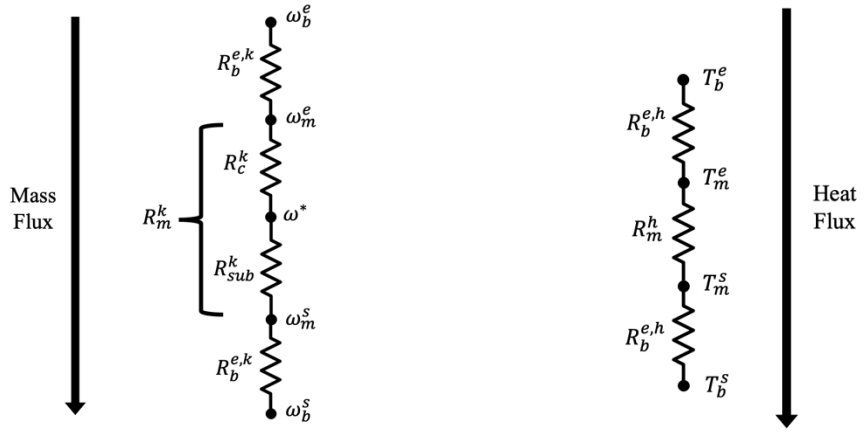

Figure 4.3) Resistance-in-series model in the exchanger for (a) mass transfer and (b) heat transfer

The heat and mass transfer resistances of the bulk flow can be calculated as:

$$R_b^h = \frac{1}{hA} \tag{35}$$

$$R_b^k = \frac{1}{kA} \tag{36}$$

Where, h is the convection heat transfer coefficient of the bulk flow, k is the mass transfer coefficient, A is the effective membrane area and R_b^h and R_b^m denote the heat and mass transfer resistances, respectively. Heat and mass transfer resistances of the membrane can be calculated in a similar way.

The heat transfer resistance R_m^h of the membrane is governed by conduction, and is

$$R_m^h = \frac{t_m}{\lambda A} \tag{37}$$

Here λ is the conductivity of the membrane, A is the effective membrane area and t_m is the thickness of the membrane. This resistance is typically negligible.

Membrane mass transfer resistance can be expressed in terms of its permeability [32]:

$$R_m^k = \frac{t_m}{P_m R_u T} \tag{38}$$

In the above equation, t_m, R_u, T and P_m denote the thickness of the membrane, universal gas constant, temperature and permeability of the membrane.

The transport through the membrane is balanced by convection transport in the bulk flow on each side of the membrane. Heat transfer on the supply and exhaust sides obey the following two equations [26]:

$$\rho^s v^s a C_p^s \frac{\partial T_b^s}{\partial y} + 2h(T_b^s - T_m^s) = 0 \tag{39}$$

$$\rho^e v^e a C_p^e \frac{\partial T_b^e}{\partial x} + 2h(T_b^e - T_m^e) = 0 \tag{40}$$

Similarly, the mass conservation equations for the supply and exhaust sides are [26]:

$$v^s a\frac{\partial \omega_b^s}{\partial y} + \ 2k(\omega_b^s - \omega_m^s) = 0 \tag{41}$$

$$v^e a\frac{\partial \omega_b^e}{\partial x} + \ 2k(\omega_b^e - \omega_m^e) = 0 \tag{42}$$

The boundary conditions at the membrane must be specified differently for dry and condensing portions of the energy exchanger. For dry regions [26]:

$$\frac{(T_b^e - T_m^e)}{R_b^{e,h}} + \dot{m}_{wv}L = \ \frac{(T_m^e - T_m^s)}{R_m^h} \tag{43}$$

$$\frac{(T_m^e - T_m^s)}{R_m^h} - \dot{m}_{wv}L = \ \frac{(T_m^s - T_b^s)}{R_b^{s,h}} \tag{44}$$

$$\frac{(\omega_b^e - \omega_m^e)}{R_b^{e,k}} = \ \frac{(\omega_m^e - \omega_m^s)}{R_m^k} \tag{45}$$

$$\frac{(\omega_m^e - \omega_m^s)}{R_m^k} = \ \frac{(\omega_m^s - \omega_b^s)}{R_b^{s,k}} \tag{46}$$

$$\dot{m}_{wv} = \ \frac{(\omega_m^e - \omega_m^s)}{R_m^k} \tag{47}$$

For condensation regions, due to condensation equation (43) becomes:

$$\frac{(T_b^e - T_m^e)}{R_b^{e,h}} + \dot{m}_{wv}L + \dot{m}_{cond}L = \ \frac{(T_m^e - T_m^s)}{R_m^h} \tag{48}$$

Where $\dot{m}_{cond}$ can be calculated from the following equation [67]:

$$\dot{m}_{cond} = \frac{\left(\omega_b^e - \omega_m^e(saturated\ at\ T_m^e)\right)}{R_b^{e,k}} \tag{49}$$

Additionally, equation (45) becomes:

$$\frac{\left(\omega_b^e - \omega_m^e(saturated\ at\ T_m^e)\right)}{R_m^k} = \frac{(\omega_m^s - \omega_m^e)}{R_b^{s,k}} \quad (50)$$

The heat and mass transfer convection coefficients, which govern transport from the bulk flow to the membrane or the condensed water film, are calculated according to [32]. A Nusselt correlation for developing flow in non-circular ducts is used [107].

$$Nu(Z^*) = \left[\left(\frac{C_4 f(Pr)}{\sqrt{Z^*}}\right)^m + \left(\left(C_2 C_3 \left(\frac{fRe}{Z^*}\right)^{1/3}\right)^5 + \left(C_1\left(\frac{fRe}{8\sqrt{\pi}\epsilon^{\Upsilon}}\right)\right)^5\right)^{m/5}\right]^{1/m} \quad (51)$$

In the above equation, constants C_1 to C_4 are specific to the boundary condition and the type of Nusselt number. m is called the blending parameter and is defined by the following equation:

$$m = 2.27 + 1.65Pr^{1/3} \quad (52)$$

ϵ is the aspect ratio of the triangular channel

$$\epsilon = \frac{a}{b} \quad (53)$$

where, a is the height of the triangular channel and b is its base. Υ is the shape factor and for an isosceles triangle with a height shorter than its base $\Upsilon = -0.3$. Finally, Z^* is a non-dimensional length defined by:

$$Z^* = \frac{Z/L}{Re\ Pr} \quad (54)$$

Where L is the square root of channel cross-sectional area, Pr is the Prandtl number, $Re = \frac{\rho v \mathrm{L}}{\mu}$ is the Reynolds number and Z is the streamwise location in the channel. In order to minimize the error in the estimation of the Nusselt number, the coefficients in equation (51) are chosen for uniform wall temperature and the Nusselt is calculated locally. The local heat transfer coefficient is then given by:

$$h(Z^*) = \frac{Nu(Z^*)\lambda_{air}}{L} \quad (55)$$

The heat and mass transfer analogy and the calculated heat transfer coefficient are then used to estimate the mass transfer coefficient:

$$k(Z^*) = \frac{h(Z^*)}{Le^{2/3} C_p} \tag{56}$$

In the above equation, *Le* is the Lewis number, which is assumed to be 0.85 [103]. Zhang et al. [108], showed that the existence of metal surfaces, which act like fins, between the channels in an energy exchanger can significantly affect the analogy between heat and mass transfer. The surfaces are highly conductive to heat whereas they are almost impermeable to water vapor. As a result, different boundary conditions apply to heat and mass transfer in the channels.

In order to account for the fin effect, Engarnevis et al. [32] used correction factors to modify the constants C_1 to C_3 in equation (51). Their correction factor, C_f, is defined as:

$$C_f = \frac{Nu_{fin}}{Nu_{no\ fin}} \times \frac{L}{d_h} \tag{57}$$

In the above equation, d_h is the hydraulic diameter of the channel $\left(\frac{4 \times Area}{Perimeter}\right)$, Nu_{fin} is the Nusselt number extracted from [109] and $Nu_{no\ fin}$ is the Nusselt number calculated from equation (51). To calculate the correction factor for the heat transfer coefficient, $Nu_{no\ fin}$ is extracted from the data for the infinitely conductive fins while for the mass transfer coefficient it is extracted from the data for the non-conductive (adiabatic) fin.

4.2.3 Empirical Membrane Resistance Model

The properties of the T4 membrane used in the energy exchanger investigated in this chapter are extensively investigated in [1,23] and Chapter 2. The T4 membrane, manufactured by CORE Energy Recovery Solutions has a total thickness of about 110 microns and is made up of a thin (<5 microns) layer of a polyether-polyurethane copolymer coated on one surface of a microporous silica polyethylene substrate [24]. In the exchanger used in this study, the dense coating layer is faced towards the exhaust flow while the substrate layer is in contact with the supply flow. As explained in Chapter 2, the membrane permeability is measured at dry conditions at 3 different temperatures (5°C, 35°C and 50°C) at different combinations of feed and sweep humidity in the range of 0% to 95%. It is shown that the permeability is a function of temperature, the humidity of both feed (higher humidity) and sweep (lower humidity) flows and the orientation of the membrane (which side of the membrane – porous substrate or dense coating layer – is in contact with the flow with higher humidity). In that paper it is demonstrated that the dependence of the

permeability on the orientation and separate feed and sweep humidity is removed if the average relative humidity experienced by the coating layer is considered. Therefore, in this study the average humidity of the coating layer is calculated and used for estimating the permeability of the composite membrane. In order to calculate the average relative humidity experienced by the coating layer, the permeability of the substrate layer of the T4 composite membrane reported in Chapter 2 is used (2.1x 10^6 Barrer at 50 °C and 50% RH). As explained by Engarnevis et al. [32], the resistance-in-series model can also be used for the composite membranes. In this model, the coating and substrate layers of a composite membrane act similar to series of resistances, where the resistance of each layer is determined by its permeability. The mass transfer resistance of the substrate layer can be calculated as:

$$R_{sub}^{k} = \frac{t_{sub}}{P_{sub} R_u T} \tag{58}$$

Where, t_{sub} is the thickness of the substrate layer and P_{sub} is its permeability. Using the resistance of the substrate layer, the moisture content at the interface of the coating and substrate layer (ω^*) can be calculated as:

$$\omega^* = \omega_m^s + \dot{m}_{wv} R_{sub}^{k} \tag{59}$$

The mean moisture content experienced by the membrane can then be calculated by:

$$\omega_{mean} = \frac{\omega^* + \omega_m^e}{2} \tag{60}$$

Finally, the mean relative humidity experienced by the coating can be calculated using the following equation [110]:

$$RH_{mean} = \frac{\omega_{mean} P}{(0.622 + \omega_{mean}) p_g} \times 100 \tag{61}$$

Since the thickness of the membrane is very small, the temperature difference across the membrane is insignificant and the saturated water vapor pressure, p_g in equation (61) is calculated at the average temperature of the two sides of the membrane.

Figure 4.4 shows the resistance of the composite membrane, at 5°C and 35°C, as a function of the mean relative humidity experienced by the coating layer, calculated using equation (38) and the permeability data in Chapter 2. In order to simplify subsequent calculations, second degree

polynomials are fitted to the membrane resistance data for each temperature. To calculate the resistance of the membrane at any temperature and mean coating relative humidity, the resistance at the required mean coating relative humidity is calculated using the polynomial equations shown in Figure 4.4 for 5°C and 35°C, then the resistance at the required temperature is calculated by linearly interpolating or extrapolating the resistance values at 5°C and 35°C.

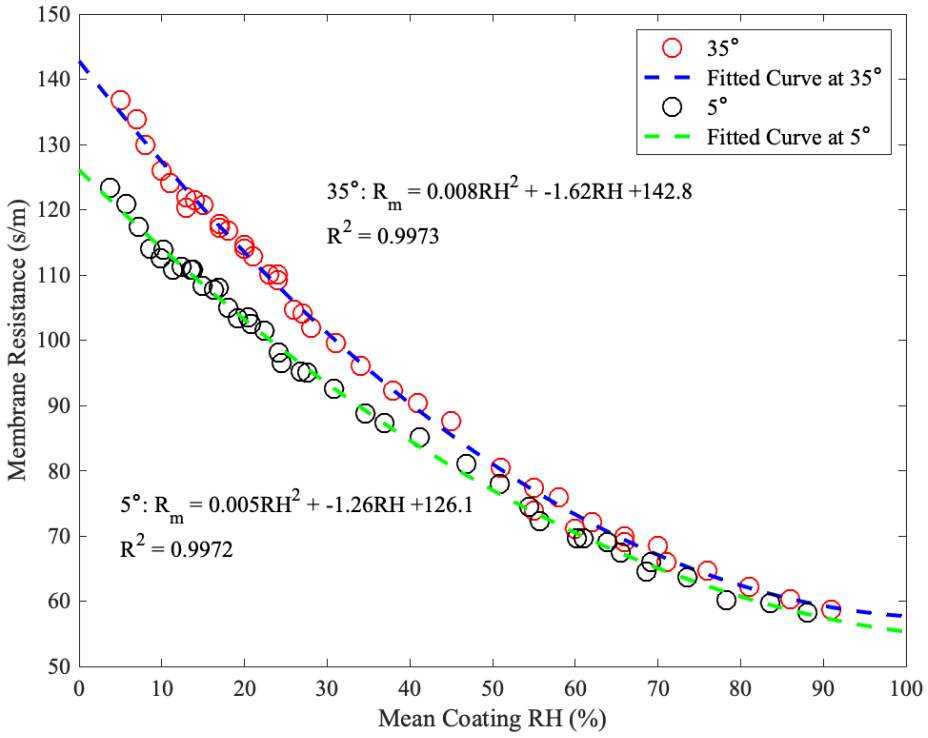

Figure 4.4) Membrane resistance as a function of mean coating RH at 5°C and 35°C

The permeability of the membrane to liquid water and water vapor can be different and therefore measurement of the permeability of the membrane to liquid water is required. The same test setup and procedure as explained in Chapter 2 is used for the liquid water permeability measurements. Figure 4.5 shows the schematic of the moisture transfer test cell in liquid water permeability measurements. As is indicated in the figure, a flow of liquid water (replacing the feed flow in Chapter 2) and a dry sweep flow pass over the membrane in the test cell, where water permeates through the membrane and humidifies the sweep flow.

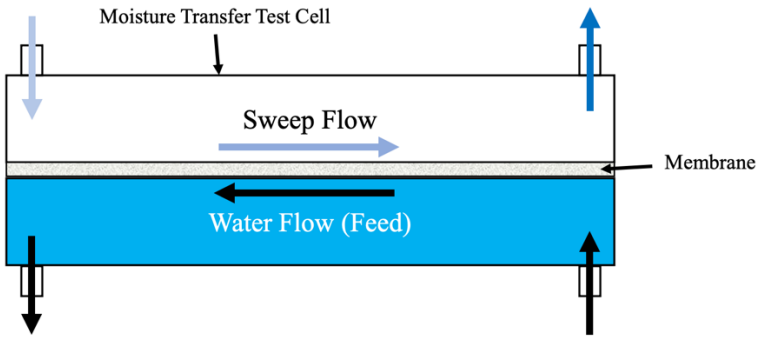

Figure 4.5) Moisture transfer test cell of Chapter 2 used for liquid water permeability measurements

Baker [52] explains that the permeation process of any liquid at temperature T through a membrane is the same as the permeation of its saturated vapor at temperature T and the same equations can be used for calculating the permeability in both scenarios. As a result, the same equations and procedure used in Chapter 2 for water vapor are used to calculate the permeability for liquid water while the water vapor pressure at the surface of the membrane in the feed side is assumed to be the saturation pressure at T.

The permeability of the composite membrane for liquid water is measured at 5°C and 35°C and the results are compared with the permeability of the membrane for water vapor at coating mean relative humidity of 97% in Table 4.1. Since in the studied exchanger the dense coating layer of the membrane is in contact with the exhaust flow, condensation only occurs at the surface of the coating layer. As a result, the permeability values are only reported for the condensation on dense coating layer scenario.

Table 4.1) Permeability (in 10^6 Barrer) of the membrane for liquid water (on dense coating layer) and water vapor

Permeant / Temperature (°C)	Water vapor, mean coating RH 97%	Liquid water
5	2.37	9.95
35	2.12	8.69

As is indicated in the table, the permeability of the membrane to liquid water is significantly higher than to water vapor. In the model, the permeability of the membrane for liquid water at any temperature is calculated by interpolating or extrapolating using the values at 5°C and 35°C.

4.2.4 Iterative Solution Procedure

For solving the differential equations (39) to (42), the forward finite difference method is used. The solution procedure is as follows:

1. Initialize the temperature and humidity fields in both supply and exhaust sides and the resistance of the membrane.
2. Assume dry conditions, calculate humidity and temperature at the surfaces of the membrane using equations (43) to (47).
3. Modify the resistance of the membrane using the surface values calculated in step 2.
4. Repeat steps 2 to 4 until the membrane resistance and the surface values are converged.
5. If the dew point temperature at the surface of the membrane at the exhaust side is lower than the calculated surface temperature $\left(T^{e}_{dew,m} < T^{e}_{m}\right)$, update the temperature and humidity of both bulk streams using equations (39) to (42) and skip to step 9 .
6. If the dew point temperature at the surface of the membrane at the exhaust side is equal to or higher than the calculated surface temperature $\left(T^{e}_{dew,m} \geq T^{e}_{m}\right)$, assume wet conditions.
7. Calculate humidity and temperature at the surfaces of the membrane using equations (43) to (50) and membrane resistance for liquid water in Table 1.
8. Update the temperature and humidity of both bulk streams using equations (39) to (42).
9. Repeat steps 2 to 8 for all of the grid until the temperature and humidity fields in both supply and exhaust bulk flows converge.

The effect of grid size on the accuracy of the results was tested by changing the grid size from 196 (assuming two adjacent channels as one) to 784 and a maximum difference of 0.1% was observed. After the temperature and humidity fields in the exchanger are determined, performance factors of the exchanger can be calculated. Sensible and latent effectiveness are usually calculated using the average temperature and humidity of the supply and exhaust flows; however, in this study, to facilitate the comparison of the heat and mass transfer in the supply and exhaust flows, the effectiveness values for supply and exhaust sides are calculated separately from equations (30) to (33).

4.3 Results and Discussion

4.3.1 Model Validation

In order to validate the model, the measured sensible and latent effectiveness of the supply and exhaust sides in the experiments performed on the same exchanger in Chapter 3 are used (Figure 4.6). The inlet temperature and humidity of the supply flow of the exchanger for all of the graphs in Figure 4.6 are 4°C and 78%, respectively. The flowrate in Figure 4.6a and 4.6c is 90 CFM while in Figure 4.6b it is 60 CFM. The exhaust inlet temperature in Figure 4.6a and Figure 4.6b is 25°C

while it is 20°C in Figure 4.6c. As is indicated in the figure, the predictions of the model are quite consistent with the experimental results; an RMS difference of 2.1% exists between the measured and predicted sensible and latent effectiveness values. Furthermore, the predicted onset of condensation based on both sensible and latent effectiveness curves is consistent with the onset implied by the experimental results.

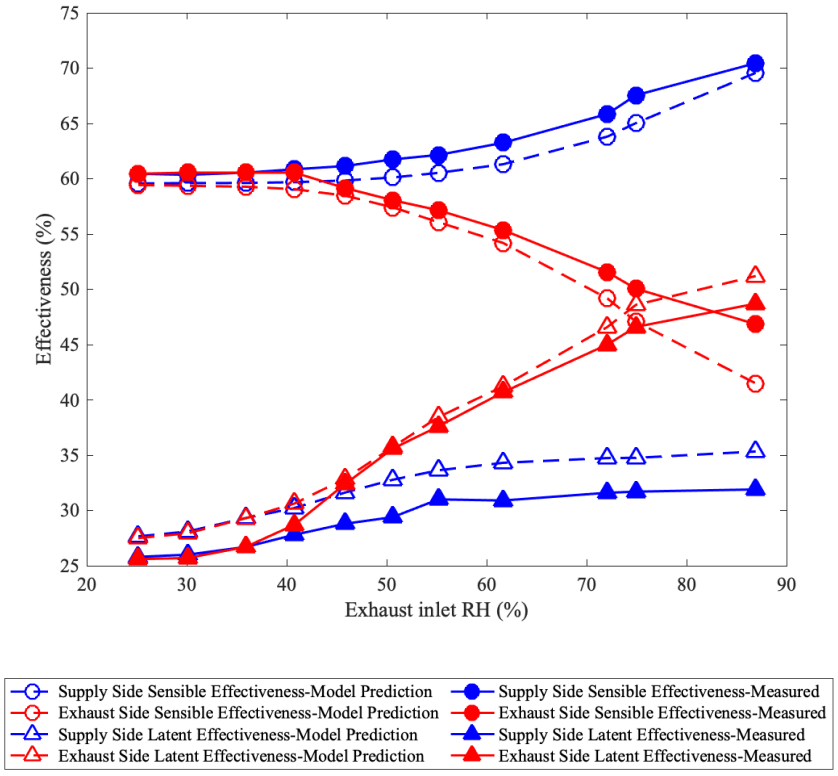

a) Flowrate 90 CFM, Exhaust inlet temperature 25°C

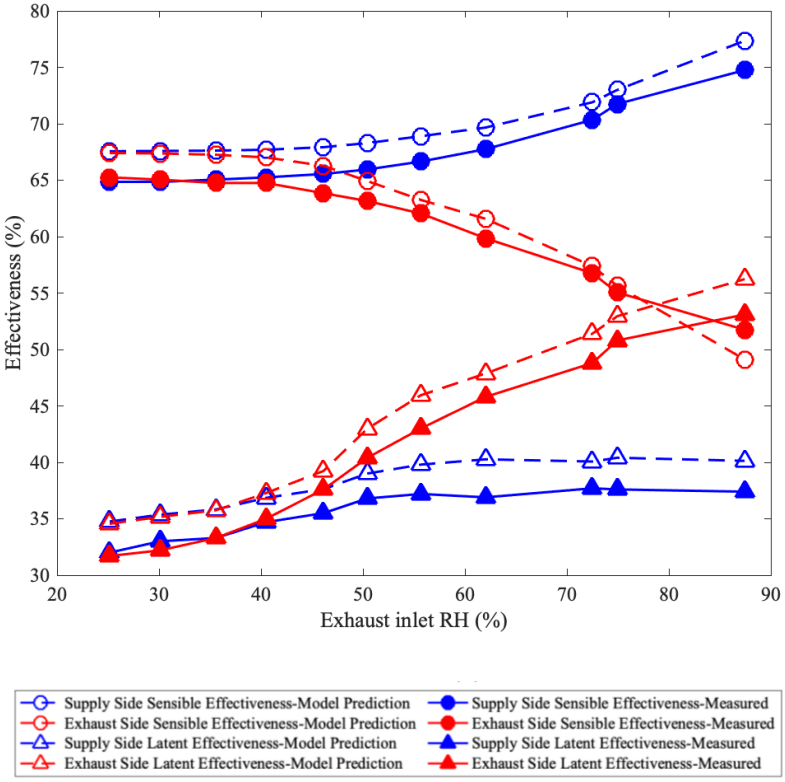

b) Flowrate 60 CFM, Exhaust inlet temperature 25°C

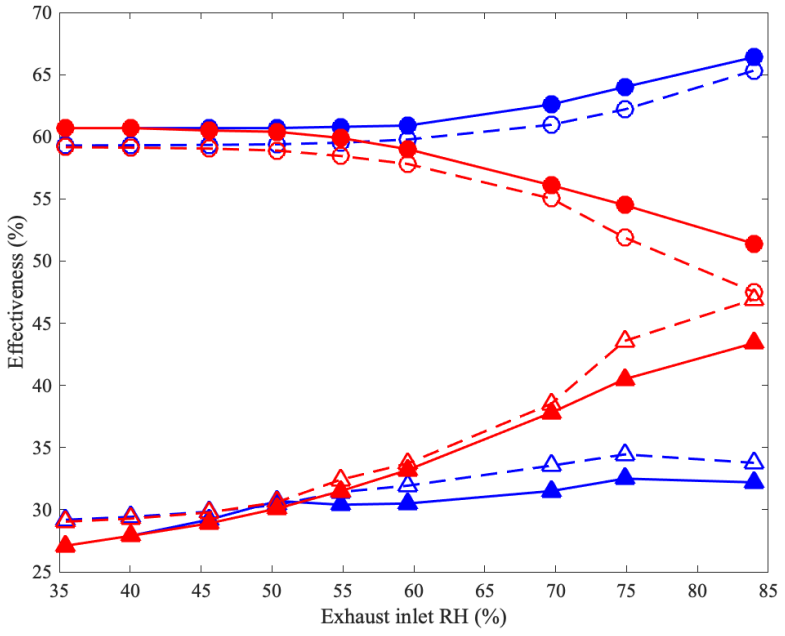

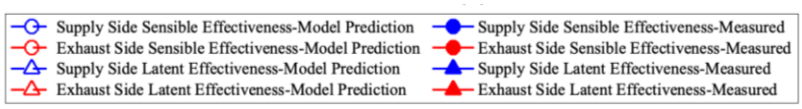

c) Flowrate 90 CFM, Exhaust inlet temperature 20°C

Figure 4.6) Validation of the model (dashed curves) with experimental results from Chapter 3 (solid lines), supply inlet temperature = 4 ℃, supply inlet relative humidity = 78%.The divergence of supply and exhaust

If an energy exchanger is operated at steady state without condensation, conservation of energy requires that the sensible and latent effectiveness of the supply and exhaust sides be equal. Figure 4.6 shows that at low exhaust inlet relative humidity the sensible and latent effectiveness of the supply and exhaust sides are indeed equal. At high exhaust inlet relative humidity, however, the sensible and latent effectiveness of the two sides diverge; the point at which the effectiveness curves of the two sides diverge can be assumed to be the onset of condensation. When determining the onset of condensation from the sensible and latent effectiveness graphs, however, it should be noted that in addition to the uncertainties in the measured effectiveness values, temperature and humidity values also have uncertainties (±0.1°C, ±0.06 gr/kg). Comparing equations (43) and (48), it is evident that the occurrence of condensation releases extra heat in the exchanger which eventually further increases the outlet temperature of both supply and exhaust sides. Based on equations (30) and (31), this increase in temperature increases the sensible effectiveness of the supply side and decreases the sensible effectiveness of the exhaust side. The latent effectiveness of both supply and exhaust sides increases with increasing relative humidity of the exhaust inlet for dry supply conditions. This is due to the fact that, as is indicated in Figure 4.4, the mass transfer resistance of the composite membrane decreases with increasing mean coating relative humidity. As a result, more water vapor is extracted from the exhaust side and is transferred to the supply side, which increases the latent effectiveness of both flows. Increasing the exhaust inlet relative humidity increases the supply and exhaust latent effectiveness even with the occurrence of condensation, but the exhaust side latent effectiveness increases more significantly. This inequality can be attributed to the fact that water starts to accumulate in the exhaust side of the exchanger and not all of the condensed water permeates through the membrane and as a result, the latent effectiveness of the two sides are unequal. The increase in the supply and exhaust side latent effectiveness even after the occurrence of condensation can also be explained by the effect of humidity on the mass transfer resistance of the membrane. Increasing humidity experienced by the membrane decreases the membrane resistance in the region without condensation, moreover, as is shown in Figure 4.4, the permeability of the composite membrane for liquid water is much higher than for water vapor. As a result, the overall mass transfer resistance of the membrane decreases after condensation, which increases the water vapor transfer rate in the exchanger and the latent effectiveness of both sides.

4.3.2 Effect of Variations in Permeability

In order to investigate the effect of the dependence of membrane permeability on humidity and temperature and the phase of water (vapor or liquid), the permeability of the membrane is assumed constant and equal to its value at 10°C and 50% mean coating relative humidity. Using this constant permeability for the membrane in the model, the performance factors of the exchanger under the operating conditions of 4.6c (supply inlet temperature = 4°C, supply inlet relative humidity = 78%, exhaust inlet temperature = 20°C, Flowrate = 90 CFM) are calculated and compared in Figure 4.7 with the variable permeability predictions.

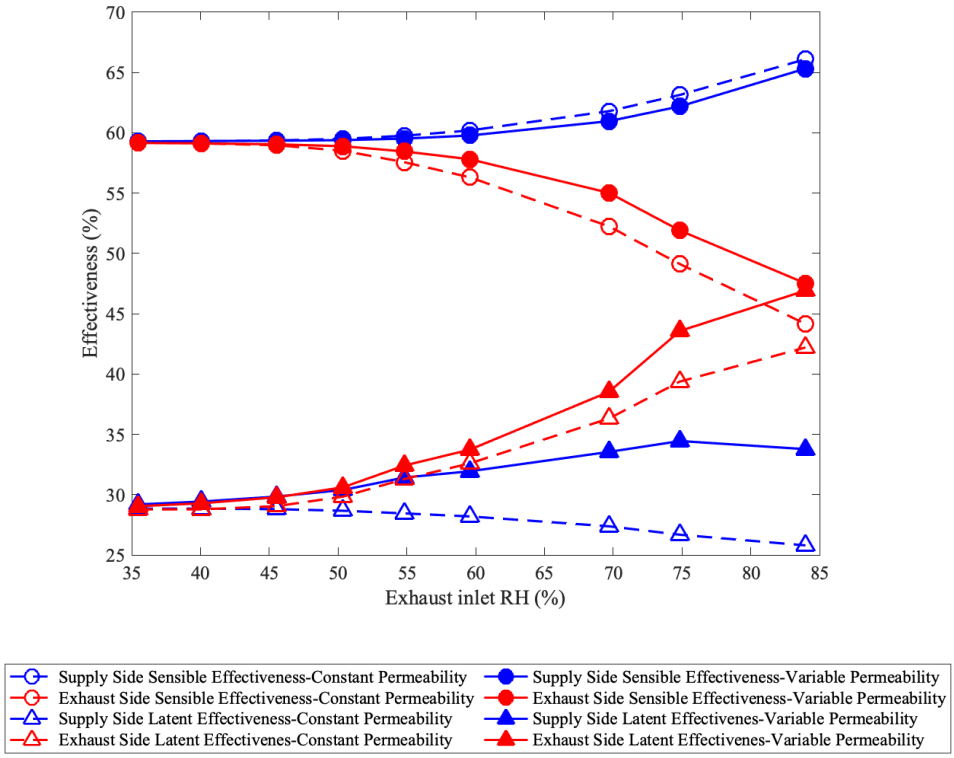

Figure 4.7) Predicted sensible and latent effectiveness with constant permeability (dashed lines) and variable permeability (solid lines), supply inlet temperature = 4 ℃, supply inlet relative humidity = 78%, exhaust inlet temperature = 20 ℃, Flowrate = 90 CFM (Figure 4.6c).

The constant permeability assumption does not significantly affect the predicted sensible effectiveness at low exhaust inlet relative humidity although at high exhaust inlet relative humidity it can result in higher RMS errors of up to 4%. Similarly, at low exhaust inlet relative humidity, the predicted latent effectiveness of both supply and exhaust sides with constant and variable

membrane permeability assumptions are almost equal. At higher exhaust inlet relative humidity, the latent effectiveness of the exhaust side with constant permeability has the same trends as the variability case, although its predicted value can have RMS errors of up to 6%. The constant permeability assumption has the most significant impact on the supply side latent effectiveness. With this assumption, the latent effectiveness of the supply side slightly decreases with increasing exhaust inlet relative humidity, in contrast with the variable permeability predictions, which shows an increasing trend. As explained in Chapter 2, the occurrence of condensation decreases the moisture content difference between the two sides of the membrane. However, the higher permeability of the membrane for liquid water dominates this lower humidity difference and overall increases the water vapor flux, resulting in higher latent effectiveness. With the assumption of constant membrane permeability, however, the decrease in the moisture content difference is not negated with increased permeability, and as a result the flux of water vapor decreases, which in turn decreases the latent effectiveness of the supply side. Another effect of the constant permeability assumption is on the onset and rate of condensation. The difference between the sensible and latent effectiveness of the two sides is directly related to the rate of condensation. A higher rate of condensation is associated with more released heat, which increases the difference between the sensible effectiveness of the two sides. Furthermore, a higher condensation rate means that more water is extracted from the exhaust side, not all of which permeates to the supply side, leading to an increased difference between the latent effectiveness of the two sides. Figure 4.7 shows that the constant permeability assumption increases the difference between the sensible and latent effectiveness of the two sides, which means that the predicted rate of condensation is higher and as a result the onset of condensation is earlier.

4.3.3 Condensation Limits

As was discussed in section 4.3.1, condensation increases the sensible and latent effectiveness of the supply side. This is actually desirable as energy exchangers are mainly used to precondition the supply side air so higher sensible and latent effectiveness for the supply side means more significant preconditioning of the air. However, as stated in the introduction, condensation can also have harmful effects on the exchanger, especially if the water is not drained properly. As a result, it is necessary to know the operating conditions at which condensation occurs and at what operating conditions condensation is significant enough to require further attention. In this section, the difference between the sensible and latent effectiveness of the supply and exhaust sides is used as a proxy for the significance of condensation in the energy exchanger. The amplitude of the difference between the effectiveness of the two sides is related to the rate of condensation and the point at which the difference becomes more than zero can be assumed to be the onset of condensation. Figure 4.8 shows the effect of indoor air temperature and relative humidity on the occurrence of condensation. The outdoor air temperature and relative humidity are assumed constant at 1.7°C and 81.8%, respectively (AHRI standard winter condition [111]) while the indoor

air temperature and relative humidity vary between 18-30°C and 20-85% and flowrate is 90 CFM. Indoor air comfort zone extracted from [112] is also shown in the figure.

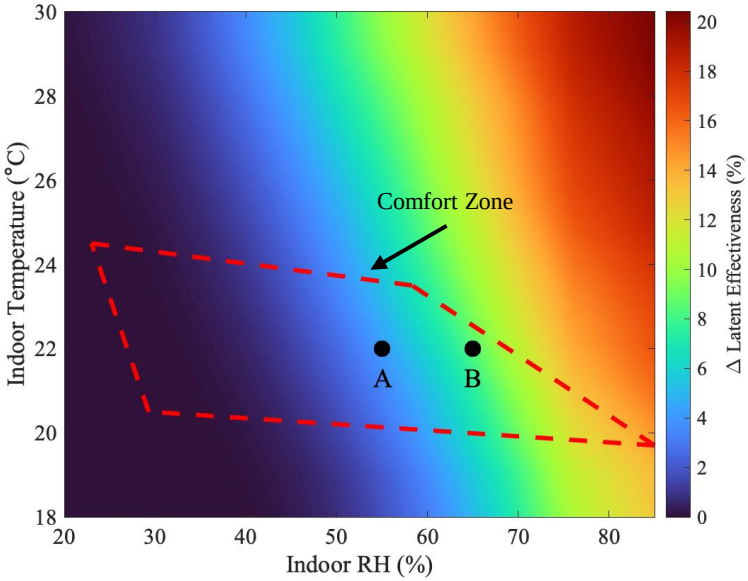

a) ΔLatent effectiveness

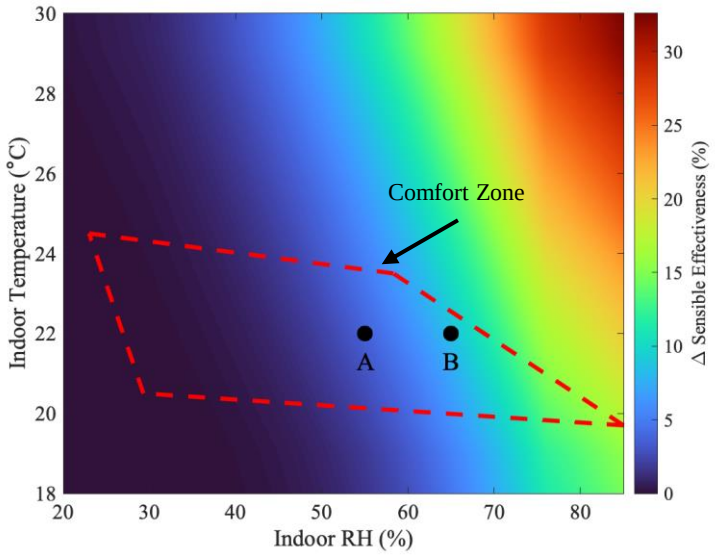

b) ΔSensible effectiveness

Figure 4.8) The effect of indoor air temperature and relative humidity on effectiveness. The outdoor air temperature and relative humidity are assumed to be respectively 1.7℃ and 81.8%. Comfort zone from ASHRAE Standard 55 is indicated on the plots.

Figure 4.8 shows that at most of the comfort zone, condensation either does not occur or is minor and it only becomes significant at high relative humidity. However, it should be noted that although the comfort zone allows for very high humidies, in practice, many ventilation systems do not allow the relative humidity to exceed 50%. Generally, at very low indoor air relative humidity, condensation does not occur for any indoor temperature. As the relative humidity increases, condensation initiates, which results in a positive difference between the sensible and latent effectiveness of the supply and exhaust sides. Additionally, after the start of condensation, increasing the relative humidity increases the magnitude of the difference and thus the significance of condensation. This can be attributed to the fact that when the relative humidity of the exhaust side is increased, so too does the region in which condensation occurs. Figure 4.9 shows the condensation region in the exchanger under the operating conditions shown by points A and B in Figure 4.8.

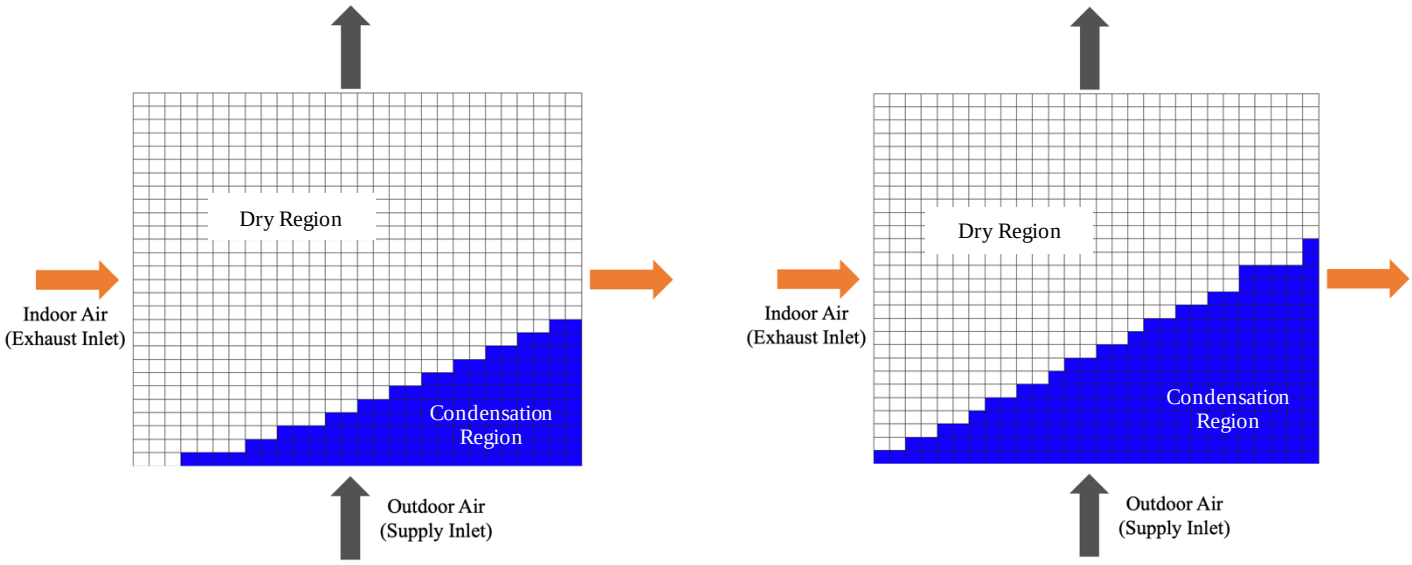

a) A, Exhaust inlet RH 55%

b) B, Exhaust inlet RH 65%

Figure 4.9) The effect of exhaust inlet relative humidity on the condensation area in the exchanger for points A (a) and B (b) in Figure 4.8, supply inlet temperature = 1.7 ℃, supply inlet relative humidity = 81.8%, exhaust inlet temperature = 25 ℃, Flowrate = 90 CFM.

Additionally, increasing the indoor temperature also increases the chances of occurrence of condensation. Finally, Figure 4.8 shows that the impact of condensation on the sensible

effectiveness is more significant than on the latent effectiveness, since the Δsensible effectiveness is larger than the Δlatent effectiveness when condensation occurs.

Condensation in the exchanger at different combinations of indoor and outdoor temperatures is investigated in Figure 4.10. The outdoor and indoor air relative humidity are both assumed constant at 50%, the outdoor and indoor air temperatures vary between 1-10°C and 18-30°C, respectively, and the flowrate is 90 CFM. Thermal comfort zone at indoor relative humidity of 50% extracted from [112] is also shown in the figure.

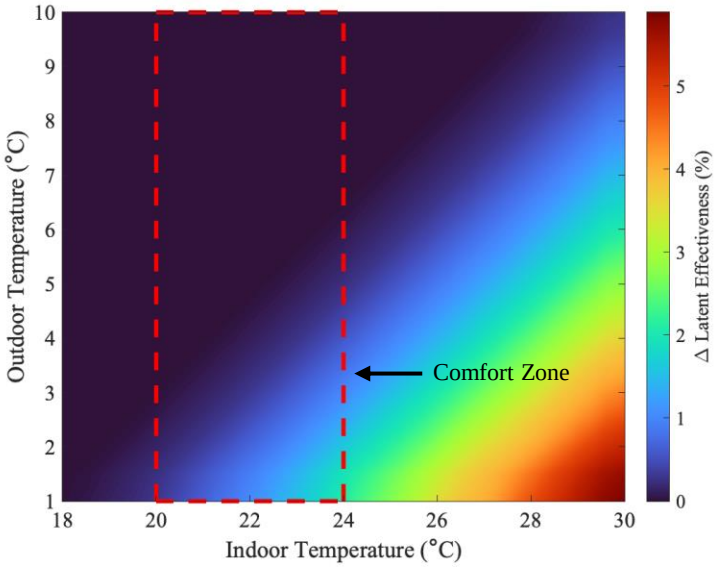

a) ΔLatent effectiveness

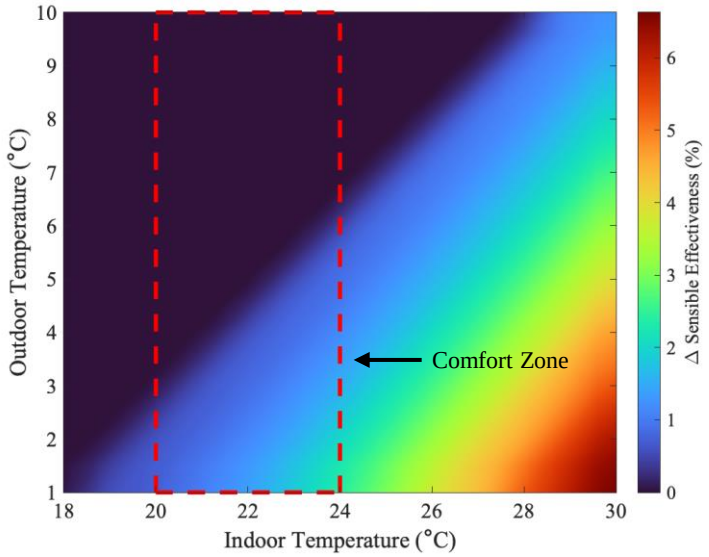

b) ΔSensible effectiveness

Figure 4.10) The effect of indoor and outdoor air temperatures on significance of condensation. The outdoor and indoor air relative humidity are assumed to be 50%. Comfort zone from ASHRAE Standard 55 is indicated on the plots.

Figure 4.10 shows that, at indoor air temperatures within the comfort zone, condensation either does not occur or is minor. Moreover, as expected, increasing the indoor air temperature and decreasing the outdoor air temperature make the energy exchanger more prone to condensation. Furthermore, as also observed in Figure 4.8, the effect of condensation on sensible effectiveness is more significant.

All previous results presented have concerned condensation in winter conditions (heating mode). However, condensation can also occur in summer conditions (cooling mode), but significant condensation in summer requires high temperature and humidity. For instance, the model developed in this study predicts that at an outdoor temperature and relative humidity of 38°C and 85% and an indoor temperature and relative humidity of 24°C and 50%, condensation will occur over 20% of the exchanger which would results in an 8% difference between the sensible effectiveness of the two sides and a 10% difference between the latent effectiveness. It should also be noted that in summer conditions, as condensation occurs at the supply side, unlike winter conditions, the sensible effectiveness of exhaust side is larger than the supply side and the latent effectiveness of the supply side is larger than the exhaust side. A thorough study of condensation in summer conditions is beyond the scope of this work.

4.4 Conclusions

A model for predicting the occurrence of condensation in membrane energy exchangers was developed and validated against experimental measurements. The model considers the variations in the membrane permeability due to temperature, humidity and the phase of the water (gas/liquid) and can predict the performance of the exchanger when condensation occurs. It was shown that the occurrence of condensation increases the sensible effectiveness of the supply side while it decreases the sensible effectiveness of the exhaust side. Condensation increases the latent effectiveness of both supply and exhaust sides. The importance of variations in the membrane permeability was investigated by comparing the results of the original model with the model assuming a constant permeability. Failure to consider the variation in the permeability of the membrane resulted in errors of up to 10% and 13% in the prediction of sensible and latent effectiveness and 25% in prediction of condensation rate. The impact of different operating conditions on condensation was determined. Increasing the indoor temperature and relative humidity increases the likelihood of condensation and the significance of condensation while increasing the outdoor temperature has the opposite effect. It was also shown that at normal building operating temperature and humidity, condensation does not occur or is minor and it only becomes significant if the building is poorly ventilated and the indoor temperature and relative humidity are high. Surprisingly, condensation has a favorable effect on the thermal performance of the membrane energy exchanger in winter conditions because it increases the supply side sensible and latent effectiveness. However, condensation could increase the pressure drop across the exchanger, may enhance the growth of micro-organism, and is associated with frosting at lower temperatures, all of which are undesirable. As a result, ventilation systems using membrane energy exchangers that are at risk of condensation must be carefully designed to properly handle the condensed water.

Chapter 5: Conclusions and Future Work

5.1 Conclusions

In this study, condensation without frost formation in membrane-based energy exchangers was experimentally investigated and a heat and mass transfer model was developed to predict the occurrence of condensation.

In order to better understand the effects of condensation in the exchanger and to increase the validity of the developed model, first, the water vapor permeation properties of two widely used membranes (commercially known as T4 (MX4) and HP2) were studied in Chapter 2. The results of the permeability experiments showed that decreasing temperature and increasing humidity increase the permeability of both membranes. Additionally, the orientation of the membranes also had a significant impact on the permeability, the permeability of both membranes was higher when the dense coating layer of the membrane was in contact with the flow with the higher humidity. Moreover, it was revealed that, unlike the popular notion that only the feed flow humidity determines the permeability of the membrane, the humidity of both feed and sweep flows affect the permeability. This dependence of permeability on orientation and both feed and sweep humidity, however, disappeared when the measured permeability values were reported as a function of the average relative humidity that the dense coating layer experiences. As a result, this new method was proposed as an alternative way for the presentation of permeability measurements. The new method is especially helpful when measurements of different test setups are getting compared or when the measured permeability values are used to develop empirical membrane models.

In Chapter 3, a widely used cross-flow energy exchanger was tested under condensation conditions. It was shown that condensation increases the sensible effectiveness of the supply side while it decreases the sensible effectiveness of the exhaust side. Furthermore, condensation increased the latent effectiveness of both supply and exhaust sides; however, the increase in the latent effectiveness of the exhaust side was more significant. Condensation also affected the pressure drop in the exhaust side at which condensation occurs. It was shown that initially, condensation increases the pressure drop in the exhaust side significantly; however, the increase in pressure drop stops after a while and eventually, the pressure drop reaches a plateau. The channel blockage and increase in pressure drop, however, did not affect the effectiveness significantly.

Due to the limitations of the test setup and the time-consuming nature of the tests conducted in Chapter 3, condensation in ethe exchanger could not be evaluated in a wide range of operating

conditions. As a result, a heat and mass transfer model was developed to predict the occurrence of condensation in a wide range of operating conditions. Moreover, the results of the permeability measurements of Chapter 2 were used to add an empirical membrane model to the heat and mass transfer model. As a result, the model also considered the variations in the permeability of the membrane. The results of the model showed that, failure to include the variations in the permeability of the membrane could result in errors of up to 25% in the predicted condensation rate. Moreover, it could result in errors in the prediction of the operating conditions that result in condensation and the sensible and latent effectiveness of the exchanger under condensation. Finally, the model was used to investigate the occurrence of condensation in a wide range of operating conditions, and it was shown that condensation will only significantly affect the exchanger when the room temperature and humidity are high.

Overall, the results of this study show that condensation has a favorable effect on the thermal performance of the exchanger in winter conditions as it increases the sensible and latent effectiveness of the supply side. However, condensation also increases the pressure drop and if not properly drained, water could accumulate in the recovery ventilation unit or be moved to other sections of the HVAC system. Additionally, condensation in membrane-based energy exchangers will not be significant if the building is properly ventilated and the temperature and humidity of the room is within the comfort zone. All of the abovementioned conclusions are made using the effectiveness values to determine the onset of condensation. However, It should be noted that there are two types of errors in determination of the onset of condensation with sensible and effectiveness values. One is the error in measured effectiveness values and the other one is the error in the temperature and humidity values and both of these uncertainties should be taken into account. Finally, it was shown that the variations in the permeation properties of the membrane media used in energy exchangers could have significant effects on the prediction of the occurrence of condensation. As a result, in all studies that investigate condensation and frost formation in energy exchangers that possess membranes with variable permeability, the variations in permeability should be considered to avoid significant errors.

5.2 Recommendations for Future Work

The permeability presentation method introduced in Chapter 2 is only tested for composite membranes with coating layers that have concentration dependent permeability. In order to further validate this method, it should also be checked for composite membranes with concentration independent permeability dense layer or composite membranes with multiple layers with concentration dependent permeability.

In order to increase the accuracy of the predicted operating conditions that result in condensation, sensible effectiveness, latent effectiveness and pressure drop methods can be used together. This

means that the onset of condensation can be predicted using all 3 methods which is expected to decrease the error in the final predicted condensation operating conditions. The experiments conducted in Chapter 3 were mainly focused on the short-term effects of condensation on the exchanger (onset of condensation) and the long-term effects of condensation such as channel blockage, pressure drop, water leakage from the exchanger or changes in effectiveness were only briefly studied; however, in the actual usage of energy exchangers, condensation might occur for a long time, as a result, this deserves to be investigated in a separate study. For instance, the effect of the direction of exchanger (vertical, horizontal or 45 °) on the progress of pressure drop could be investigated. Additionally, the experiments in this chapter were only conducted in winter conditions; however, condensation could also occur in summer conditions. As a result, the experiments could be repeated for summer operating conditions.

Similar to the experiments, the model developed in Chapter 4 was only focused on the onset of condensation in the exchanger. This model could be extended to investigate the transient effects of condensation such as the accumulation of water in the exchanger which would change the flow distribution and increase the pressure drop. Additionally, the developed model is expected to predict the occurrence of condensation in the exchanger in summer conditions as well; however, the model is only validated with condensation in winter conditions. Thus, the model should also be validated with experimental measurements in summer conditions and be used to find the summer operating conditions that result in condensation.

Bibliography

[1] A. Engarnevis, Impact of humidity, temperature, and particulate fouling on membrane-based energy exchangers, University of British Columbia, 2018. https://doi.org/10.14288/1.0371165.

[2] U. IEA, US Energy Information Administration, International Energy Outlook 2017 Overview, Int. Energy Outlook. (n.d.) 143.

[3] A. Sieminski, Annual energy outlook 2015, US Energy Information Administration. (2015).

[4] E.U.D. Handbook, Natural Resources Canada, June, 2004.

[5] B.E.D. Book, Us department of energy, 2011, 2010.

[6] Ashrae, 2013 ASHRAE Handbook: Fundamentals, Ashrae, 2013.

[7] H. Tsutsumi, S. Tanabe, J. Harigaya, Y. Iguchi, G. Nakamura, Effect of humidity on human comfort and productivity after step changes from warm and humid environment, Building and Environment. 42 (2007) 4034–4042. https://doi.org/10.1016/j.buildenv.2006.06.037.

[8] L.Z. Zhang, J.L. Niu, Energy requirements for conditioning fresh air and the long-term savings with a membrane-based energy recovery ventilator in Hong Kong, Energy. 26 (2001) 119–135.

[9] L. Wang, P. Haves, J. Breshears, The Energy Saving Potential of Membrane-Based Enthalpy Recovery in Vav Systems for Commercial Office Buildings, Lawrence Berkeley National Lab.(LBNL), Berkeley, CA (United States), 2012.

[10] L.-Z. Zhang, Progress on heat and moisture recovery with membranes: From fundamentals to engineering applications, Energy Conversion and Management. 63 (2012) 173–195. https://doi.org/10.1016/j.enconman.2011.11.033.

[11] A. Handbook, HVAC systems and equipment, chapter, 1996.

[12] R. Baker, Future directions of membrane gas-separation technology, Membrane Technology. 2001 (2001) 5–10.

[13] B. Yang, W. Yuan, F. Gao, B. Guo, A review of membrane-based air dehumidification, Indoor and Built Environment. 24 (2015) 11–26.

[14] A.S. ASHRAE, Standard 90.1-2016. Energy standard for buildings except low rise residential buildings, American Society of Heating, Refrigerating and Air-Conditioning Engineers, Inc. (2016).

[15] S. ASHRAE, Standard 189.1-2014 Standard for the Design of High-performance Green Buildings, American Society of Heating, Refrigerating, and Air-Conditioning Engineers. (2014).

[16] M. Rafati Nasr, M. Fauchoux, R.W. Besant, C.J. Simonson, A review of frosting in air-to-air energy exchangers, Renewable and Sustainable Energy Reviews. 30 (2014) 538–554. https://doi.org/10.1016/j.rser.2013.10.038.

[17] H. Lin, S.M. Thompson, A. Serbanescu-Martin, J.G. Wijmans, K.D. Amo, K.A. Lokhandwala, T.C. Merkel, Dehydration of natural gas using membranes. Part I: Composite membranes, Journal of Membrane Science. 413–414 (2012) 70–81. https://doi.org/10.1016/j.memsci.2012.04.009.

[18] H. Sijbesma, K. Nymeijer, R. van Marwijk, R. Heijboer, J. Potreck, M. Wessling, Flue gas dehydration using polymer membranes, Journal of Membrane Science. 313 (2008) 263–276. https://doi.org/10.1016/j.memsci.2008.01.024.

[19] C.A. Scholes, G.W. Stevens, S.E. Kentish, Membrane gas separation applications in natural gas processing, Fuel. 96 (2012) 15–28. https://doi.org/10.1016/j.fuel.2011.12.074.
[20] A. Figoli, S. Simone, Membranes for sustainable food packaging, Membrane Processes for Sustainable Growth. (2013) 101–119.
[21] A. Gugliuzza, E. Drioli, A review on membrane engineering for innovation in wearable fabrics and protective textiles, Journal of Membrane Science. 446 (2013) 350–375. https://doi.org/10.1016/j.memsci.2013.07.014.
[22] K.R. Kistler, E.L. Cussler, Membrane Modules for Building Ventilation, Chemical Engineering Research and Design. 80 (2002) 53–64. https://doi.org/10.1205/026387602753393367.
[23] R.N. Huizing, Electrospun nanofibrous membranes for water vapour transport applications, University of British Columbia, 2017. https://doi.org/10.14288/1.0344019.
[24] R.N. Huizing, Coated membranes for enthalpy exchange and other applications, US9255744B2, 2016. https://patents.google.com/patent/US9255744B2/en (accessed August 5, 2021).
[25] S. Koester, M. Falkenberg, M. Logemann, M. Wessling, Modeling heat and mass transfer in cross-counterflow enthalpy exchangers, Journal of Membrane Science. 525 (2017) 68–76. https://doi.org/10.1016/j.memsci.2016.10.030.
[26] L.Z. Zhang, Y. Jiang, Heat and mass transfer in a membrane-based energy recovery ventilator, Journal of Membrane Science. 163 (1999) 29–38. https://doi.org/10.1016/S0376-7388(99)00150-7.
[27] L.-Z. Zhang, Heat and mass transfer in plate-fin enthalpy exchangers with different plate and fin materials, International Journal of Heat and Mass Transfer. 52 (2009) 2704–2713. https://doi.org/10.1016/j.ijheatmasstransfer.2008.12.014.
[28] W. Yaïci, M. Ghorab, E. Entchev, Numerical analysis of heat and energy recovery ventilators performance based on CFD for detailed design, Applied Thermal Engineering. 51 (2013) 770–780. https://doi.org/10.1016/j.applthermaleng.2012.10.003.
[29] L.-Z. Zhang, Convective mass transport in cross-corrugated membrane exchangers, Journal of Membrane Science. 260 (2005) 75–83. https://doi.org/10.1016/j.memsci.2005.03.029.
[30] L.-Z. Zhang, Numerical study of heat and mass transfer in an enthalpy exchanger with a hydrophobic-hydrophilic composite membrane core, Numerical Heat Transfer, Part A: Applications. 51 (2007) 697–714. https://doi.org/10.1080/10407780600879048.
[31] K. Zaw, M.R. Safizadeh, J. Luther, K.C. Ng, Analysis of a membrane based air-dehumidification unit for air conditioning in tropical climates, Applied Thermal Engineering. 59 (2013) 370–379. https://doi.org/10.1016/j.applthermaleng.2013.05.029.
[32] A. Engarnevis, R. Huizing, S. Green, S. Rogak, Heat and mass transfer modeling in enthalpy exchangers using asymmetric composite membranes, Journal of Membrane Science. 556 (2018) 248–262. https://doi.org/10.1016/j.memsci.2018.03.007.
[33] T.C. Merkel, V.I. Bondar, K. Nagai, B.D. Freeman, I. Pinnau, Gas sorption, diffusion, and permeation in poly(dimethylsiloxane), Journal of Polymer Science Part B: Polymer Physics. 38 (2000) 415–434. https://doi.org/10.1002/(SICI)1099-0488(20000201)38:3<415::AID-POLB8>3.0.CO;2-Z.
[34] S.A. Stern, V.M. Shah, B.J. Hardy, Structure-permeability relationships in silicone polymers, Journal of Polymer Science Part B: Polymer Physics. 25 (1987) 1263–1298. https://doi.org/10.1002/polb.1987.090250607.

[35] R.W. Baker, J.G. Wijmans, Y. Huang, Permeability, permeance and selectivity: A preferred way of reporting pervaporation performance data, Journal of Membrane Science. 348 (2010) 346–352. https://doi.org/10.1016/j.memsci.2009.11.022.
[36] E. Favre, N. Morliere, D. Roizard, Experimental evidence and implications of an imperfect upstream pressure step for the time-lag technique, Journal of Membrane Science. 207 (2002) 59–72. https://doi.org/10.1016/S0376-7388(02)00039-X.
[37] S. Koester, F. Roghmans, M. Wessling, Water vapor permeance: The interplay of feed and permeate activity, Journal of Membrane Science. 485 (2015) 69–78. https://doi.org/10.1016/j.memsci.2015.03.019.
[38] R.S. Prabhakar, R. Raharjo, L.G. Toy, H. Lin, B.D. Freeman, Self-Consistent Model of Concentration and Temperature Dependence of Permeability in Rubbery Polymers, Ind. Eng. Chem. Res. 44 (2005) 1547–1556. https://doi.org/10.1021/ie0492909.
[39] P.M. Hauser, A.D. McLaren, Permeation through and Sorption of Water Vapor by High Polymers, Ind. Eng. Chem. 40 (1948) 112–117. https://doi.org/10.1021/ie50457a032.
[40] M.J. Thundyil, Y.H. Jois, W.J. Koros, Effect of permeate pressure on the mixed gas permeation of carbon dioxide and methane in a glassy polyimide, Journal of Membrane Science. 152 (1999) 29–40. https://doi.org/10.1016/S0376-7388(98)00153-7.
[41] L. Liu, N. Jiang, C.M. Burns, A. Chakma, X. Feng, Substrate resistance in composite membranes for organic vapour/gas separations, Journal of Membrane Science. 338 (2009) 153–160. https://doi.org/10.1016/j.memsci.2009.04.019.
[42] S. Koester, J. Lölsberg, L. Lutz, D. Marten, M. Wessling, On individual resistances of selective skin, porous support and diffusion boundary layer in water vapor permeation, Journal of Membrane Science. 507 (2016) 179–187. https://doi.org/10.1016/j.memsci.2015.12.070.
[43] L. Liu, Y. Chen, S. Li, M. Deng, The Effect of a Support Layer on the Permeability of Water Vapor in Asymmetric Composite Membranes, Separation Science and Technology. 36 (2001) 3701–3720. https://doi.org/10.1081/SS-100108357.
[44] G.Z. Ramon, M.C.Y. Wong, E.M.V. Hoek, Transport through composite membrane, part 1: Is there an optimal support membrane?, Journal of Membrane Science. 415–416 (2012) 298–305. https://doi.org/10.1016/j.memsci.2012.05.013.
[45] G.Z. Ramon, E.M.V. Hoek, Transport through composite membranes, part 2: Impacts of roughness on permeability and fouling, Journal of Membrane Science. 425–426 (2013) 141–148. https://doi.org/10.1016/j.memsci.2012.08.004.
[46] L.-Z. Zhang, A lattice Boltzmann simulation of mass transport through composite membranes, AIChE Journal. 60 (2014) 3925–3938. https://doi.org/10.1002/aic.14564.
[47] R. Huizing, W. Mérida, F. Ko, Impregnated electrospun nanofibrous membranes for water vapour transport applications, Journal of Membrane Science. 461 (2014) 146–160. https://doi.org/10.1016/j.memsci.2014.03.019.
[48] L.-Z. Zhang, Evaluation of moisture diffusivity in hydrophilic polymer membranes: A new approach, Journal of Membrane Science. 269 (2006) 75–83. https://doi.org/10.1016/j.memsci.2005.06.020.
[49] S. Metz, W. Vandeven, J. Potreck, M. Mulder, M. Wessling, Transport of water vapor and inert gas mixtures through highly selective and highly permeable polymer membranes, Journal of Membrane Science. 251 (2005) 29–41. https://doi.org/10.1016/j.memsci.2004.08.036.

[50] A. Gabelman, S.-T. Hwang, Hollow fiber membrane contactors, Journal of Membrane Science. 159 (1999) 61–106. https://doi.org/10.1016/S0376-7388(99)00040-X.
[51] S.J. Metz, Water vapor and Gas Transport through Polymeric Membranes, (2003). https://research.utwente.nl/en/publications/water-vapor-and-gas-transport-through-polymeric-membranes (accessed August 16, 2021).
[52] R.W. Baker, Membrane technology and applications, 3rd ed, John Wiley & Sons, Chichester, West Sussex ; Hoboken, 2012.
[53] J. Min, T. Hu, Moisture permeation through porous membranes, Journal of Membrane Science. 379 (2011) 496–503. https://doi.org/10.1016/j.memsci.2011.06.028.
[54] M. Mulder, Basic Principles of Membrane Technology, Springer Netherlands, Dordrecht, 1991. https://doi.org/10.1007/978-94-017-0835-7.
[55] R.N. Huizing, H. Chen, F.K.B. WONG, Blended membranes for water vapor transport and methods for preparing same, US10139116B2, 2018. https://patents.google.com/patent/US10139116B2/en (accessed August 5, 2021).
[56] H. Czichos, T. Saito, L.E. Smith, Springer Handbook of Metrology and Testing, Springer Science & Business Media, 2011.
[57] A. Stroeks, The moisture vapour transmission rate of block co-poly(ether–ester) based breathable films. 2. Influence of the thickness of the air layer adjacent to the film, Polymer. 42 (2001) 09903–09908. https://doi.org/10.1016/S0032-3861(01)00565-1.
[58] O. Dufaud, E. Favre, L.M. Vincent, A Laboratory for Gaseous Diffusion Through Permeable Solids: The Time Lag, Chemical Engineering Education. 34 (2000) 172–177.
[59] F23 Committee, Test Methods for Water Vapor Diffusion Resistance and Air Flow Resistance of Clothing Materials Using the Dynamic Moisture Permeation Cell, ASTM International, n.d. https://doi.org/10.1520/F2298-03R09E01.
[60] P. Gibson, C. Kendrick, D. Rivin, L. Sicuranza, M. Charmchi, An Automated Water Vapor Diffusion Test Method for Fabrics, Laminates, and Films, Journal of Coated Fabrics. 24 (1995) 322–345. https://doi.org/10.1177/152808379502400407.
[61] R. Huizing, Design and Membrane Selection for Gas to Gas Humidifiers for Fuel Cell Applications, (2007). https://uwspace.uwaterloo.ca/handle/10012/3048 (accessed September 29, 2021).
[62] S. Metz, W. Ven, M. Mulder, M. Wessling, Mixed gas water vapor/N transport in poly(ethylene oxide) poly(butylene terephthalate) block copolymers, Journal of Membrane Science. 266 (2005) 51–61. https://doi.org/10.1016/j.memsci.2005.05.010.
[63] H. Azher, C. Scholes, S. Kanehashi, G. Stevens, S. Kentish, The effect of temperature on the permeation properties of Sulphonated Poly (Ether Ether) Ketone in wet flue gas streams, Journal of Membrane Science. 519 (2016) 55–63. https://doi.org/10.1016/j.memsci.2016.07.015.
[64] R.R.L. Bhopal, Investigation of water vapour permeation and antibacterial properties of nano silver loaded cellulose acetate film, Int. Food Res. J. 17 (2010) 623–639.
[65] O.L. Sprockel, W. Prapaitrakul, P. Shivanand, Permeability of Cellulose Polymers: Water Vapour Transmission Rates, Journal of Pharmacy and Pharmacology. 42 (2011) 152–157. https://doi.org/10.1111/j.2042-7158.1990.tb05375.x.
[66] P.P. Roussis, Diffusion of water vapour in cellulose acetate: 1. Differential transient sorption kinetics and equilibria, Polymer. 22 (1981) 768–773. https://doi.org/10.1016/0032-3861(81)90012-4.

[67] V.I. Deshko, A.Y. Karvatskii, I.O. Sukhodub, Heat and mass transfer in cross-flow air-to-air membrane heat exchanger in heating mode, Applied Thermal Engineering. 100 (2016) 133–145. https://doi.org/10.1016/j.applthermaleng.2016.01.139.
[68] S. Gendebien, S. Bertagnolio, V. Lemort, Investigation on a ventilation heat recovery exchanger: Modeling and experimental validation in dry and partially wet conditions, Energy and Buildings. 62 (2013) 176–189. https://doi.org/10.1016/j.enbuild.2013.02.025.
[69] H. Viitanen, J. Vinha, K. Salminen, T. Ojanen, R. Peuhkuri, L. Paajanen, K. Lähdesmäki, Moisture and bio-deterioration risk of building materials and structures, Journal of Building Physics. 33 (2010) 201–224.
[70] W.J. Fisk, R.E. Chant, K.M. Archer, D. Hekmat, F.J. Offermann, Performance of residential air-to-air heat exchangers during operation with freezing and periodic defrosts, ASHRAE Transactions. 91 (1985) 159–172.
[71] E.P.R.C.B. Bradley, D.R. Fisher, A Model to Compare Freezing Control Stratigies for Residential Air-to-Air Heat Recovery Ventilators, ASHRAE Transactions. 95 (1989) 454–483.
[72] E.G. Phillips, D.R. Fisher, R.E. Chant, P. ENG, B. BRADLEY, Freeze-control strategy and air-to-air energy recovery performance, ASHRAE Journal. 34 (1992) 44–49.
[73] J.Y. Jang, H.H. Bae, S.J. Lee, M.Y. Ha, Continuous heating of an air-source heat pump during defrosting and improvement of energy efficiency, Applied Energy. 110 (2013) 9–16.
[74] J. Zhang, A.S. Fung, Experimental study and analysis of an energy recovery ventilator and the impacts of defrost cycle, Energy and Buildings. 87 (2015) 265–271. https://doi.org/10.1016/j.enbuild.2014.11.050.
[75] K. Park, D. Lee, H.J. Chung, Y. Kim, Performance Improvement of Condensation Reduction and Removal in Heat Recovery Ventilators Using Purge Methods, Energies. 13 (2020) 6152. https://doi.org/10.3390/en13226152.
[76] M. Rafati Nasr, M. Kassai, G. Ge, C.J. Simonson, Evaluation of defrosting methods for air-to-air heat/energy exchangers on energy consumption of ventilation, Applied Energy. 151 (2015) 32–40. https://doi.org/10.1016/j.apenergy.2015.04.022.
[77] J.C. Min, M. Su, L.N. Wang, Experimental and theoretical investigations of membrane-based energy recovery ventilator performance, Int. J. Air-Cond. Ref. 20 (2012) 1150004. https://doi.org/10.1142/S2010132511500040.
[78] Y.P. Zhou, J.Y. Wu, R.Z. Wang, Performance of energy recovery ventilator with various weathers and temperature set-points, Energy and Buildings. 39 (2007) 1202–1210. https://doi.org/10.1016/j.enbuild.2006.12.010.
[79] J. Liu, W. Li, J. Liu, B. Wang, Efficiency of energy recovery ventilator with various weathers and its energy saving performance in a residential apartment, Energy and Buildings. 42 (2010) 43–49. https://doi.org/10.1016/j.enbuild.2009.07.009.
[80] M.Aa. Gjennestad, E. Aursand, E. Magnanelli, J. Pharoah, Performance analysis of heat and energy recovery ventilators using exergy analysis and nonequilibrium thermodynamics, Energy and Buildings. 170 (2018) 195–205. https://doi.org/10.1016/j.enbuild.2018.04.013.
[81] J. Ko, J. Park, J.-W. Jeong, Energy saving potential of a model-predicted frost prevention method for energy recovery ventilators, Applied Thermal Engineering. 185 (2021) 116450. https://doi.org/10.1016/j.applthermaleng.2020.116450.

[82] M. Jafarizave, A. Khaleghi, M. Rezakazemi, Development of CFD model for membrane-based energy recovery ventilators, Chemical Engineering Research and Design. 145 (2019) 226–234. https://doi.org/10.1016/j.cherd.2019.03.019.
[83] R. Al-Waked, D. Bani Mostafa, M.S. Nasif, Performance of energy recovery ventilators under different climatic regions, Energy Efficiency. 14 (2020) 8. https://doi.org/10.1007/s12053-020-09917-w.
[84] H. Han, K. Kim, K.-J. Jang, G.-S. Han, I.-B. Lee, Energy Consumption and Indoor Environment of Broiler Houses with Energy Recovery Ventilators, Applied Engineering in Agriculture. 29 (2013) 751–759. https://doi.org/10.13031/aea.29.9968.
[85] S.-H. Nam, H. Han, Computational modeling and experimental validation of heat recovery ventilator under partially wet conditions, Applied Thermal Engineering. 95 (2016) 229–235. https://doi.org/10.1016/j.applthermaleng.2015.11.023.
[86] S. Anisimov, A. Jedlikowski, D. Pandelidis, Frost formation in the cross-flow plate heat exchanger for energy recovery, International Journal of Heat and Mass Transfer. 90 (2015) 201–217. https://doi.org/10.1016/j.ijheatmasstransfer.2015.06.056.
[87] R.B. Holmberg, Sensible and Latent Heat Transfer in Cross-Counterflow Gas-To-Gas Heat Exchangers, Journal of Heat Transfer. 111 (1989) 173–177. https://doi.org/10.1115/1.3250640.
[88] Y. Mercadier, T. Duong, F. Lagace, Dynamic performance of a cross flow heat recovery ventilator operating under frost conditions, in: Proceedings of the Fourth International Symposium on Thermal Engineering and Science for Cold Regions, 1993: pp. 113–121.
[89] T.R. Nielsen, J. Rose, J. Kragh, Dynamic model of counter flow air to air heat exchanger for comfort ventilation with condensation and frost formation, Applied Thermal Engineering. 29 (2009) 462–468. https://doi.org/10.1016/j.applthermaleng.2008.03.006.
[90] B.-H. Jeon, J.-W. Kim, S.-K. Lee, Y.-J. Lee, Y.-C. Ahn, A study on the dew condensation according to the operational conditions of a heat-recovery ventilator, Korean Journal of Air-Conditioning and Refrigeration Engineering. 25 (2013) 529–533.
[91] J. Rose, T.R. Nielsen, J. Kragh, S. Svendsen, Quasi-steady-state model of a counter-flow air-to-air heat-exchanger with phase change, Applied Energy. 85 (2008) 312–325. https://doi.org/10.1016/j.apenergy.2007.07.009.
[92] P. Liu, M. Rafati Nasr, G. Ge, M. Justo Alonso, H.M. Mathisen, F. Fathieh, C. Simonson, A theoretical model to predict frosting limits in cross-flow air-to-air flat plate heat/energy exchangers, Energy and Buildings. 110 (2016) 404–414. https://doi.org/10.1016/j.enbuild.2015.11.007.
[93] M. Rafati Nasr, F. Fathieh, D. Kadylak, R. Huizing, R.W. Besant, C.J. Simonson, Experimental methods for detecting frosting in cross-flow air-to-air energy exchangers, Experimental Thermal and Fluid Science. 77 (2016) 100–115. https://doi.org/10.1016/j.expthermflusci.2016.04.009.
[94] Z.J. Shen, J.C. Min, Outdoor air state that may cause moisture condensation in membrane-type total heat exchangers using different membrane materials, Energy Reports. 6 (2020) 227–233. https://doi.org/10.1016/j.egyr.2019.08.049.
[95] Free Online Interactive Psychrometric Chart, (n.d.). http://www.flycarpet.net/en/psyonline (accessed October 10, 2021).
[96] J. Fernández-Seara, R. Diz, F.J. Uhía, A. Dopazo, J.M. Ferro, Experimental analysis of an air-to-air heat recovery unit for balanced ventilation systems in residential buildings, Energy

Conversion and Management. 52 (2011) 635–640. https://doi.org/10.1016/j.enconman.2010.07.040.
[97] Y. Zhang, Y. Jiang, L.Z. Zhang, Y. Deng, Z. Jin, Analysis of thermal performance and energy savings of membrane based heat recovery ventilator, Energy. 25 (2000) 515–527. https://doi.org/10.1016/S0360-5442(99)00087-0.
[98] W.J. Fisk, R.E. Chant, K.M. Archer, D. Hekmat, F.J. Offermann, Onset of freezing in residential air-to-air heat exchangers, ASHRAE Transactions. 91 (1985) 145–158.
[99] A.V. Arundel, E.M. Sterling, J.H. Biggin, T.D. Sterling, Indirect health effects of relative humidity in indoor environments., Environmental Health Perspectives. 65 (1986) 351–361.
[100] A. Engarnevis, R. Huizing, S. Green, S. Rogak, Particulate fouling assessment in membrane based air-to-air energy exchangers, Energy and Buildings. 150 (2017) 477–487. https://doi.org/10.1016/j.enbuild.2017.05.046.
[101] L.-Z. Zhang, Heat and mass transfer in a quasi-counter flow membrane-based total heat exchanger, International Journal of Heat and Mass Transfer. 53 (2010) 5478–5486.
[102] L. Zhang, Z. Chen, Convective heat transfer in cross-corrugated triangular ducts under uniform heat flux boundary conditions, International Journal of Heat and Mass Transfer. 54 (2011) 597–605. https://doi.org/10.1016/j.ijheatmasstransfer.2010.09.010.
[103] J. Min, M. Su, Performance analysis of a membrane-based energy recovery ventilator: Effects of outdoor air state, Applied Thermal Engineering. 31 (2011) 4036–4043. https://doi.org/10.1016/j.applthermaleng.2011.08.006.
[104] J. Min, M. Su, Performance analysis of a membrane-based energy recovery ventilator: Effects of membrane spacing and thickness on the ventilator performance, Applied Thermal Engineering. 30 (2010) 991–997. https://doi.org/10.1016/j.applthermaleng.2010.01.010.
[105] M.S. Nasif, R. Al-Waked, M. Behnia, G. Morrison, Modeling of air to air enthalpy heat exchanger, Heat Transfer Engineering. 33 (2012) 1010–1023.
[106] L.Z. Zhang, J.L. Niu, Effectiveness correlations for heat and moisture transfer processes in an enthalpy exchanger with membrane cores, J. Heat Transfer. 124 (2002) 922–929.
[107] Y.S. Muzychka, M.M. Yovanovich, Laminar Forced Convection Heat Transfer in the Combined Entry Region of Non-Circular Ducts, Journal of Heat Transfer. 126 (2004) 54–61. https://doi.org/10.1115/1.1643752.
[108] L.-Z. Zhang, Laminar flow and heat transfer in plate-fin triangular ducts in thermally developing entry region, International Journal of Heat and Mass Transfer. 50 (2007) 1637–1640.
[109] L.-Z. Zhang, Heat and mass transfer in plate-fin sinusoidal passages with vapor-permeable wall materials, International Journal of Heat and Mass Transfer. 51 (2008) 618–629. https://doi.org/10.1016/j.ijheatmasstransfer.2007.04.050.
[110] Y.A. Cengel, M.A. Boles, M. Kanoglu, Thermodynamics: an engineering approach, McGraw-hill New York, 2011.
[111] AHRI Standard 1060 (IP), Performance rating of air-to-air exchangers for energy recovery ventilation equipment, (2013).
[112] ASHRAE Standard 55, Thermal environmental conditions for human occupancy, American Society of Heating, Refrigerating and Air Conditioning Engineers. (1992).
[113] Thermodynamics: An Engineering Approach, 2018. https://www.mheducation.com/highered/product/thermodynamics-engineering-approach-cengel-boles/M9781259822674.html (accessed August 16, 2021).

[114] J.F. Crifo, Inferences Concerning Water Vapour Viscosity and Mean Free Path at Low Temperatures, Astronomy and Astrophysics. 223 (1989) 365.
[115] W. Sutherland, LII. The viscosity of gases and molecular force, The London, Edinburgh, and Dublin Philosophical Magazine and Journal of Science. 36 (1893) 507–531. https://doi.org/10.1080/14786449308620508.
[116] R.B. Montgomery, VISCOSITY AND THERMAL CONDUCTIVITY OF AIR AND DIFFUSIVITY OF WATER VAPOR IN AIR, Journal of the Atmospheric Sciences. 4 (1947) 193–196. https://doi.org/10.1175/1520-0469(1947)004<0193:VATCOA>2.0.CO;2.
[117] P.T. Tsilingiris, Thermophysical and transport properties of humid air at temperature range between 0 and 100°C, Energy Conversion and Management. 49 (2008) 1098–1110. https://doi.org/10.1016/j.enconman.2007.09.015.
[118] N.H. Chen, D.F. Othmer, New Generalized Equation for Gas Diffusion Coefficient., J. Chem. Eng. Data. 7 (1962) 37–41. https://doi.org/10.1021/je60012a011.
[119] J.R. Taylor, An Introduction to Error Analysis: The Study of Uncertainties in Physical Measurements, University Science Books, 1997.

Appendices

Appendix A Measurement of Boundary Layer Resistance

One sample of the resistance vs thickness plots discussed in section 2.2.3 is shown in Figure A.1. In the figure, the error bar on each data point represents the uncertainty of the measured total water vapor resistance for that test and the shaded error bound represents the standard error of estimate for the line regressed to the results. The intercept of the fitted line is the boundary layer resistance and the error of estimate of the intercept is considered to be the uncertainty of the calculated boundary layer resistance.

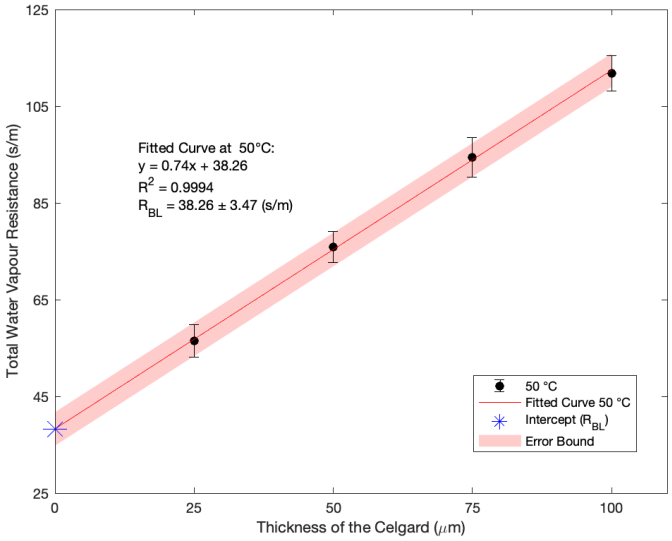

Figure A.1. Sample calculation of the boundary layer resistance at 50 °C and 6 SLPM at both feed and sweep sides.

The calculated boundary layer resistances at 30 °C and 50 °C are summarized in Table A.1.

Table A1. Boundary layer resistance of the test cell at 30 °C and 50 °C at flowrates ranging from 5 to 8 SLPM

	30 °C		50 °C	
Flowrate (SLPM)	Total Boundary Layer Resistance(s/m)	Uncertainty (s/m)	Total Boundary Layer Resistance(s/m)	Uncertainty (s/m)
5	47.10	4.41	44.71	4.87
6	43.46	3.42	38.26	3.47
7	38.00	3.34	34.76	3.30
8	34.60	2.74	33.49	3.00

In order to be able to calculate the mass transfer coefficient of the channels using equation (7), the density and viscosity of the air and the diffusivity of water vapor in air need to be calculated at different temperatures and humidity.

Assuming water vapor and air as ideal gasses, the density of the mixture of air and water vapor can be calculated using the following equation [113]:

$$\rho_{mix} = \frac{p_v}{R_v T} + \frac{p_a}{R_a T} \qquad (A.1)$$

In the above equation, p_v and p_a denote the partial pressures of water vapor and air, respectively. Partial pressure of water vapor can be calculated via the relative humidity of the flow and the partial pressure of air can be calculated using the atmospheric pressure and the partial pressure of water vapor. Furthermore, R_v and R_a are the specific gas constants of water vapour and air and T is the temperature.

The viscosity of the water vapor at temperatures higher than 250 K can be calculated from the following equation [114]:

$$\mu_{H_2O} = \frac{10^{-5}\left(\frac{T}{T_0}\right)^{0.5}}{a_0 + a_1\left(\frac{T}{T_0}\right)^{-1} + a_2\left(\frac{T}{T_0}\right)^{-2} + a_3\left(\frac{T}{T_0}\right)^{-3}} \qquad (A.2)$$

$$T_0 = 647.27,\ \ a_0 = 0.0181583,\ \ a_1 = 0.0177624,\ \ a_2 = 0.0105287,\ \ a_3 = -0.0036744$$

The viscosity of air for 0 K < T < 554 K can also be calculated using the following equation [115]:

$$\mu_{dry\ air} = \mu_0 \frac{T_0 + C}{T + C}\left(\frac{T}{T_0}\right)^{1.5} \qquad (A.3)$$

Where, μ_0 is the reference viscosity at reference temperature T_0 and C is the Sutherland's constant. The values of μ_0, T_0 and C are summarized below [116]:

$$\mu_0 = 1.818 \times 10^{-5}\ \frac{kg\ m}{s}\ ,\ T_0 = 293.15\ K\ , C = 120$$

Finally, using the viscosity of the dry air and water vapor, it is possible to calculate the viscosity of the humid air using the following equations [117]:

$$\mu_{mix} = \frac{(1 - x_v) \cdot \mu_{air}}{(1 - x_v) + x_v \cdot \Phi_{av}} + \frac{x_v \cdot \mu_v}{x_v + (1 - x_v) \cdot \Phi_{av}} \quad (A.4)$$

$$\Phi_{av} = \frac{\left(1 + \left(\frac{\mu_{air}}{\mu_v}\right)^{0.5} \cdot \left(\frac{M_v}{M_{air}}\right)^{0.25}\right)^2}{\left(8\left(1 + \frac{M_{air}}{M_v}\right)\right)^{0.5}} \quad (A.5)$$

$$\Phi_{va} = \frac{\mu_v}{\mu_{air}} \times \frac{M_{air}}{M_v} \times \Phi_{av} \quad (A.6)$$

$$x_v = \frac{p_v}{P} \quad (A.7)$$

In the above equations, μ_{air} and μ_v denote the viscosity of air and water vapour, P denotes the atmospheric pressure and M_{air} and M_v are the molar mass of air and water vapour, respectively.

The diffusivity of water vapor in air for 250K<T<1000K can be calculated using the following equation [118]:

$$D_{wv} = \frac{0.43\left(\frac{T}{100}\right)^{1.81}\left(\frac{1}{M_{air}} + \frac{1}{M_v}\right)^{0.5}}{P\left(\frac{T_{c_v} T_{c_{air}}}{10000}\right)^{0.1406}\left[\left(\frac{V_{c_v}}{100}\right)^{0.4} + \left(\frac{V_{c_{air}}}{100}\right)^{0.4}\right]^2} \quad (A.8)$$

Where T_{c_v} and $T_{c_{air}}$ are critical temperatures of water vapour and air and V_{c_v} and $V_{c_{air}}$ are critical specific volumes of water vapor and air extracted from [113].

Now it is possible to fit equation (7) to the measured boundary layer resistance values and find the constants a and b. The measured boundary layer resistance values at 30 °C are used to find the coefficients in equation (7) and the measured values at 50 °C are used to validate the model. A comparison between the measured boundary layer resistances and the predicted values using the model is made in Table A.2.

Table A.2. Comparison between the experimental results and predicted values by the model

	30 °C				50 °C			
	Experiment		Model[a]		Experiment		Model	
Flowrate (LPM)	Total Boundary Layer Resistance (s/m)	Uncertainty (s/m)	Feed Side Boundary Layer Resistance (s/m)	Sweep Side Boundary Layer Resistance (s/m)	Total Boundary Layer Resistance (s/m)	Uncertainty (s/m)	Feed Side Boundary Layer Resistance (s/m)	Sweep Side Boundary Layer Resistance (s/m)
5	47.10	4.41	23.80	23.82	44.71	4.87	21.8	21.84
6	43.46	3.42	21.32	21.34	38.26	3.47	19.52	19.56
7	38.00	3.34	19.43	19.44	34.76	3.30	17.79	17.82
8	34.60	2.74	17.92	17.93	33.49	3.00	16.41	16.44

[a] Fit parameters for equation (7) at 30 °C: a = 0.07636, b = 0.604, SSE = 3.23

Comparing the predictions of the model at 50 °C with the actual measured values and considering the sum of squared errors for the fitted equation at 30 °C, it is clear that the model predictions are very well compatible with the experimental measurements.

Using the model, it is possible to investigate the effect of temperature, flowrate and relative humidity of the flows on the boundary layer resistance in a wider range. Figure A.2 shows the effect of temperature and flowrate on the resistance of the boundary layer. As expected, increasing temperature and flowrate decreases the boundary layer resistance in the test cell considerably, so, it is important to be able to calculate the boundary layer resistance in different temperatures and flowrates.

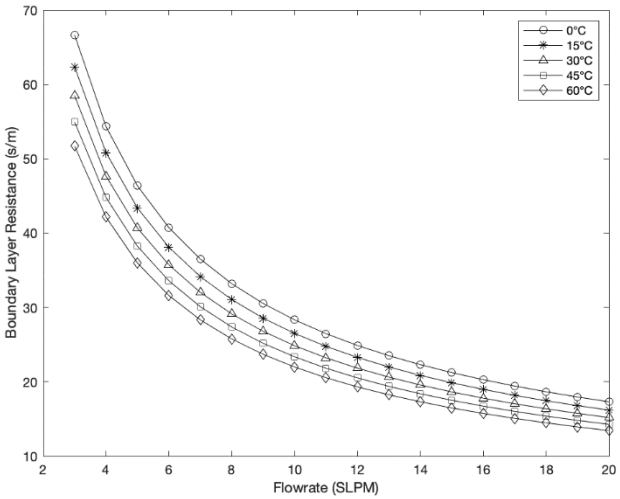

Figure A.2. The effect of flowrate and temperature on the boundary layer resistance

The effect of relative humidity of the flow is indicated in Figure A.3. Although changing the relative humidity of the flow changes some of the properties of the humid air, its effect on the boundary layer resistance is very low.

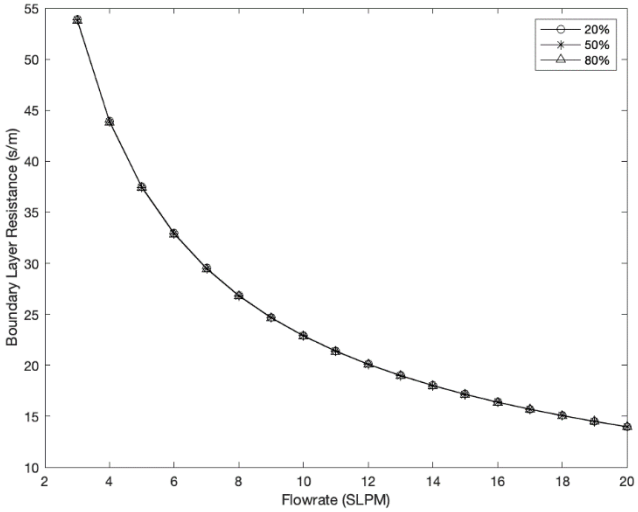

Figure A.3. The effect of RH of the flows on the boundary layer resistance

Appendix B Calculation of Resistance of the Substrate Layer

One of the widely used models for calculation of the water vapor flux through porous materials is the dusty gas model [53]. In this model, three mechanisms are used to explain the transport of water vapor through the porous material. Knudsen and molecular diffusions are considered to act like two resistances in series that together, are in parallel with the resistance representing the Poiseuille flow. Engarnevis et al.[32] used this model to calculate the resistance of the substrate layer in the composite membranes. They assumed that since the pressure difference across the membranes in the enthalpy exchangers is low (which is similar to the test cell of this study) and the coating layer blocks the Poiseuille flow, the term related to this mechanism can be neglected and the flux of water vapor through the substrate layer can be calculated using the following equation:

$$J = \frac{\varepsilon\left(p_v^* - p_{v,m}^s\right)\int_0^\infty \left(\frac{R_u T}{D_{Kn}} + \frac{R_u T}{D_{wv}}\right)^{-1} \varphi\left(d_{pore}\right)\cdot d\left(d_{pore}\right)}{t_{sub}\,\tau \int_0^\infty \varphi\left(d_{pore}\right)\cdot d\left(d_{pore}\right)} \qquad (B.1)$$

In the above equation, D_{Kn} is the Knudsen diffusivity, D_{wv} is the diffusivity of water vapour in air (calculated from equation (A.8), R_u is the universal gas constant, τ is the tortuosity, t_{sub} is the thickness of the substrate layer, ε is the surface porosity of the substrate layer, $\varphi\left(d_{pore}\right)$ is the pore size distribution and p_v^* and $p_{v_m}^{\ s}$ are the water vapor partial pressures at the intersection of the coating and substrate layers (as shown in Figure B.1) and water vapor partial pressure at the open surface of the substrate layer at the sweep side ($p_{v,m}^f$ if the substrate layer is at the feed side), respectively.

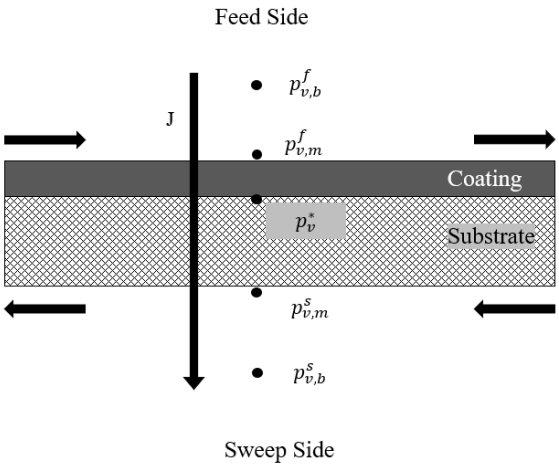

Figure B.1 Distribution of water vapor partial pressure in the test cell for the coating at feed side scenario

Knudsen diffusivity and the surface porosity of the substrate layer can be calculated using the following equations [53]:

$$D_{kn} = \frac{d_{pore}}{3}\sqrt{\frac{8R_uT}{\pi M_v}} \tag{B.2}$$

$$\varepsilon = \frac{N}{4}\int_0^{\infty} \varphi\left(d_{pore}\right)\pi d_{pore}^2 \, d\left(d_{pore}\right) \tag{B.3}$$

Where, N is the number of pores per unit area.

Based on the definition of the permeability of the membrane:

$$J = Permeability\ \frac{\Delta p_v}{\delta} \tag{B.4}$$

Where, Δp_v is the partial vapour pressure difference across the membrane and δ is the thickness of the membrane

Finally, using equations (B.1) and (B.4) the substrate permeability can be defined as below:

$$Permeability_{sub} = \frac{\varepsilon \int_0^{\infty} \left(\frac{R_u T}{D_{Kn}} + \frac{R_u T}{D_{wv}}\right)^{-1} \varphi(d_{pore}) \cdot d(d_{pore})}{\tau \int_0^{\infty} \varphi(d_{pore}) \cdot d(d_{pore})} \quad (B.5)$$

Appendix C Uncertainty Analysis of Permeability Measurements

The WVTR testing method is based on the measurement of the water vapor concentration in the air at the inlets and outlets of the test cell, as a result, the uncertainty of the humidity measurements is significantly important in determining the uncertainty of the final membrane permeability value. The polymer humidity sensors have an absolute nominal uncertainty of ±2% RH (at 50% RH) and the dew-point hygrometer has an accuracy of ±0.15 °C dew-point temperature which is ±0.4% RH at 50 °C. As most of the tests are performed with a dry sweep flow, the water vapour concentration at the sweep outlet measured by the dew-point hygrometer is used for the calculation of the permeability mostly; however, for the permeability calculations of the tests with a humid sweep flow and to calculate the water vapour concentration at the surface of the membrane, the polymer RH sensors are used in conjunction with the dew-point hygrometer. Additionally, in all tests, the polymer RH sensors are used to check the mass balance between the feed and sweep sides to reveal any leakage in the system and to compare water vapour flux through the membrane calculated from each side. The flowrate of the air streams leaving the feed and sweep sides are also frequently measured using a soap bubble flowmeter (Gilibrator-2) to further validate the sealing of the test cell. Overall, a mass balance difference of less than 5% was maintained for all the tests. In order to decrease the uncertainty in the measurements of the polymer RH sensors, they are frequently checked and leveled by the dew-point hygrometer. As a result, it can be assumed that the theoretical accuracy of the polymer RH sensors is lowered to 0.5 % RH [1].
The mass flow controllers have an accuracy of ±0.8%, the temperature-controlled chambers have temperature fluctuations of up to ±0.5 °C and temperature variations inside the chambers can be up to ±1 °C. The polymer RH sensors can also measure the temperature of the airflows with an accuracy of ±0.1 °C.

The abovementioned values for the accuracy of measurement equipment and error propagation methods are used to calculate the uncertainty [119]. Average uncertainties of 10% and 18% (95% CI) are calculated for the permeability of the composite membranes and the coating layers, respectively. An average repeatability of less than 5% is also observed for the measured permeability values.